J. A. Van den Akker

The Institute of Paper Chemistry

Appleton, Wisconsin

Doctor's Dissertation

A Study of Irreversible, Stress-Induced Changes in the Macrostructure of Paper

Irwin Bruce Sanborn

June, 1961

A STUDY OF IRREVERSIBLE, STRESS-INDUCED CHANGES IN THE MACROSTRUCTURE OF PAPER

A thesis submitted by

Irwin Bruce Sanborn

B.Ch.E. 1954, Rensselaer Polytechnic Institute
M.S. 1956, Lawrence College

in partial fulfillment of the requirements
of The Institute of Paper Chemistry
for the degree of Doctor of Philosophy
from Lawrence College,
Appleton, Wisconsin

June, 1961

TABLE OF CONTENTS

INTRODUCTION

Paper has been used for centuries, but there is still a great deal to be learned about how it responds to stress. Of course, a great amount of phenomenological information concerning the deformation of paper is available, but most of it is of little use in characterizing the mechanisms by which paper deforms. This is understandable when one considers that paper is a structure (on a fine macroscopic scale) rather than a homogeneous material. Consequently, paper responds to stress as a structure and the phenomena involved are extremely complex.

At present there are sufficient data available to demonstrate that both molecular processes and interfiber macroscopic effects play an important part in determining how paper will respond to stress. The problem which remains is to assess the relative importance of these two classes of response. When this has been done, the next step will be to develop semiquantitative theories of response useful in designing papers for specific end uses.

The objective of the work discussed in this dissertation was to learn more about how the interfiber structure of paper is altered by deformation and to determine how these changes affect the response of a sheet to stress.

HISTORICAL REVIEW

Almost all of the work involved in trying to elucidate the mechanisms by which paper deforms under stress has been done using tensile (stress-strain or creep-recovery) tests. The most obvious reason for this is that the boundary conditions of such tests are well defined.

The first workers to report studies of the deformation suffered by paper as a function of applied stress were Houston (1) and Bercsi (2) who studied the stress-strain properties of sheets with the hope of being able to predict "performance" more accurately. Unfortunately, the approach taken in each case was quite utilitarian, and although the data gathered served to demonstrate the viscoelasticity of paper, very little was learned about the mechanisms of response to stress.

The first workers to contribute to an <u>understanding</u> of the response of paper to stress were Gibbon (3) and Farebrother (4) who described simple techniques for measuring strain as a function of stress and reported a considerable amount of stress-strain and some creep data. Later in a discussion of his work Gibbon pointed out that:

1. paper is a viscoelastic material and suggested that its response to stress might best be characterized through the use of rheological methods, and

2. paper suffers considerable amounts of irrecoverable deformation as a result of stressing and hypothesized that this was due to stress-induced fiber slippage.

The next significant contribution to the literature concerning the mechanical properties of paper was made by Steenberg and co-workers (5-9).

They carried out an exhaustive study of the mechanical properties of a large number of papers and used the data to make two very important additions to the fund of knowledge concerning the response of paper to stress. First, they showed that although the prerupture response of paper is affected by variations in test conditions, such as rate of stressing or straining, specimen size or shape, etc., its prerupture properties are as reproducible as those of many other materials (5, 6). Second, they demonstrated that the mechanical properties of paper cannot be truly characterized through the use of mechanical models containing various combinations of springs and dashpots (6-9). Later, Rance (10) pinpointed the inadequacies of mechanical models by pointing out that such models fail to link sheet structure with mechanical behavior, fail to deal adequately with strain irrecoverability, and fail to account for fracture by relating it to prerupture properties.

Steenberg, et al. suggested two rather interesting concepts relating to the mechanism by which paper responds to stress. First, the idea that fibers might contain an invisible "micro-crêpe" was introduced to explain strain irrecoverability (6); second, the concept of "crystallite organization" was introduced to explain the "hump" observed in some stress-strain curves after cycling and the increase in slope of the post-yield region of other stress-strain curves (8).

Another attempt to characterize the mechanical properties of paper using essentially a phenomenological approach was made by Nissan (11-13), who assumed that the response of a sheet was governed by hydrogen bond deformation which could be related to stress by a modified type of Morse

function. The expression developed cannot be expected to give any more than a crude approximation of response because it was derived on the assumption that all bonds were acted upon in the direction of externally applied stress and because time effects and stress redistribution during deformation were neglected. This means that if the approach is not used judiciously, it degenerates into a curve-fitting technique taking advantage of the form of the Morse function to attain coincidence between predicted and observed values.

One of the most significant hypotheses concerning the mechanisms by which paper responds to stress first appeared in a paper published by Rance (14), who suggested that interfiber bond breakage controlled the rate of response to stress exhibited by a sheet. This hypothesis was formed after observing that:

1. the ultimate strain exhibited by a sheet is not greatly affected by variations in the rate of stressing or straining,

2. strain lines develop within high-density sheets when stress is applied, and

3. paper suffers large amounts of irrecoverable deformation when stress is applied.

A better understanding of the mechanism of response has led to the conclusion that Rance (10, 14, 15) was probably incorrect in concluding that the rate of response to stress was controlled by interfiber bond fracture, but this does not detract from the importance of his hypothesis for its main contribution was in emphasizing the importance of interfiber structural damage to the deformation of paper under stress.

Another important theory concerning the mechanisms of response to stress was proposed by Brezinski (16, 17). He hypothesized that intrafiber molecular processes control the rate of response and ascribe reversible deformation to reversible molecular processes--polymer chain straightening, etc.--and irreversible deformation to irreversible molecular processes--crystallite growth, etc. Subsequent studies have shown that this hypothesis was not entirely correct because it neglected stress-induced interfiber structural changes, but this is not important for its real contribution was in emphasizing the importance of fiber properties to the response exhibited by a sheet.

One of the most important contributions to an understanding of the mechanisms by which paper responds to stress has been made by Nordman, et al. (18-21), who developed a technique for measuring the optical properties of paper while it was under stress. This technique was used to obtain data which indicated that paper suffers a stress-induced increase in scattering power linearly related to the energy lost during deformation. In analyzing these data, it was assumed that the increase in scattering coefficient was due to interfiber bond fracture and a so-called bonding strength was calculated. This method of estimating bond strength has been criticized by a number of workers (22, 23) because it ignores the separating of unbonded areas, changes in intrafiber scattering, and energy losses due to fiber deformation during straining.

Because the work reported by Nordman, et al. (18-21) only supplied indirect evidence of structural damage during deformation, there was

some question as to whether the observed change in scattering power was due to interfiber damage. Some of these doubts were dispelled by Page, et al. (24, 25), who supplied direct experimental evidence that interfiber bonds were broken as a result of deformation. These workers developed a microscopic technique which allowed them to observe interfiber areas in optical contact as a sheet was subjected to stress. The data collected indicated that:

1. some bonds broke almost instantaneously while the area of others seemed to decrease rather slowly during deformation, and
2. the area of bonds never increased when stress was removed.

The importance of these observations cannot be overemphasized for they prove that interfiber bonds are broken when paper is subjected to stress.

In a recent symposium, Corte (26) described a number of techniques which he had used to characterize the porous properties of paper. Among these were included methods for measuring both the number and volume average pore size distribution within a sheet and techniques for measuring the permeability of paper to both inert and sorbable gases. Proper use of such techniques should supply a considerable amount of useful information concerning the effect of stress on the interfiber structure of a sheet, but it will not yield a quantitative characterization of the interfiber structure of paper because there is no suitable model for the structure of a porous medium. It may be possible to develop such a model by extending a statistical approach similar to the one recently reported by Kallmes and Corte (27); but until such a model

is devised there is little hope of being able to use permeability and pore size distribution techniques to get any more than a qualitative picture of interfiber structure.

One of the best ways to gain an understanding of the mechanical properties of paper is to consider a sheet to be a structure rather than a homogeneous material and then relate its mechanical properties to those of its constituent fibers. Onogi and Sasaguri (28) have made such an attempt and have related the elastic modulus, density, Poisson's ratio, and dynamic viscosity of paper to the elastic modulus, density, radius, segment length, and angular distribution of the fibers within it. This treatment would be quite useful despite the fact that it is only intended to apply in the elastic region were it not for the fact that the analysis is based on the erroneous assumption that the forces acting on all fiber elements are parallel to the direction of the externally applied stress (29). As a result the only contribution made by these workers was to demonstrate that the density of a sheet can be related to the density and shape of its constituent fibers if their arrangement within the sheet is known.

A more successful attempt to relate the mechanical properties of a web to the properties of its constituent fibers has been made by Petterson (30), who was able to predict both the elastic and plastic properties of low density, long-fibered webs from a knowledge of the elastic modulus, rupture load, rupture elongation, yield zone, and angular distribution of their constituent fibers. The theory developed is not based on a good model for paper because the system considered is

not sufficiently consolidated, but the method of attack used is very interesting because it would appear that some of the experimental and analytical techniques that were developed can be used to study more highly consolidated systems such as paper. The agreement between predicted and measured data achieved by Petterson is encouraging (the expressions developed can be used to predict both the elastic and plastic response of a web with an accuracy of 10-20%), but his results are not applicable to paper because the plastic response of his "non-woven" fabrics was directly attributable to the viscoelastic nature of their constituent fibers.

Van den Akker (29) has recently developed a mathematical theory for a fibrous structure that is intended to simulate typical paper and paperboard with regard to such factors as nature of the fibers and frequency of fiber-fiber bonding. His treatment embraces two regimes, the "elastic" and the "plastic"; for the former, expressions are developed for external load, Poisson's ratio, Young's modulus, and modulus of rigidity; for the latter the theory yields expressions for stresses in fiber-fiber bonds that relate to "torque" and "tension" types of bond failure.

To summarize the above review, it can be stated that paper is recognized as having the following characteristics:

1. It is a viscoelastic, anisotropic material made up of fibers bonded together into a highly consolidated system.
2. It derives most of its strength from the strength of its constituent fibers and the strength of the hydrogen bonds which hold the fibers together in a contiguous mass.

3. It suffers structural breakdown due to interfiber bond fracture when stress is applied.

PRESENTATION OF THE PROBLEM

The work cited in the foregoing section indicates that both inter- and intrafiber processes have an important effect upon the response of paper to stress. The purpose of this investigation was to learn more about the mechanisms by which paper deforms. The procedure followed was to use all of the information currently available to develop a qualitative theory of response that could be stated clearly and concisely; then the theory was used to develop explicit objectives for the work and as an aid in interpreting the data obtained.

Originally, it was hoped that this study would yield data which could be used to determine the relative importance of inter- and intrafiber processes of deformation, but this objective had to be modified because of experimental difficulties*. The result was that attention was concentrated on interfiber processes of deformation, and it was decided that the objectives of the investigation should be:

1. to seek additional evidence that interfiber structural damage caused by fiber-fiber bond breakage is induced by stress, and
2. to learn more about the mechanisms by which paper responded to stress.

The method of attack used to study the mechanisms by which paper deforms consisted of three steps:

*The permeability data that were obtained could not be treated in such a way that changes in interfiber structure could be characterized quantitatively. As a result, changes in interfiber structure could not be differentiated from changes in intrafiber structure, and the relative importance of inter- and intrafiber processes of deformation could not be evaluated.

1. First-creep and creep-recovery measurements were made to characterize the mechanical properties of specimens.
2. Transmittance and reflectance data were collected to determine the effect of deformation on the optical scattering power of paper.
3. Air permeability and gas drive tests were carried out to study the effect of stress on the porous properties of a sheet.

The data gathered by these experiments were used to answer three important questions:

1. How does stress-induced deformation affect the scattering power of paper when long-term, time-dependent processes of deformation are allowed to become important?
2. How does deformation affect the porous structure of paper?
3. What do the stress-induced changes in scattering power and porous properties imply about the mechanisms of deformation?

BACKGROUND INFORMATION

Before any progress toward an understanding of how paper responds to stress could be made, all of the information available had to be used to obtain a good insight into the mechanisms of deformation. The first step taken was to recognize that paper is a heterogeneous material made of fibers bonded together in a structure which suffers structural damage when subjected to stress (18-21, 24, 25). This means that paper must be thought of as a structure if the response of a sheet is to be understood.

Van den Akker (31) has described a typical paper as a relatively strong, well-consolidated system of fibers, with many points of bonding between any given fiber and its neighbors, and with its fibers lying primarily in the x-y plane of the sheet (lying generally within small angular ranges of such planes). He has expressed the opinion that, for strains up to the point of structural damage, the fibers are not free to twist and change shape, or slide over each other when the sheet is stressed. In more recent work (29) he discusses, from a theoretical point of view, the disruptive shear stresses that may exist in fiber-fiber bonds when the sheet is strained in the "plastic regime."

A number of studies supplying a great deal of information concerning how paper deforms under stress have been performed. One of the most important was carried out by Brezinski (16, 17) who found that:

1. the primary and first-creep response of paper shows a degree of ideality typical of processes controlled by molecular mechanisms,

2. paper appears to conform to a mechanical equation of state, and

3. part of the so-called irreversible deformation suffered by a sheet during a creep-recovery cycle at low relative humidity is recovered upon humidification.

The data collected by Brezinski clearly demonstrate the importance of intrafiber molecular processes to specimen deformation, but his interpretation of the data has been criticized because he did not ascribe sufficient importance to interfiber, macroscopic processes going on during deformation. Subsequent work has substantiated this criticism.

Other data which also indicates that intrafiber processes have an important effect upon the response shown by a sheet have been supplied by Van den Akker, et al. (32). These workers devised a technique for observing the zone of rupture in a sheet during tensile failure. The data obtained demonstrated that:

1. many fibers broke during disruption of a sheet, and

2. the ratio of broken to pulled-out fibers in the zone of rupture increased as the degree of bonding within a sheet increased.

These observations indicate that the fibers within a sheet are well bonded together and that they are subjected to large stresses during deformation. Thus, it is to be expected that the properties of the fibers within a sheet will have an effect upon the mechanical properties exhibited by that sheet.

Rance (10, 14, 15) has suggested that interfiber, macroscopic processes, such as fiber-fiber bond breakage, control the rate at which paper deforms under load. He reached this conclusion on the basis of information already presented (see page 4 of this dissertation), but his

interpretation of the data has been criticized because he did not recognize the importance of intrafiber processes of deformation.

Subsequent experiments have supplied good evidence that the breaking of fiber-fiber bonds constitutes an important aspect of sheet deformation. The most important of these are the studies conducted by Nordman, et al. (18-21) and Page, et al. (24, 25).

In a study carried out by Jayne (33), who developed a technique for measuring the stress-strain characteristics of individual pulp fibers, it was shown that the response to stress of such fibers is primarily (but not entirely) elastic. These results have been verified by workers at The Institute of Paper Chemistry (34) and serve to demonstrate that the marked viscoelasticity of paper arises partially from some mechanism in addition to fiber element deformation.

An investigation which illustrates one of the possible effects of interfiber bond fracture has been made by Schulz (35), who studied the effect of wet straining on the mechanical properties of dry sheets. Schulz found that variations in internal stress distribution induced by wet straining had a pronounced effect on both the "instantaneous" and time-dependent response of a dry sheet to stress. This suggests that interfiber bond breakage may alter the response of paper by causing stress redistribution to take place within it during deformation.

With the above facts in mind it should be possible to develop a qualitative theory of response compatible with all of the experimental data currently available. In developing such a theory it should be

remembered that the hypotheses suggested by Brezinski (16, 17) and Rance (10, 14, 15) have been criticized because the former did not recognize the importance of interfiber, macroscopic effects while the latter failed to recognize the importance of intrafiber effects.

It is now hypothesized that the rate of response shown by a sheet at any instant is controlled by molecular mechanisms, but that this rate is altered by interfiber macroscopic effects in two ways. First, the fracture of fiber-fiber bonds decreases the load-bearing area and, second, it causes a stress redistribution to take place within a sheet. Neither of these phenomena can affect the fundamental mechanisms by which deformation takes place, but they can alter both the rate and amount of deformation by changing the driving force (stress) to which the fiber elements within a sheet are subjected. All of the experimental data obtained during this investigation have been analyzed with this hypothesis in mind. It is hoped that this has resulted in an understanding of the significance of the data which might not have been achieved otherwise.

EXPERIMENTAL PROCEDURES AND TECHNIQUES

Before the experimental techniques used in this investigation are described, some space should be devoted to a description of the experimental program that was used. Figure 1 contains a diagrammatic presentation of the program and demonstrates two important facts. First, four techniques--the creep and creep-recovery, the light-scattering, the air permeability, and the gas drive method--were used to study the effect of stress on the interfiber structure of paper; second, two completely different procedures were used to collect data.

The first procedure, which shall be referred to as the parallel testing procedure, was used to obtain light-scattering data and contained three steps:

1. The optical properties of a number of specimens (usually seven) were measured.
2. Each specimen was subjected to a different creep-recovery cycle.
3. The optical properties of each specimen were measured again and the effect of deformation was evaluated.

The advantages of this procedure were its simplicity and ability to gather large amounts of information with a minimum of effort. The principal disadvantage of the procedure was that specimen-to-specimen variations were not eliminated.

The second procedure, referred to as the series testing procedure, was used to study stress-induced changes in porous properties, such as

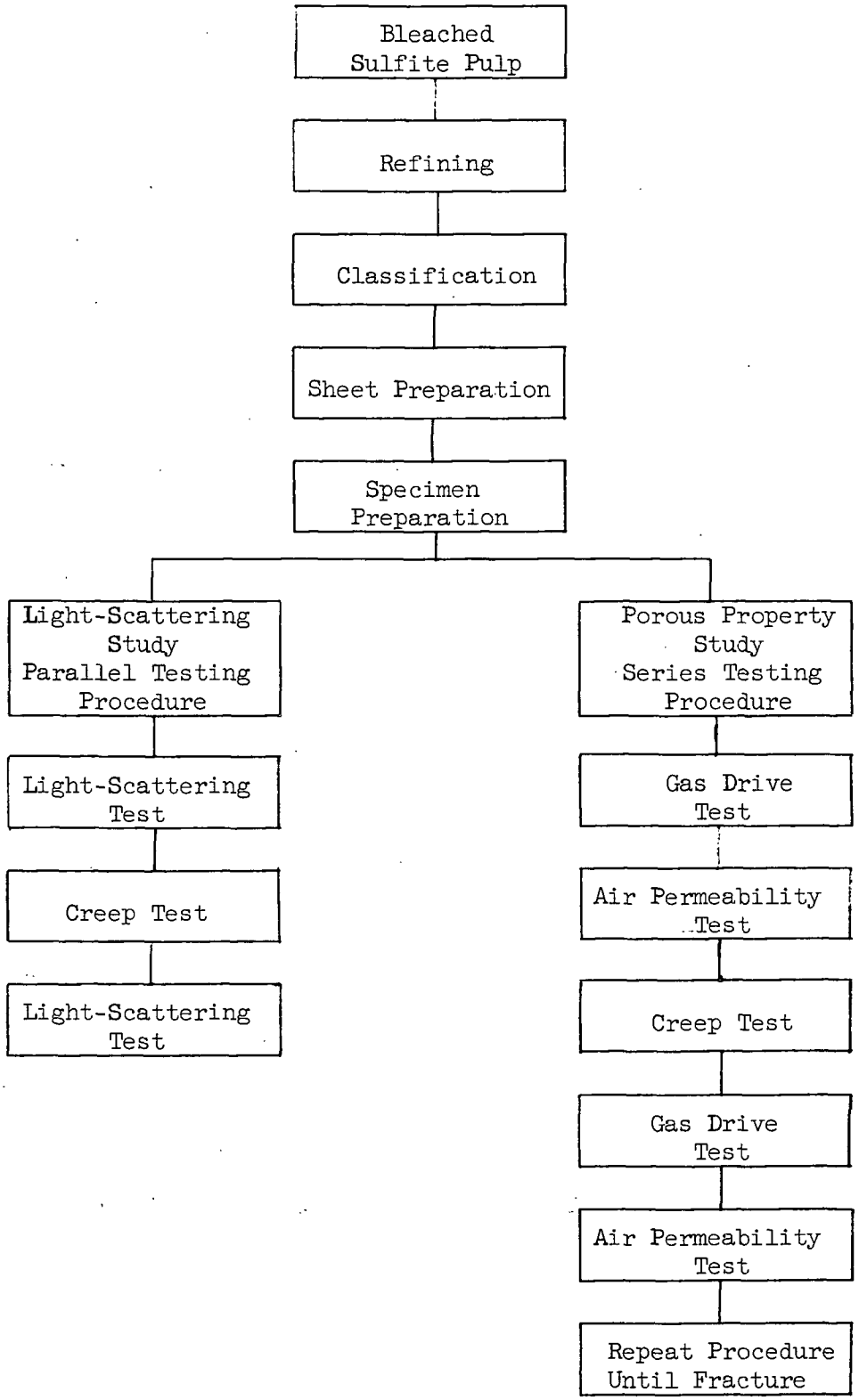

Figure 1. Experimental Program

permeability and pore size distribution. This procedure contained many steps.

1. The porous properties of a specimen were measured.
2. The specimen was subjected to a creep-recovery cycle.
3. The porous properties of the specimen were measured again and the effect of the creep-recovery cycle was evaluated.
4. Steps 2 and 3 were repeated with the creep-recovery cycle being increased in severity each time until fracture occurred.

The great advantage of the series testing procedure was the elimination of specimen-to-specimen variations, but this advantage was offset by the time required to carry out the program of testing.

PREPARATION OF SPECIMENS

Because stress-induced changes in interfiber structure were to be studied during this investigation, it was decided that sheets with a relatively simple interfiber structure, comparatively free of fines and fiber fibrils, should be used. Therefore, a long-fibered, bleached, sulfite pulp containing 60-80% spruce, 10-20% hemlock, 10-20% balsam fir, and 5-10% larch fiber was used in the study; it was subjected to the following treatment before being used to prepare handsheets:

1. Twenty 100-gram batches of never-dried pulp were ball-mill refined for 30 minutes according to Institute Method 402 (36), dewatered on a large Buchner funnel, and blended.

2. Ninety 20-gram batches of refined pulp were classified according to Institute Method 415 (37) and only those portions held on a 20-mesh screen were retained.
3. Each of the 90 batches of classified pulp was dewatered on a British sheet mold, and then all 90 were blended at a consistency of 2%, dewatered with a laboratory wash-box, centrifuged, bagged, and stored in a cold room to await future use.

The pulp obtained was a lightly beaten, long-fibered stock that had good strength properties and gave handsheets with a relatively simple inter-fiber structure.

Originally, it was believed that the strength of the specimens studied during this investigation would have to be varied over a wide range by a method which had very little effect on the characteristics of the fibers and interfiber structure of the specimens*. The most logical method of accomplishing this variation in strength was to subject the handsheets from which specimens were to be prepared to different amounts of wet pressing prior to drying. It was found that conventional methods of wet pressing did not cause a sufficiently large variation in strength properties. The result was that the technique of pressing to dryness described below was adopted to get the required spread in mechanical properties. Later, it was found that the study

*This was a result of an original intention to assess the relative importance of inter- and intrafiber processes of deformation when a sheet is subjected to tensile stress.

of but one type of material was sufficient. These specimens were prepared in the following manner:

1. Sufficient pulp for a 9 by 9-inch, 100 g./sq. m. handsheet was weighed into a small polyethylene sack, soaked overnight with 100 cc. of deionized water, and disintegrated for 5 minutes in a malted milk mixer before being added to the deckle box of a 9 by 9-inch sheet mold.
2. In the deckle box, the pulp was diluted to a consistency ~ 0.005→0.006 % of about ~~0.0015%~~ with deaerated, deionized water, and drawn through a 110 by 90-mesh "flat weave" wire to form a handsheet. This sheet was couched off the wire and covered with wet blotters that had previously been sprayed with clear lacquer to promote release after pressing.
3. The wet sheet, its couch, and cover blotters were placed between eight dry blotters and pressed in a hydraulic press at 50 p.s.i.g. until dry. During this period, water removal was achieved by blotter replacement after contact times of 5, 10, 15, and 30 minutes.
4. When essentially dry--10-15% moisture--the sheet was stripped from its couch and cover blotters, taped to a glass plate with gummed kraft paper, and allowed to equilibrate with the atmosphere in a humidity room maintained at 50% relative humidity and 73°F.
5. After a number of handsheets had equilibrated, three 6.14 by 15.98-cm. specimens were cut from each sheet with a razor blade*.

*A template constructed in such a way that 21 fiducial marks could be made at 0.25-inch intervals along both edges of the five-inch central section of a specimen was also used.

6. Finally, when all the specimens had been cut out and marked with identification numbers, they were placed in a dark drawer in a constant-temperature, constant-humidity room to await future use.

CREEP AND CREEP-RECOVERY PROPERTIES

During this investigation creep and creep-recovery techniques were used to characterize the mechanical response of specimens to stress. These techniques were used because they have well-defined boundary conditions and yield data that can be interpreted in terms of fundamental mechanisms of deformation. Two pieces of equipment were used to make creep and creep-recovery measurements.

The first apparatus to be described is quite similar to the one used by Brezinski (16, 17) and is shown in Fig. 2 and 3. From these figures, it can be seen that the top specimen clamp hung from a pin (A) and that the lower clamp was attached to a weight can filled with lead shot by a rod (B). The position of the two clamps during a test was determined through the use of two contactors (C & D) attached to a traveling rod (E) held against the shaft of a micrometer (F) by a spring (G). These contactors operated by using a swing bar (H) to make and break electrical contact between the contactor bodies (I), which were grounded to the frame of the apparatus, and the contactor bars (J) which were connected to a low-voltage electrical circuit, also grounded to the frame. Thus, the position of either specimen clamp could be determined merely by driving the traveling rod (E) up and down with the micrometer (F) and

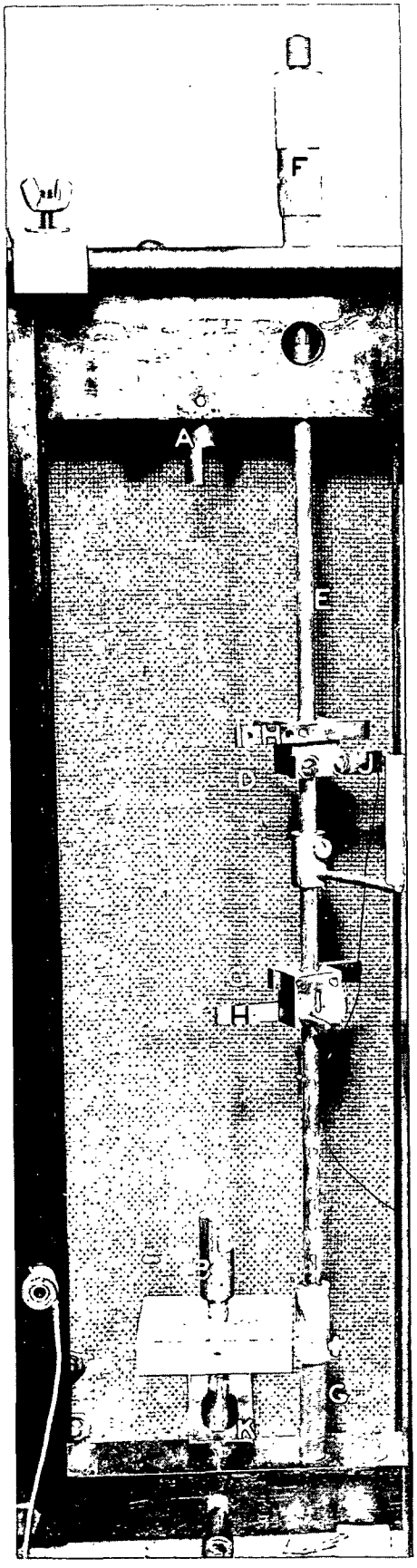

Figure 2. Creep Tester Without Specimen Clamps

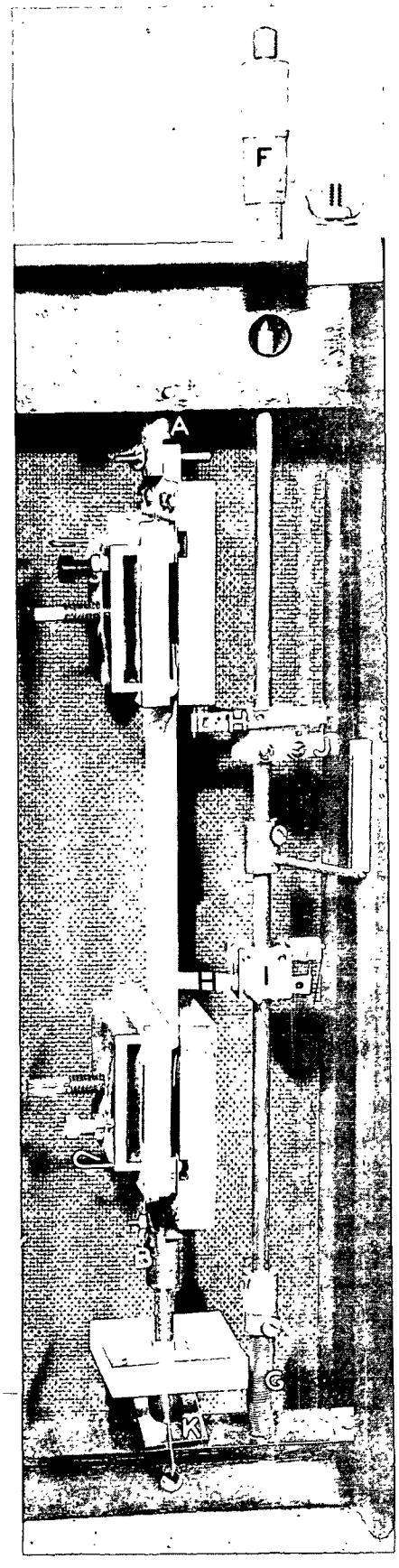

Figure 3. Creep Tester With Specimen Clamps

noting the micrometer reading when the external electrical circuit was broken by the rotation of the swing bar (H) as it contacted the face of a specimen clamp.

The specimen clamps used with the creep-testing equipment just described were of special design and constructed in such a manner that a specimen could be clamped at a known pressure between a cylindrical rod and a flat face. The design of the clamps is illustrated in Fig. 4, which shows how the jaws were controlled by turning a differential screw (A). Control of the clamping pressure was achieved through the use of a cantilever contactor (B) which was separated from a plug contactor (C) and broke an external electrical circuit when sufficient pressure was brought to bear on a loading beam (D) by the differential screw[1]. When a specimen was to be gripped by the clamp, it was placed between the jaws of the device and the differential screw was turned until the specimen was gripped with sufficient force to prevent jaw pull-out[2].

The technique used to obtain creep and creep-recovery data with the equipment described above was as follows:

1. A specimen was placed in the mounting jig pictured in Fig. 5 and clamped between two 2.75-inch wide line contact clamps (see Fig. 4) with a gage length of 5.002 inches (see Fig. 6).
2. The specimen was placed in a creep-testing station similar to the one shown in Fig. 2 and 3 and the position of each

[1] This design was adapted from that of the IPC zero-span testing device (38).

[2] During this investigation, the applied force at which the contactors (B & C) separated was 100 lb./in. The contactors on each clamp were set by a dead-weight loading technique.

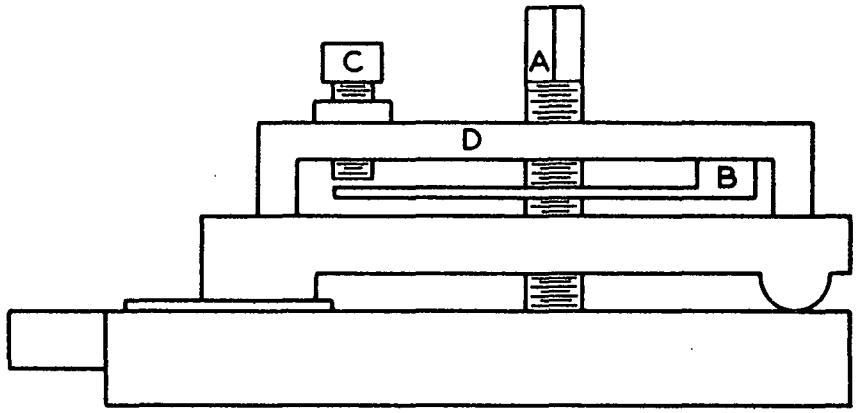

SIDE VIEW

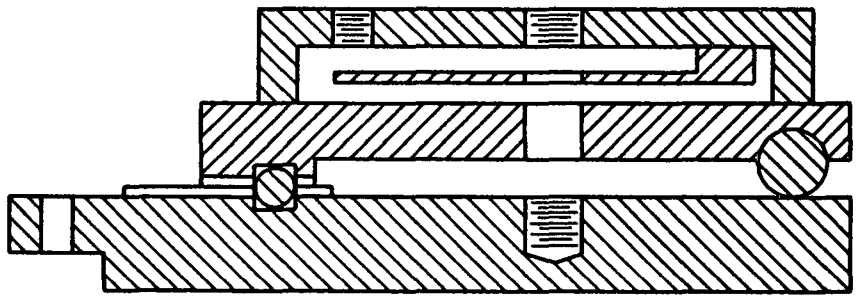

CROSS-SECTIONAL VIEW THROUGH TAPS FOR CONTACTOR C AND DIFFERENTIAL SCREW A

Figure 4. Sketch of Line Contact Clamps

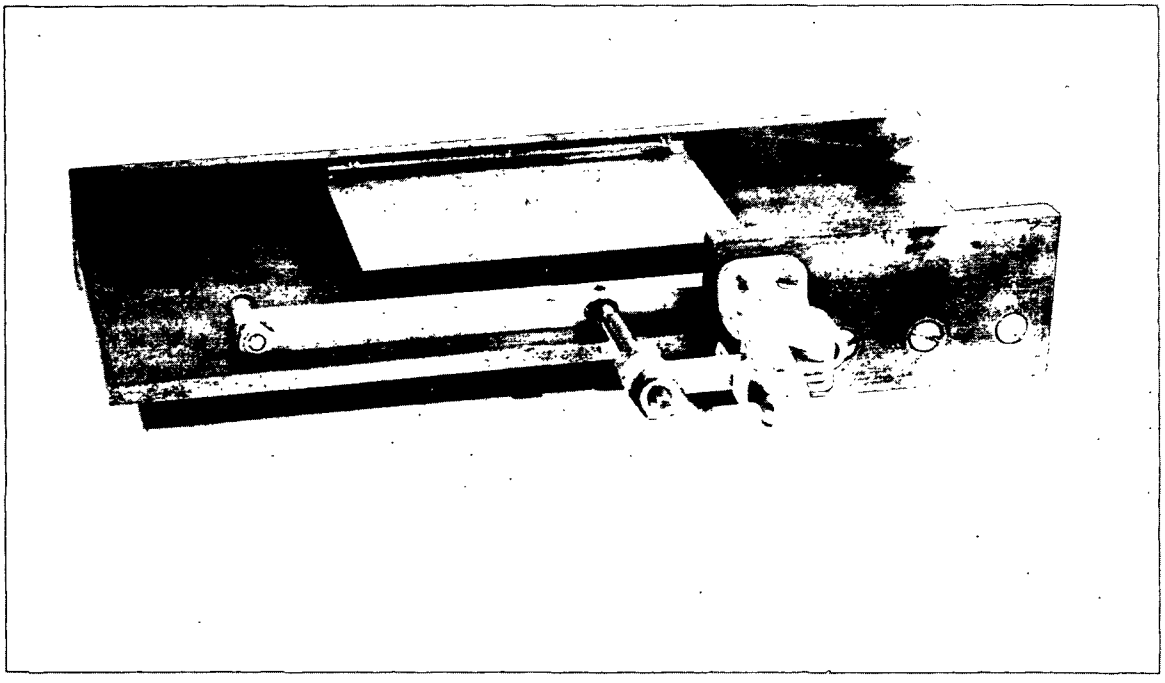

Figure 5. Specimen Mounting Jig Without Clamps

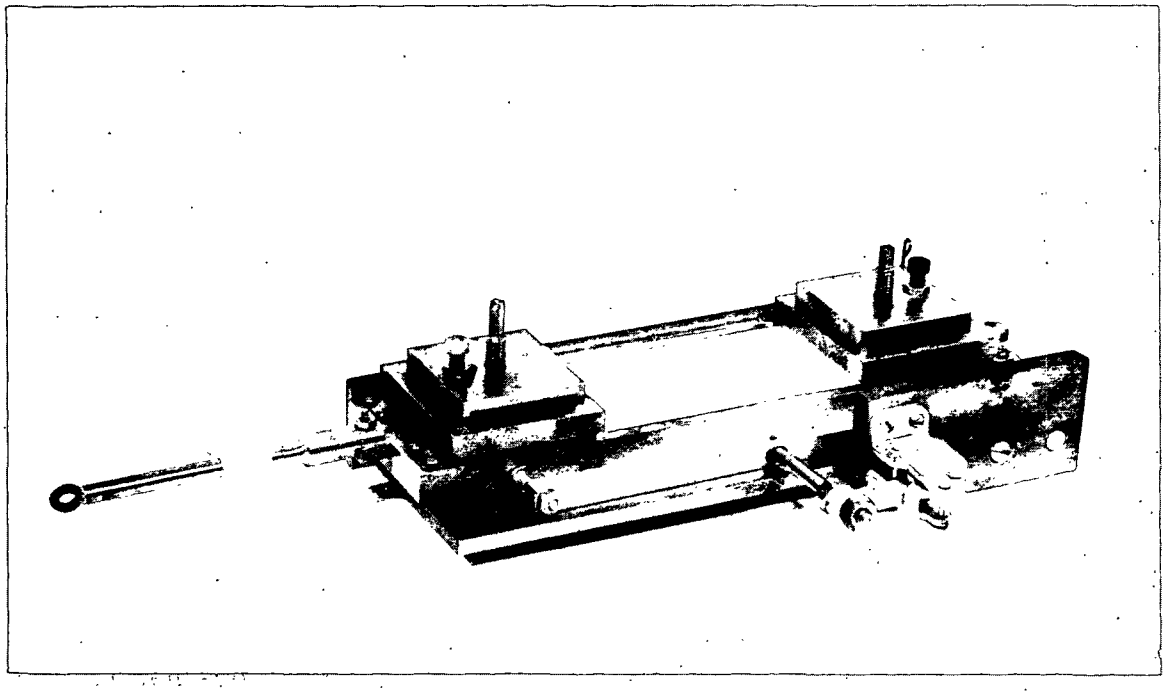

Figure 6. Specimen Mounting Jig With Clamps

clamp was determined with the weight of the bottom clamp holding the specimen taut[1].

3. A creep test was carried out by gently hanging a weight can on the rod (B) and using the micrometer (F) to measure the position of both clamps as a function of time[2].

4. The creep test was ended by removing the weight can from the rod (B) and was usually followed by a creep-recovery test which was carried out by again using the micrometer to measure the position of both clamps as a function of time[3].

5. The recovery test was ended by taking the specimen out of the testing station and removing it from the specimen clamps with the aid of the mounting jig.

Load-extension data were required if the energy irreversibly lost during a creep-recovery cycle was to be estimated[4]. The equipment just described could not supply such information, and another piece of apparatus had to be used. The IPC load-elongation tester (39), modified as

---

[1] The weight of the bottom, jaw (2.47 lb.) caused a 0.003-inch extension of the specimens. This was taken into account when the data gathered were analyzed.

[2] All creep and creep-recovery tests lasted exactly 24 hours during this investigation unless the creep test was terminated by rupture.

[3] All recovery measurements were made with the weight of the lower clamp holding the specimen taut; but when measurements were not being made, the weight of the bottom clamp was supported by a leaf spring (K) (see Fig. 2 and 3). (The 0.003-inch extension caused by the weight of the bottom jaw was corrected for during subsequent calculations.)

[4] In Appendix I, it is demonstrated that the energy irreversibly lost during a creep-recovery cycle is equal to the area enclosed by the load, creep, and deload curves of the cycle on a load-versus-extension plot.

shown in Fig. 7, was used to collect the information that was needed. The top clamp of the tester was assumed to remain stationary during a creep-recovery cycle, which meant that only the bottom jaw moved during a test. The position of this clamp was determined through the use of the traveling bar (A), which had a revolution counter attached to its main drive screw, and a contactor (B) located at the bottom of the weight can (C)[1].

Only load, deload, and creep data were gathered on the IPC load-elongation tester. The technique used was as described below.

1. One end of a 1.0 by 5.5-inch specimen was clamped in the upper line-contact jaw of the IPC load-elongation tester using the mounting jig that was provided.
2. Both the specimen and clamp were placed in the testing station of the load-elongation tester and the other end of the specimen was clamped in the lower, line-contact jaw which was still attached to the traveling bar in the usual fashion[2].
3. The lower, line-contact jaw was detached from the traveling bar and attached to the weight can, which was supported by the traveling bar until the creep test was started.

---

[1]Contact between the traveling bar (A) and the contactor (B) was detected through the use of an external, low-voltage, electrical circuit which was grounded to the frame of the tester on one side and attached to the lower clamp on the other.

[2]A gage length of 5.000 inches was used.

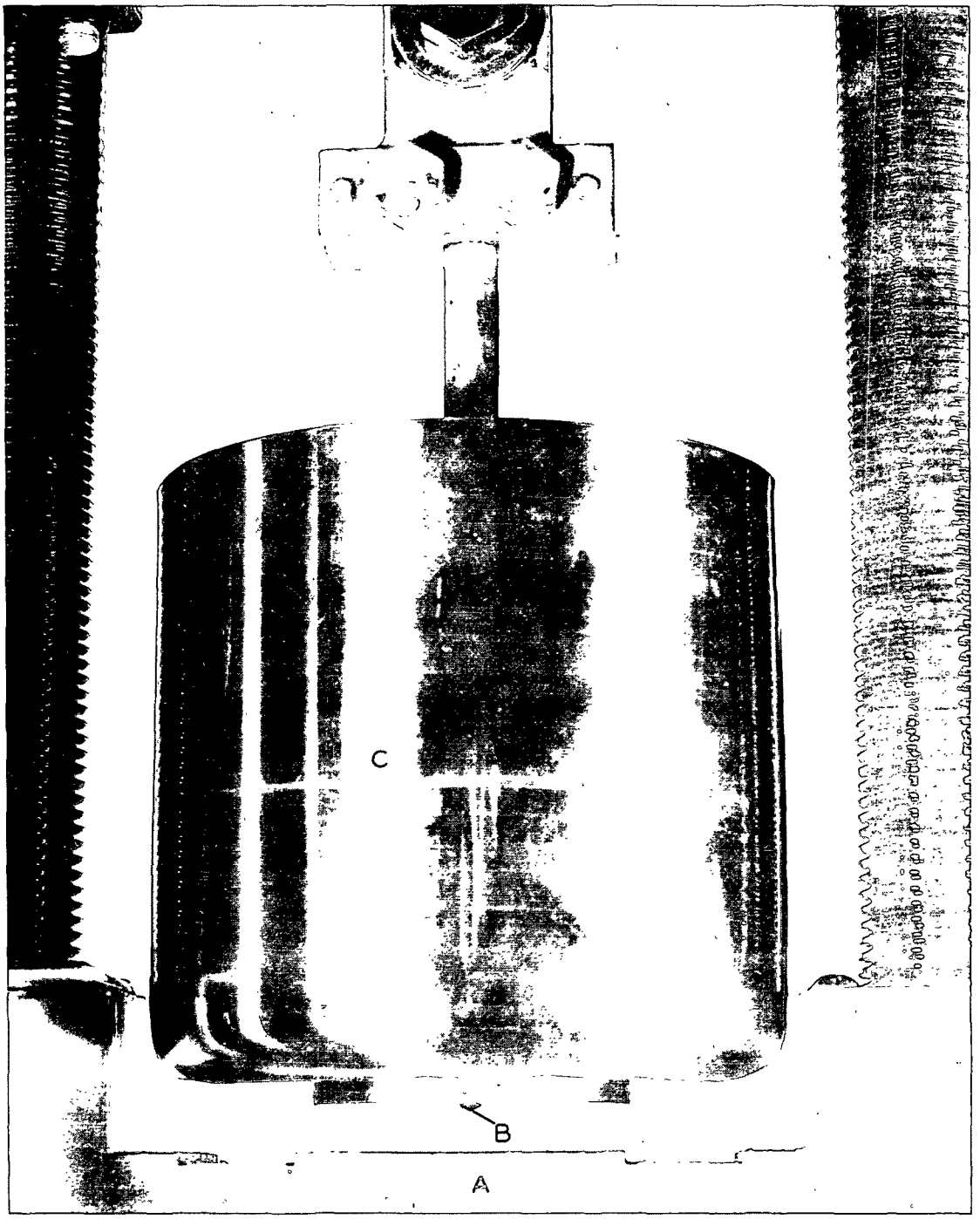

Figure 7. Testing Station of the IPC Load-Elongation Tester

4. A creep test was started by running the traveling bar down at a constant speed and recording a load-elongation curve for the application of load.
5. Creep measurements were made for 24 hours with the help of the contactor (B), the traveling bar, and an external, electrical circuit.
6. The creep test was ended by running the traveling bar up at a constant speed and recording a deload-versus-extension curve.
7. When a complete load, creep, and deload cycle had been completed, the specimen was removed from the clamps holding it, allowed to recover for 24 hours, and then subjected to additional testing.

OPTICAL PROPERTIES

One objective of this investigation was to learn more about how creep stressing affects the optically apparent exposed surface within a specimen. The parallel testing procedure was used to measure the optical properties of a number of specimens before and after they had been subjected to creep-recovery cycles. The data obtained were analyzed through the use of the Kubelka-Munk theory of light scattering (40, 41), which can be stated mathematically as follows*:

$$d \ln[I_r/I_t] = -2(s + k)dW + [(I_t/I_r) - (I_r/I_t)]sdW \qquad (1)$$

*Although the original Kubelka-Munk equation was stated in terms of differential thickness, Van den Akker (42) has shown that it can also be stated rigorously in terms of differential basis weight.

where I_r and I_t are the intensities of the reflected and transmitted portions of the incident light, and s, k, and W are the specific scattering coefficient, specific absorption coefficient, and basis weight of a sheet. Kubelka (43) has solved Equation (1) and shown that the transmittance, T, reflectance (when backed by a black body), R_o, specific scattering coefficient, s, specific absorption coefficient, k, and basis weight, W, of a sheet are related as shown below.

$$(s + k)/s = \alpha = (1 + R_o^2 - T^2)/2R_o \qquad (2)$$

$$sW = (1/\beta)[\text{arc sinh}(\beta/T) - \text{arc sinh}(\beta)] \qquad (3)$$

where $\beta = (\alpha^2 - 1)^{1/2}$. This means that it was necessary to measure only the transmittance, T, reflectance, R_o, and basis weight, W, of a specimen before and after a creep-recovery cycle if the effect of deformation on the optically apparent exposed surface of that specimen was to be determined.

The apparatus used to collect light-scattering data during this investigation was a Hardy General Electric recording spectrophotometer (GERS) (44, 45). The GERS was modified slightly for this work because a special integrating cavity had to be used to determine transmittance, T^*. This cavity is shown in Fig. 8 and 9.

The experimental technique used to gather light-scattering data during this study was as follows.

*Dearth and Shillcox (46) have shown that the use of the special integrating cavity yields data on scattering coefficient that are in excellent agreement with those obtained with the spherical cavity and reflectance determinations.

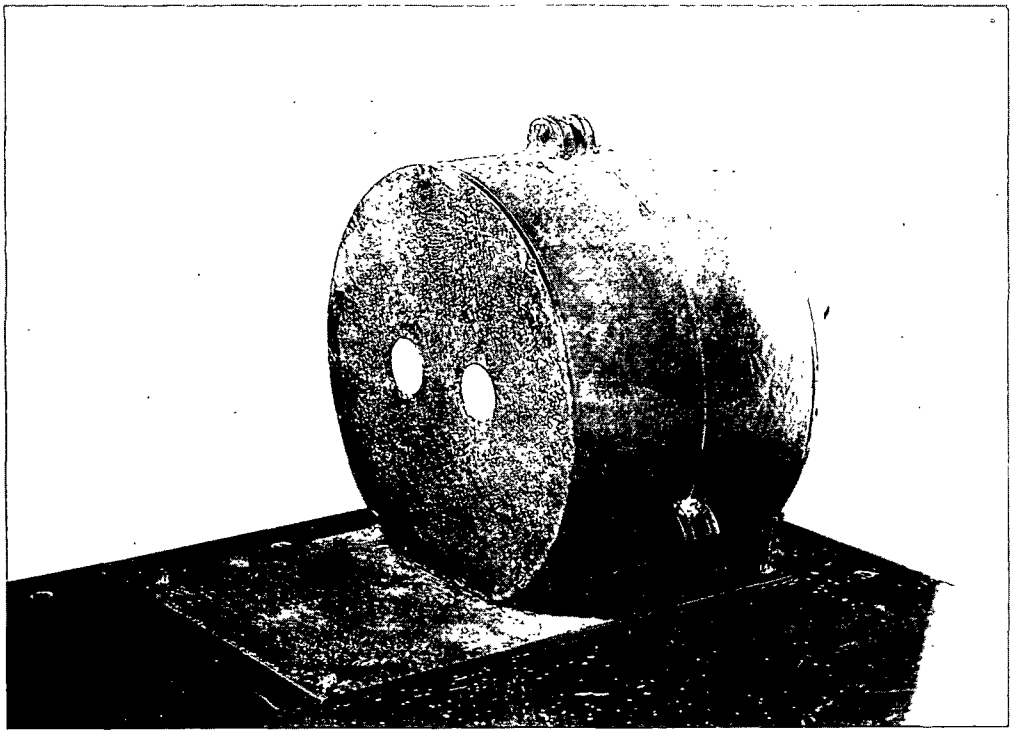

Figure 8. Integrating Cavity Without Specimen Holder

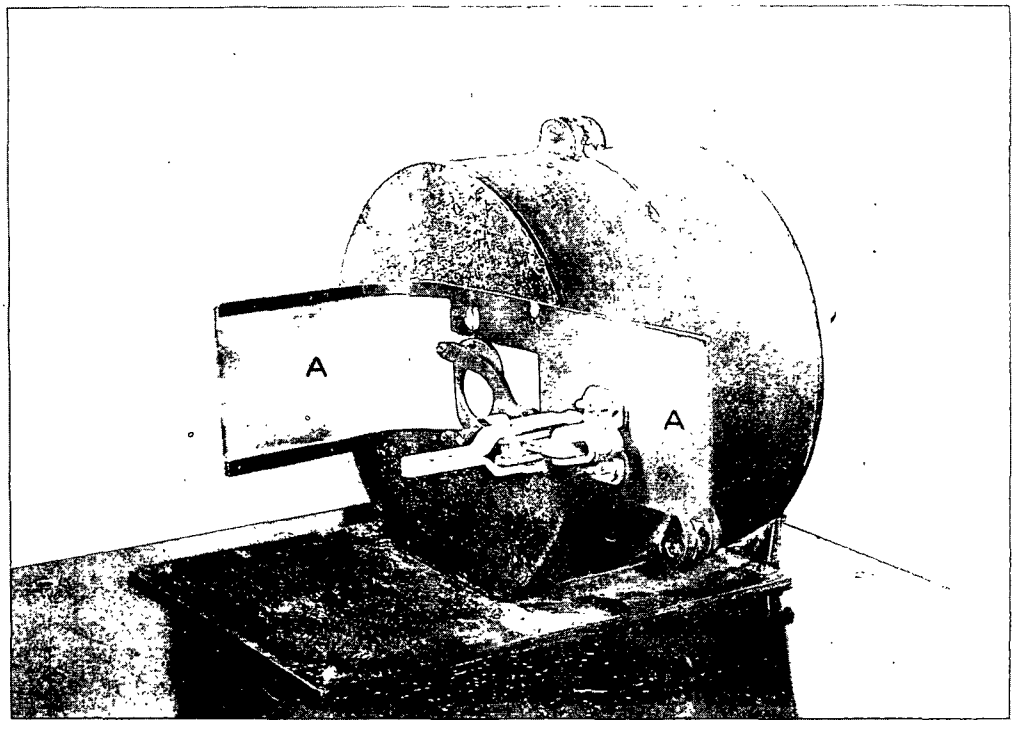

Figure 9. Integrating Cavity With Specimen Holder

1. The GERS was turned on, allowed to warm up for a short time, the wavelength of its incident beams was set at 650 mμ by adjustment of the monochromater, and a pair of matched magnesium carbonate blocks were placed over the exit ports of the integrating cavity.
2. A specimen was placed in the specimen holder (A) and its transmittance was measured at 38 different, preselected spots which were located through the use of a cross hair on the holder and fiducial marks on the specimen.
3. When the necessary transmittance data had been obtained, the specimen was removed from the holder, and the two magnesium carbonate blocks were replaced by a barium sulfate plaque at the exit port for the reference beam.
4. The reflectance, $\underline{R}_o$, of the specimen was measured at six randomly selected points by holding it against the sample beam exit port of the integrating cavity with a black velvet-lined cavity.
5. When all the necessary optical data had been collected, the specimens were conditioned in a constant-temperature, constant-humidity room and weighed.

PERMEABILITY PROPERTIES

One of the important questions to be answered by this study was, "How does deformation affect the porous structure of paper?" Air permeability studies were very useful in gathering information to answer this question. Air permeability data were used in two ways. First, they were

employed to determine the changes in permeability properties induced by stress; second, they were used to decide if the Kozeny-Carman method of data reduction (47) could be used to estimate either the absolute value of or stress-induced changes in interfiber exposed surface. A summary of the Kozeny-Carman approach along with a description of the method used to analyze permeability data is given below.

It is an experimental fact that for viscous flow the permeability coefficient, K, exhibited by a porous medium is linearly related to the mean pressure, $\bar{P}$, of the gas passing through it. This can be expressed mathematically by the equation:

$$K = c\bar{P} + d \qquad (4)$$

where $K = u\bar{P}L/\Delta P$, u is the linear velocity, $\bar{P}$ the pressure, L the thickness, and ΔP the pressure drop across the porous medium.

Carman (47) has shown that terms c and d in Equation (4) can be related to more fundamental constants by means of the equations, $c = B_o/n$ and $d = 4K_o\bar{v}/3$, where B_o and K_o are the air permeability and slip constants of a medium and n and $\bar{v}$ are gas viscosity and mean thermal molecular velocity. Carman also went on to show that if a medium satisfied the limitations inherent in the Kozeny-Carman treatment, its permeability and slip constants could be related to even more fundamental bed parameters by means of Equations (5) and (6).

$$B_o = pm^2/k' = p^3/k_o t'S^2 \qquad (5)$$

$$K_o = \delta_1 pm/t' = \delta_1 p^2/t'S \qquad (6)$$

where $\underline{p}$ is the porosity, $\underline{m}$ is the mean hydraulic radius, $\underline{k}'$ is the Kozeny constant, $\underline{k}_o$ is a shape factor, $\underline{t}'$ is the tortuosity, $\underline{S}$ is the surface area exposed to the flowing fluid per unit volume of bed, $\delta_1 = (3\pi/16)[(2 - \underline{f}_1)/\underline{f}_1]$ and $\underline{f}_1$ is the fraction of molecules diffusely reflected from the pore walls of the medium.

The thickness of the specimens studied during this investigation was measured with a Federal gage (48) using a pressure of 6.4 lb./sq. in. on a 0.125-inch diameter platen. In addition, the specimen holder pictured in Fig. 10 was also attached to the gage. The holder served two important functions. First, it held a specimen flat as thickness measurements were made and, second, it was used to locate 38 preselected points on each specimen through the use of a cross hair and fiducial marks. The reason that these 38 points on each specimen had to be located was that the series testing procedure demanded that the thickness of each specimen be measured at the same points each time. The technique used in measuring sheet thickness was to insert a specimen into the holder, measure its thickness at 38 preselected points, remove the specimen from the holder, and use the data collected to calculate an accurate, harmonic mean thickness for the specimen. This procedure was repeated for each specimen just before it was to be submitted to each permeability and pore size distribution study in a series testing procedure.

The apparatus used to obtain flow rate-pressure drop data as a function of mean pressure is sketched diagrammatically in Fig. 11. This device was designed to collect data at pressures either above or below one atmosphere, and operated in the following manner:

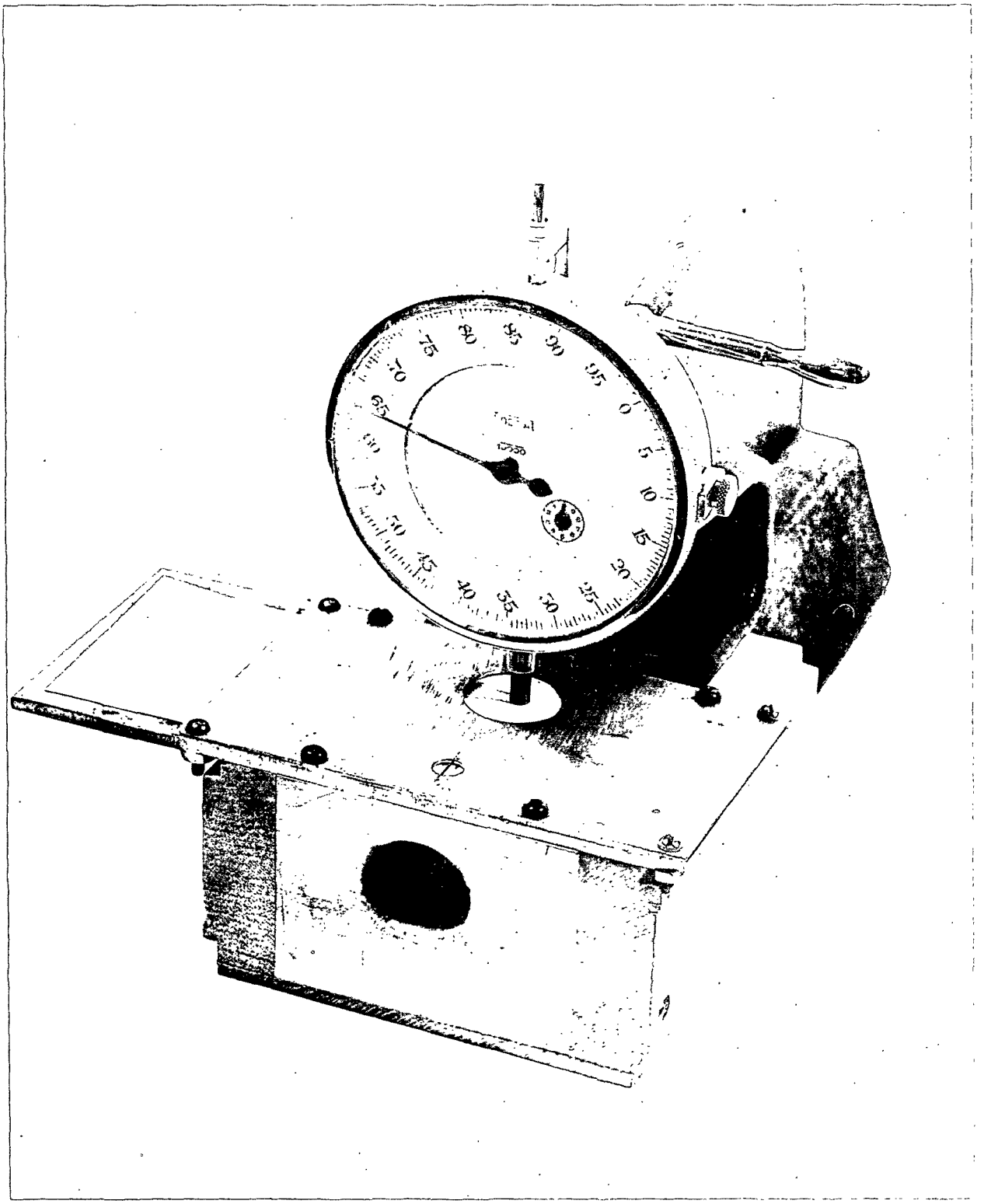

Figure 10. Federal Gage and Specimen Holder

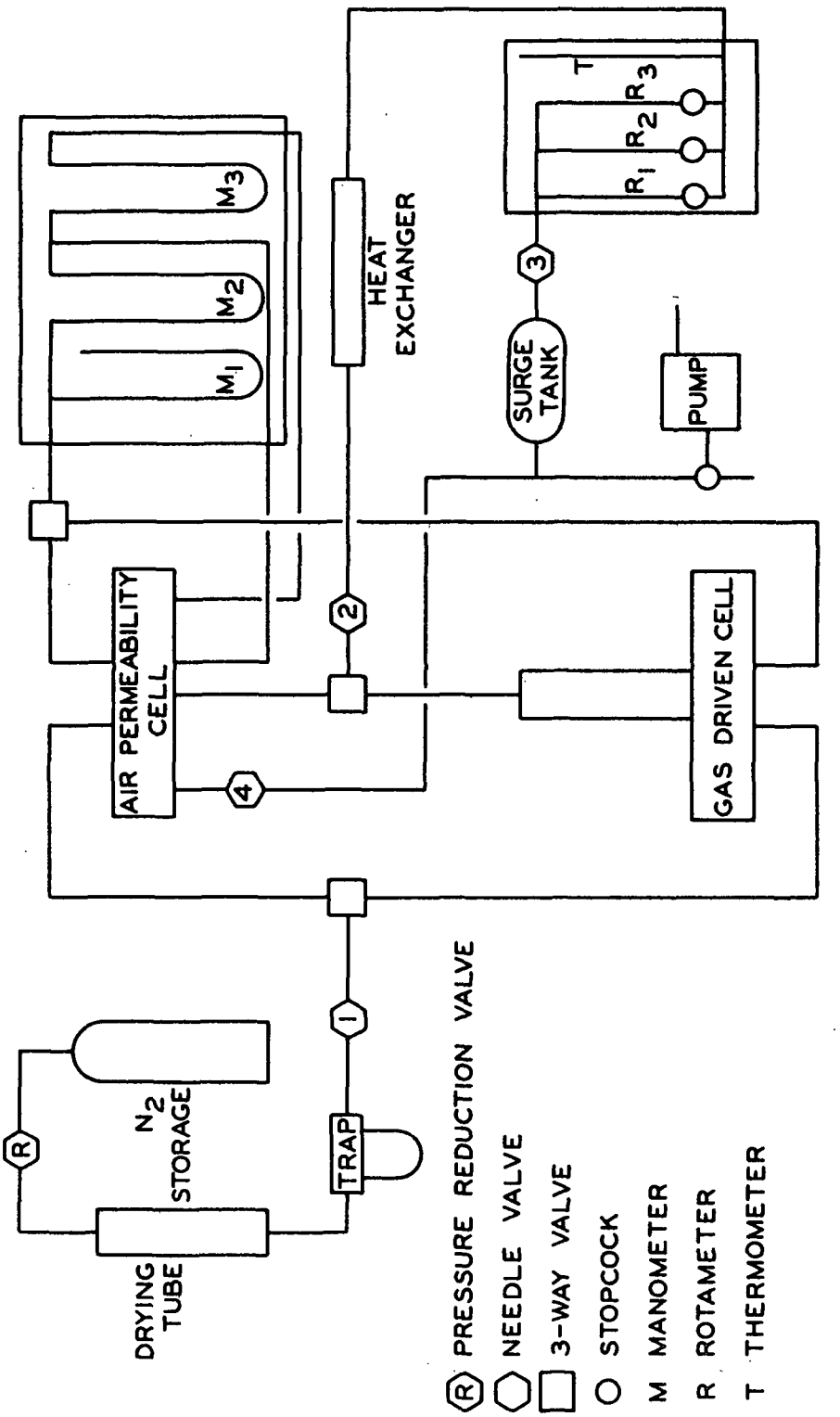

Figure 11. Sketch of Flow Rate-Pressure Drop Apparatus

1. Water-pumped nitrogen was released from a storage tank and bled across an Airco 8456, two-stage pressure-reduction valve into a drying tube--three feet of 3-inch diameter black iron pipe capped at each end--filled with Davidson Pa-400 refrigeration-grade silica gel.
2. After escaping from the drying tube, the dry nitrogen passed through a Norgren 30-AE filter trap and reached a Hoke needle valve (1) where its pressure was reduced to the desired level and it was introduced into the top of the permeability test cell shown in Fig. 12 and 13.
3. After passing through the specimen and escaping from the permeability test cell, the gas passed through another Hoke needle valve (2)[1] and a finned, copper-tubing heat exchanger before reaching a complex which contained an 18-inch mercury thermometer (0-50°C.) and three Fisher-Porter triflat rotameters mounted in parallel.
4. In this complex, the temperature and flow rate of the nitrogen were measured and then it passed through still another Hoke needle valve (3)[1] and into a surge tank from which it either escaped or was pumped to the atmosphere by a Duo-Seal vacuum pump[2].

---

[1]Either needle valve (2) or (3) could be used to control the flow rate through the permeability apparatus. Valve (2) was used when data were being gathered at pressures greater than one atmosphere while valve (3) was used when the equipment was being operated at a vacuum.

[2]The Duo-Seal pump was used only when the apparatus was being operated under a vacuum.

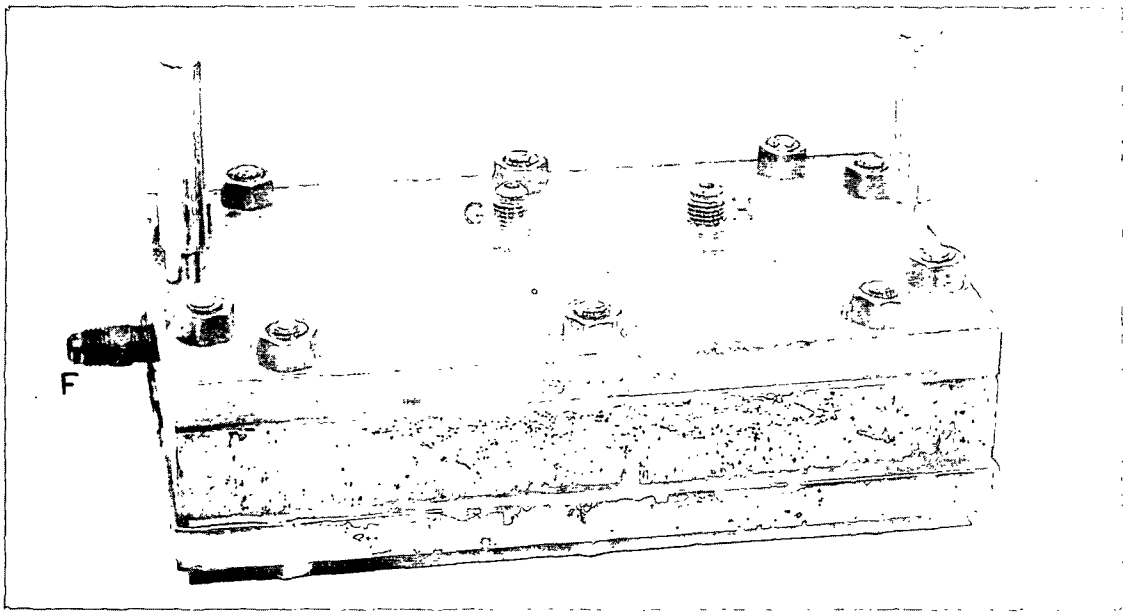

Figure 12. Permeability Test Cell Closed

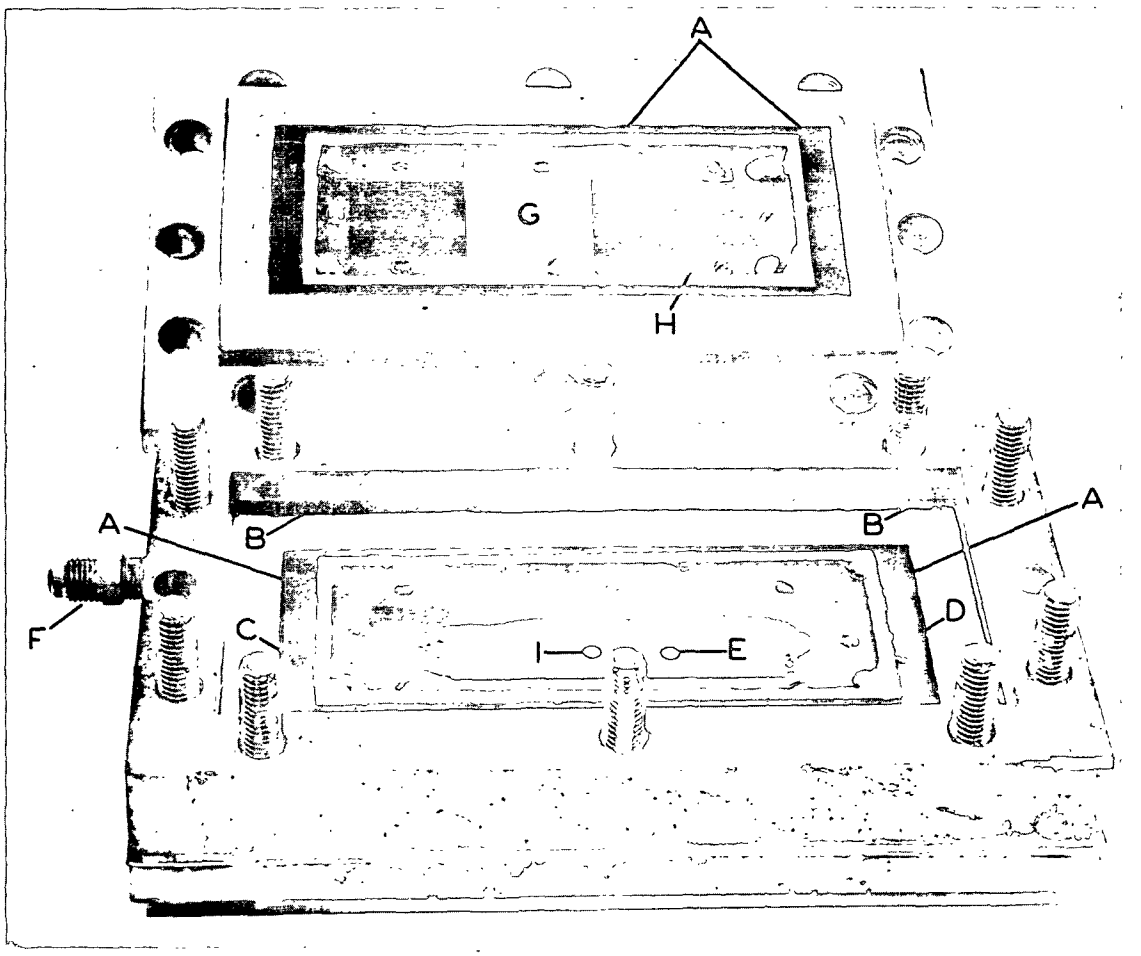

Figure 13. Permeability Test Cell Open

Photographs of the permeability test cell used in this study are presented in Fig. 12 and 13. It will be seen that the cell was equipped with two guard rings. The inner guard ring (A) was used to isolate a specimen during testing so that precise flow rate-pressure drop data could be gathered without fear of complications due to edge effects. This guard ring was equipped with two taps--a bleeder tap (C) and a manometer tap (D). The bleeder tap (C) was used to control the pressure within the guard ring (A). The manometer tap (D) was connected to another manometer tap (E) in the bottom plate by an octoil-s filled Meriam U-type manometer which was used to make sure that the pressures in the guard ring (A) and on the downstream side of the specimen were equivalent. The only function of the outer guard ring (B), which was connected to the entering gas line by an inlet tap (F), was to maintain the pressure drop between the two guard rings at a low level so that leaks between them would be minimized.

The top plate of the permeability test cell contained two taps--a baffled inlet tap (G) and a manometer tap (H). The inlet tap (G) served to introduce the permeating gas into the cell from which it escaped by way of an outlet tap (I). The manometer tap (H) was connected to two manometers. One of these was used to measure the pressure drop across a specimen during permeation, while the other was used to measure the gage pressure at the manometer tap (H). The manometer used to measure the pressure drop was a slant-mounted, octoil-s filled Meriam U-type manometer. The manometer used to measure the gage pressure was an upright, mercury-filled Meriam U-type manometer.

The experimental technique used to characterize the permeability of specimens during this investigation was as follows:

1. The thickness of a specimen was measured at 38 pre-selected points, using the Federal gage and specimen holder shown in Fig. 10.
2. The specimen was placed in the permeability test cell shown in Fig. 12 and 13, conditioned for four hours by allowing dry nitrogen to pass through it, and then flow rate-pressure drop measurements were made at a number of mean pressures ranging from 1.6 to 0.3 bars.
3. When sufficient flow rate-pressure drop data had been obtained, the specimen was removed from the test cell and stored in a humidity room to await future testing.
4. Finally, the thickness and flow rate-pressure drop data were used to estimate the effect of variations in mean pressure on specimen permeability coefficient, and this information was used to estimate the permeability and slip constants of the specimen.

PORE SIZE DISTRIBUTION PROPERTIES

The measurement of pore size distribution was another technique used to evaluate the effect of deformation on the porous properties of paper. Such data were used to answer two important questions concerning how deformation affected the porous structure of paper. First, they were used to determine whether stress-induced changes in the pore size distribution within a sheet took place; second, they were used to learn how

these alterations in distribution occurred. Both pieces of information were very useful in demonstrating that deformation did alter the inter-fiber structure of paper and in explaining the anomalies in permeability properties caused by stress application.

Although there are several methods for measuring the pore size distribution within a porous medium, it seemed best to use a technique particularly sensitive to large pores--3 to 10 μ--because it was suspected that stress-created pinholes might be responsible for the increase in specimen permeability induced by stress. In this case, the gas drive method was used. This technique has been used by soil scientists for many years (50), but Corte (26) was apparently the first to report its use with paper. The principle used by the technique is that an increase in the pressure drop across a porous medium partially saturated with liquid causes more pores to be drained of liquid. This means that the increased rate of flow that results is caused by two effects. First, there is the effect of the increase in the pressure drop across the medium, and second, the opening up of new flow channels for the non-wetting fluid. This can be stated mathematically as follows:

$$dQ = Q_v dN + Q d\Delta P/\Delta P \tag{7}$$

or

$$dQ/d\Delta P = (Q_v dN/d\Delta P) + Q/\Delta P \tag{8}$$

where Q is the volume flow rate, Q_v the volume flow rate through each pore brought into action, N the number of pores, and ΔP the pressure drop. The capillary pressure equation states that $\Delta P = 2\gamma/R$ if the

contact angle is taken as 0°, where γ and R are surface tension and effective pore radius. Therefore,

$$d\Delta P = -2\gamma dR/R^2 \qquad (9)$$

Now, if Equation (9) is combined with (8) and it is remembered that, for cylindrical pores, $Q_v = \pi R^4 \Delta P/8nL$ where n and L are gas viscosity and pore length, respectively,

$$(dQ/d\Delta P) - (Q/\Delta P) = -(\pi R^6 \Delta P/16\gamma nL)dN/dR \qquad (10)$$

which through the use of the capillary pressure equation may be converted to:

$$dN/dR = -[(\Delta P)^5 nL/4\pi\gamma^5][(dQ/d\Delta P) - (Q/\Delta P)] \qquad (11)$$

The gas drive technique can be used to get an estimate of both the pore size distribution within a specimen and its relative permeability when all pores with a minimum effective radius greater than some arbitrarily chosen value are open.

The apparatus used to gather flow rate-pressure drop data via the gas drive method was exactly the same as that sketched diagrammatically in Fig. 11. A different test eell was used, and only one instead of three manometers was needed, but the method of operation was exactly the same except that needle valve (1) was used to control flow rate and the valves (2) and (3) were kept wide open.

Photographs of the gas drive test cell used in this work are shown in Fig. 14 and 15. The cell was made of Lucite and built in the form of

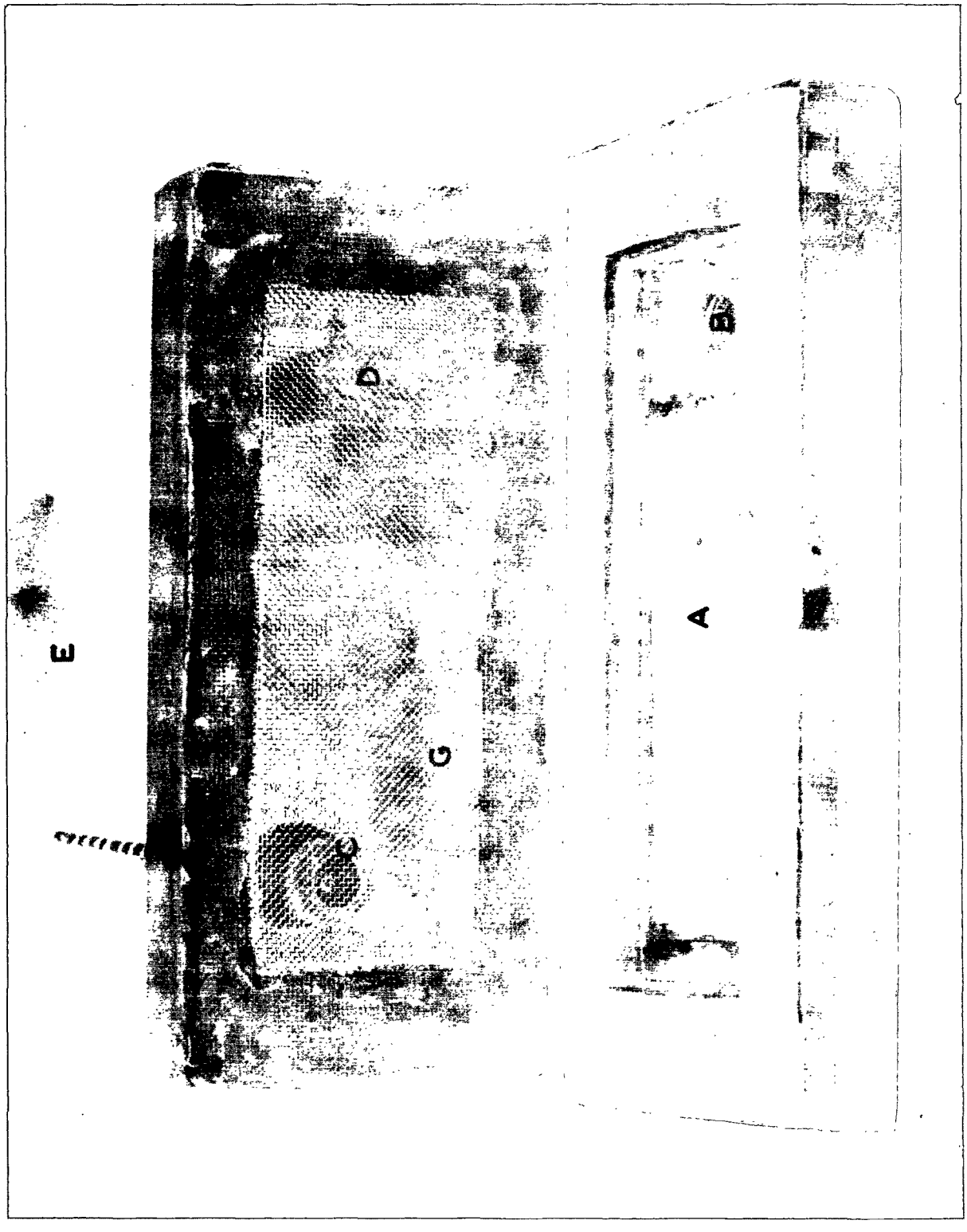

Figure 14. Gas Drive Cell Open

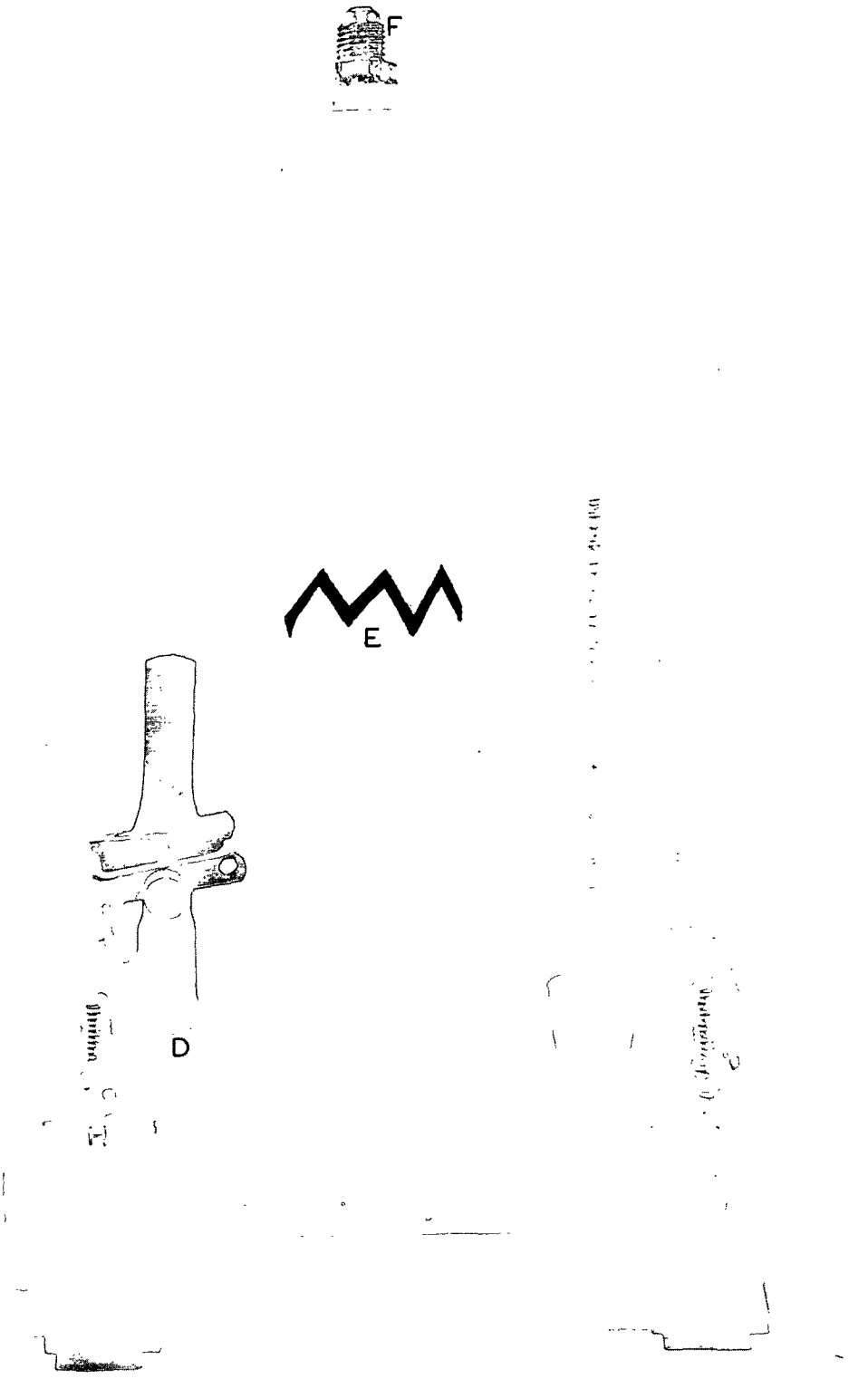

Figure 15. Gas Drive Cell Closed

a rectangle. The bottom half of the cell contained a baffled inlet (A) and a manometer tap (B). The manometer tap (B) was connected to a mercury-filled, Meriam U-type manometer which was used to measure the gage pressure of the gas on the upstream side of a specimen. Several things were attached to the top half of the cell. One of these was a thermometer well (C) through which a 5-inch mercury thermometer (0-150°C.) extended; another was an inlet port (D) through which hexyl alcohol was introduced; a third was a mist column (E)[1] which was used to eliminate liquid entrainment; a fourth was an outlet tap (F) from which the driving gas escaped; and a fifth was a screen (G), which was installed to prevent specimen bowing during gas drive studies. The two halves of the cell were faced with rubber gasketing material and held together by two steel brackets (H and I).

The technique used in carrying out gas drive measurements was quite simple.

1. A specimen of known thickness was clamped in the apparatus and conditioned for four hours by allowing dry nitrogen to pass through it.
2. When a test was to be started, 20 cc. of technical-grade hexyl alcohol were introduced through the inlet port (D) and the break-through pressure[2] was noted.

---

[1]The central section of the mist column has been removed from Fig. 15 (see broken line) so that both the cell and its outlet at the top of the mist column can be shown in the same photograph.

[2]The break-through pressure of a porous medium is equal to the pressure drop at which gas first starts to flow through a saturated bed of the material.

3. Needle valve (1) was used to vary the flow rate of dry nitrogen and flow rate-pressure drop data were gathered over a rather large range of volume flow rates--0 to 100 cc./sec.
4. When the gas drive experiment had been completed, the specimen was removed from the test cell, excess hexyl alcohol was blotted off, and the final traces of alcohol were removed by vacuum before the specimen was set aside for future use.
5. Finally, the raw flow rate-pressure drop data were used to estimate the pore size distribution within the specimen through the use of Equation (11), and relative permeabilities were calculated at a number of arbitrarily chosen minimum effective pore radii.

PRESENTATION OF DATA AND DISCUSSION OF RESULTS

MECHANICAL PROPERTIES

The first step taken in studying the mechanisms by which paper responds to stress was to characterize the mechanical properties of the material studied. This was done by obtaining stress-strain and creep-recovery data[1].

Stress-strain curves for three of the specimens used during the investigation are presented in Fig. 16[2]. These curves show the typical stress-strain response (50-A-2-3-1) as well as the maximum variability in stress-strain response (50-A-5-1-2 and 50-A-4-3-1) to be expected from the specimens. Figure 16 also demonstrates that all three specimens showed a marked yield zone typical of sheets dried under very little restraint.

The specimen-to-specimen variations in mechanical properties shown by Fig. 16 are difficult to explain because considerable care was taken in preparing the handsheets from which the specimens were obtained. It has already been mentioned that all handsheets were dried by pressing

---

[1] All of the stresses reported in this dissertation are expressed in terms of unit cross-sectional area of cellulose. They were calculated through the use of the expression:

$$\text{Stress} = \frac{(\text{Tensile Load})}{(\text{Specimen Weight})/(\text{Density of Fiber})(\text{Specimen Length})}$$

where the density of the fiber was assumed to be 1.55 g./cc.

[2] The data presented in Fig. 16 were collected with an Instron tensile tester using IPC line contact clamps (51).

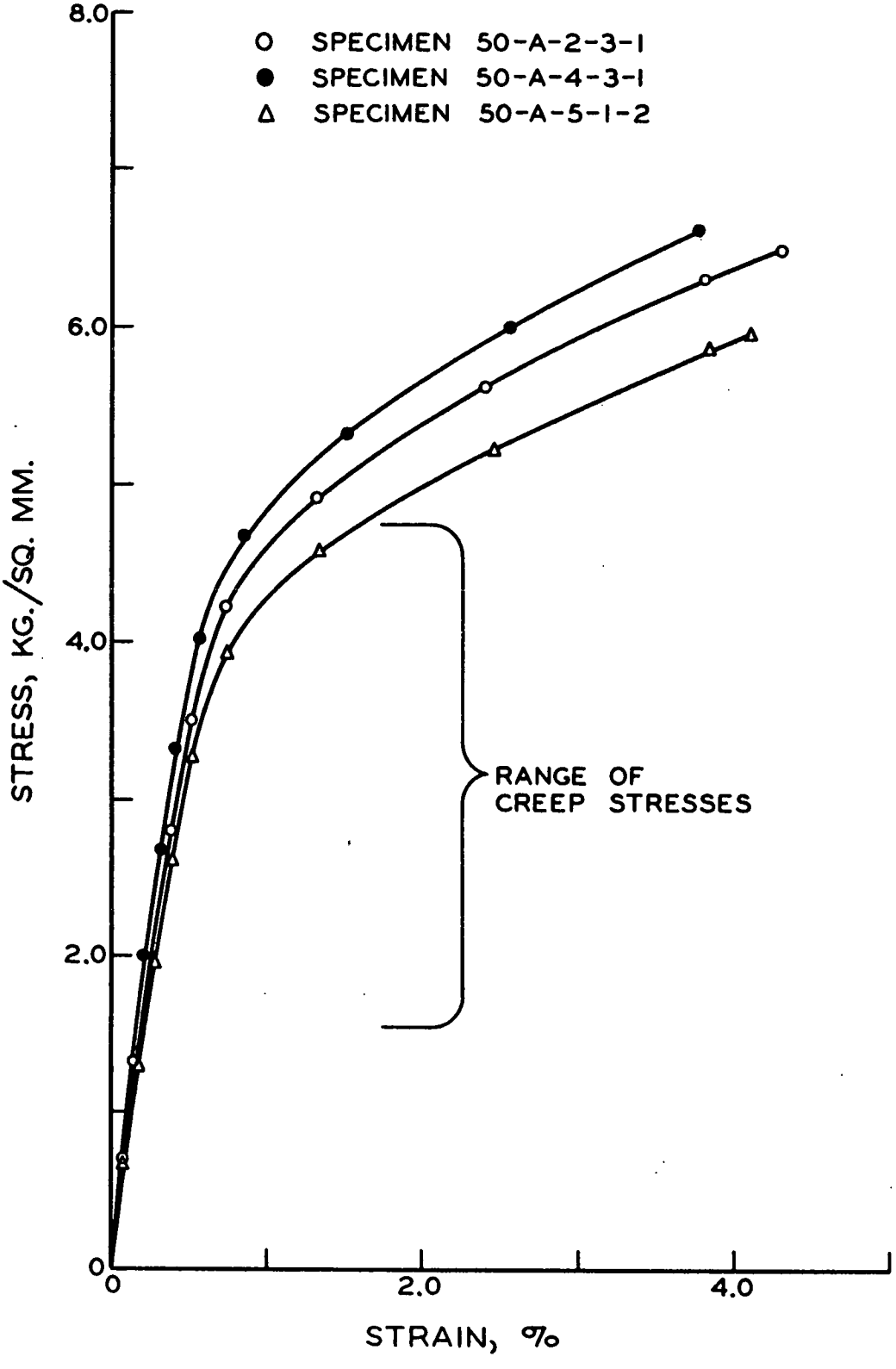

Figure 16. Typical Stress-Strain Curves

them between couch and cover blotters which had previously been sprayed with clear lacquer. These blotters curled badly when wet with water because the lacquer on their surfaces prevented expansion and contraction due to changes in moisture content. Consequently, variations in the coat weight of lacquer probably caused different blotters to respond differently to changes in moisture content. The result was that each handsheet was dried under different conditions of restraint, and this probably caused the differences in mechanical properties observed. Fortunately, these differences in conditions of restraint had no appreciable effect upon the mechanisms by which the specimens responded to stress.

Although stress-strain data were collected during this investigation the mechanical properties of specimens were usually characterized through the use of the creep-recovery technique. First-creep curves for a number of specimens used to study the effect of creep deformation on the scattering coefficient of specimens are presented in Fig. 17*. These curves were used to construct the master-creep curve shown in Fig. 18 which shows that the specimens studied conform well with a master-creep curve concept (16, 17, 52). The shifts in $\log_{10}$(time) required to form the master curve are presented in Table I. These shifts were found to be linearly related to the applied stress with a time shift of 2.34 decades/(kg./sq.mm.)required to bring about coincidence.

Figure 19 presents the first-recovery curves for the specimens from which the first-creep data just discussed were obtained. These curves

*The creep and creep-recovery data used to construct Fig. 17 through 20 are recorded in Appendix II.

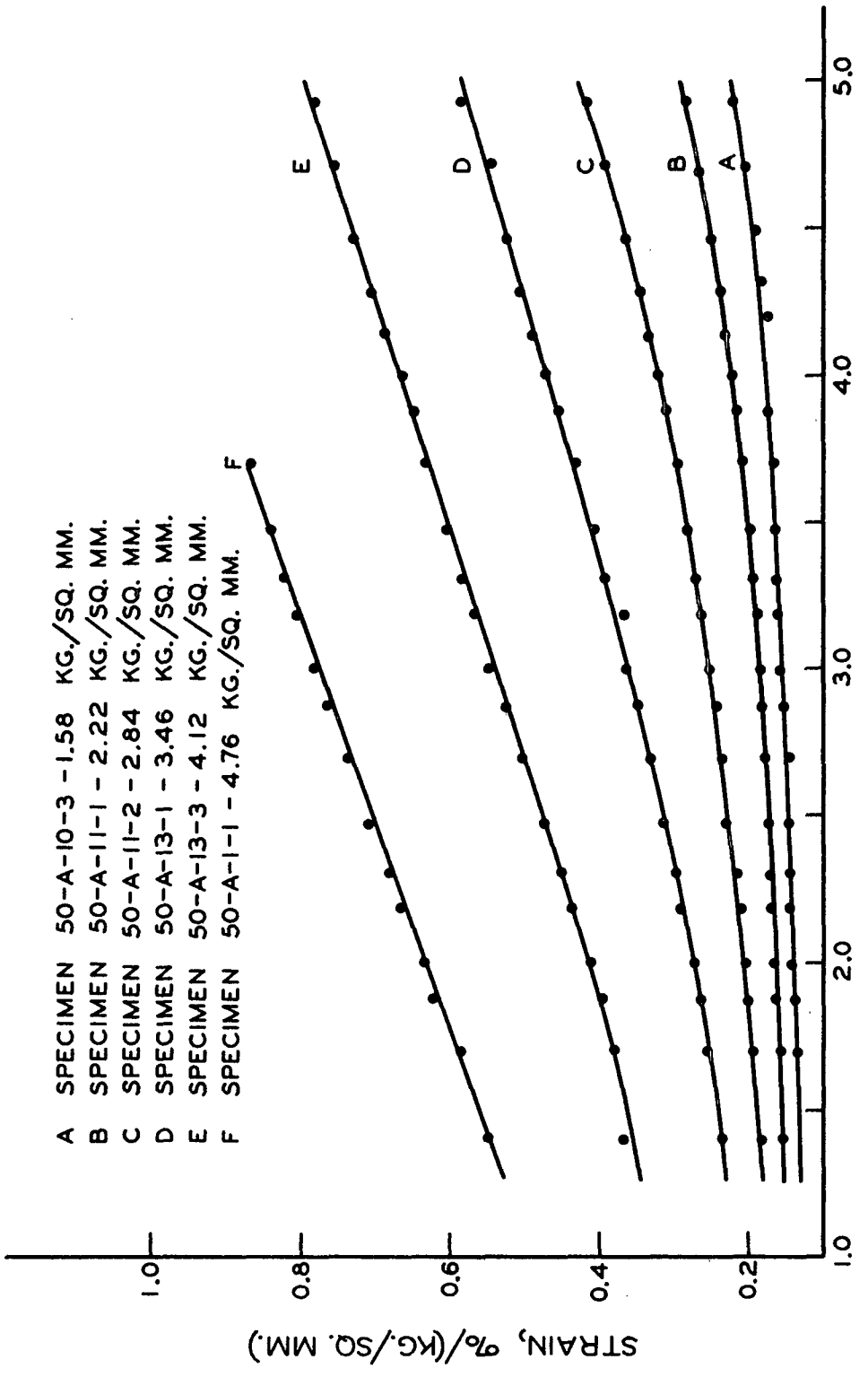

Figure 17. First-Creep Curves for Samples Used in Light-Scattering Studies

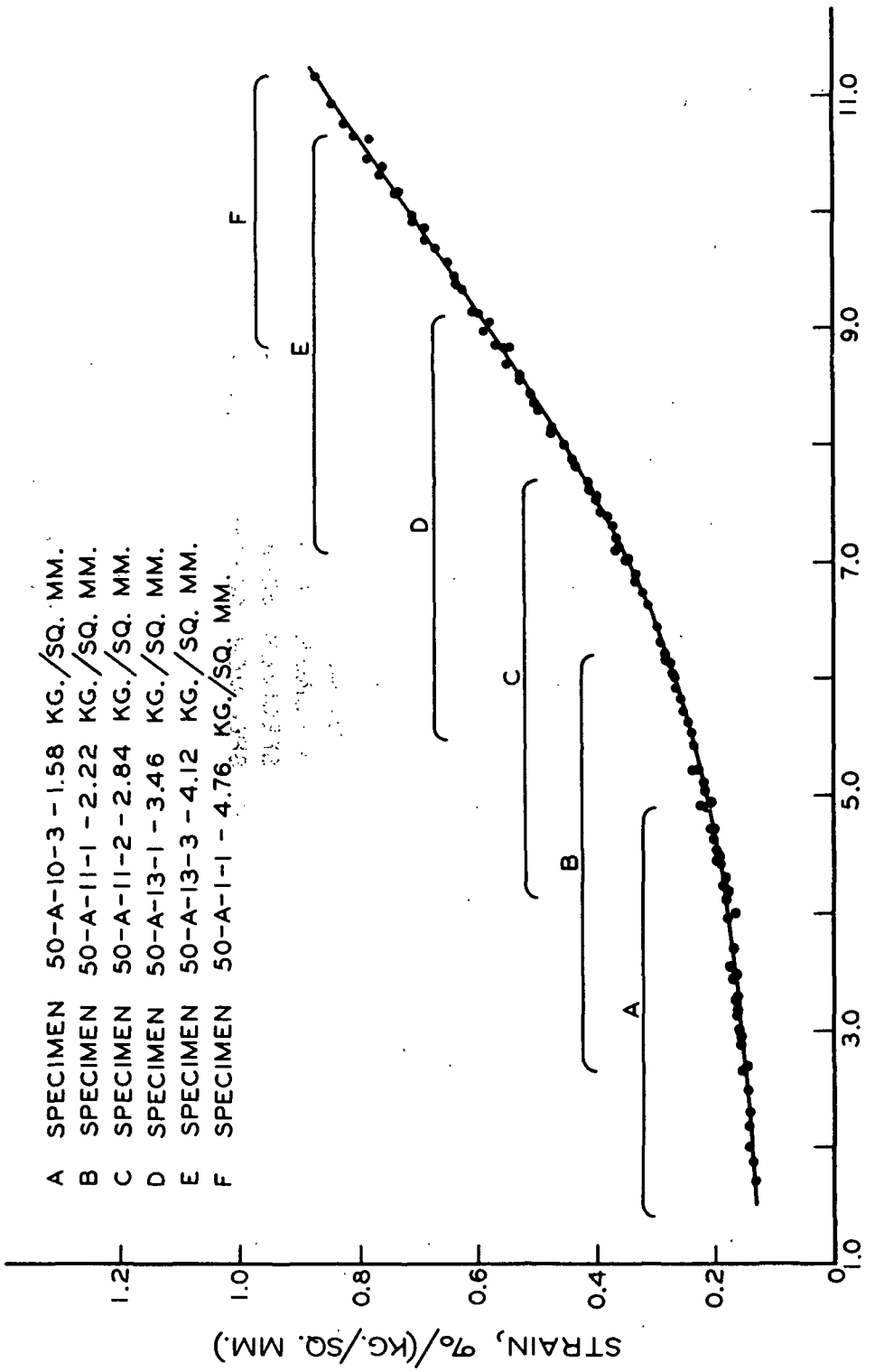

Figure 18. Master-Creep Curve for Samples Used in Light-Scattering Studies

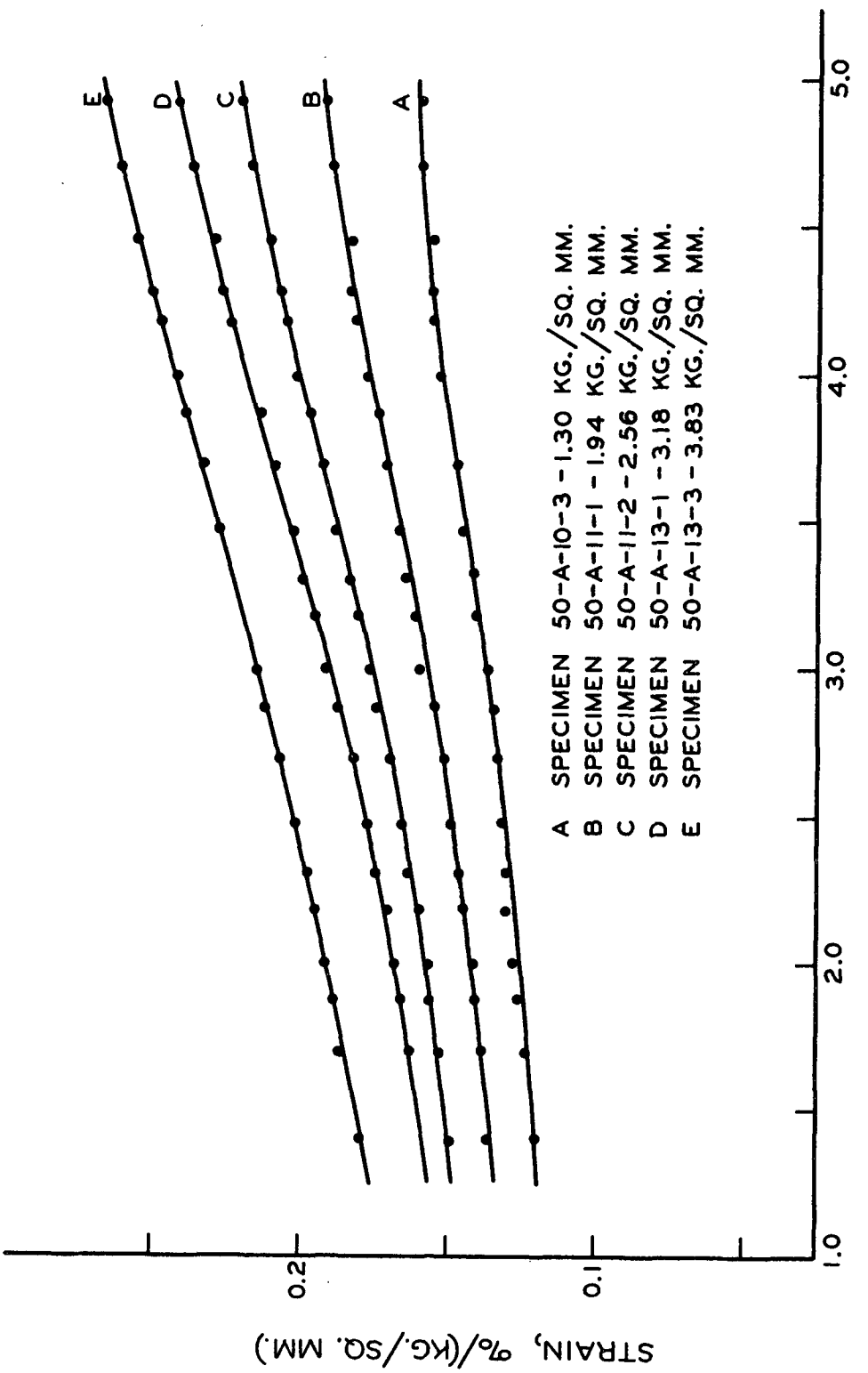

Figure 19. First-Recovery Curves for Samples Used in Light-Scattering Studies

TABLE I

TIME SHIFTS REQUIRED TO CONSTRUCT MASTER-CREEP CURVE

Specimen	Applied Stress, kg./sq.mm.	Time Shift, decades of $\log_{10}$(time)
50-A-10-3	1.58	0.00
50-A-11-1	2.22	1.25
50-A-11-2	2.84	2.75
50-A-13-1	3.46	4.14
50-A-13-3	4.12	5.70
50-A-1-1	4.76	7.47

were used to construct the master-recovery curve shown in Fig. 20, which shows that the recovery data appear to conform to a master curve concept. The time shifts required to attain coincidence are presented in Table II. These time shifts were linearly related to the stress removed at the start of the recovery tests, and it was found that a time shift of 1.66 decades/(kg./sq.mm.) was required to construct the master curve.

TABLE II

TIME SHIFTS REQUIRED TO CONSTRUCT MASTER-RECOVERY CURVE

Specimen	Applied Stress, kg./sq.mm.	Time Shift,[a] decades of $\log_{10}$(time)
50-A-10-3	1.30	0.00
50-A-11-1	1.94	1.22
50-A-11-2	2.56	2.34
50-A-13-1	3.18	3.13
50-A-13-3	3.83	4.41

[a]Each specimen supported the weight of its bottom clamp (2.47 lb.) throughout these recovery tests.

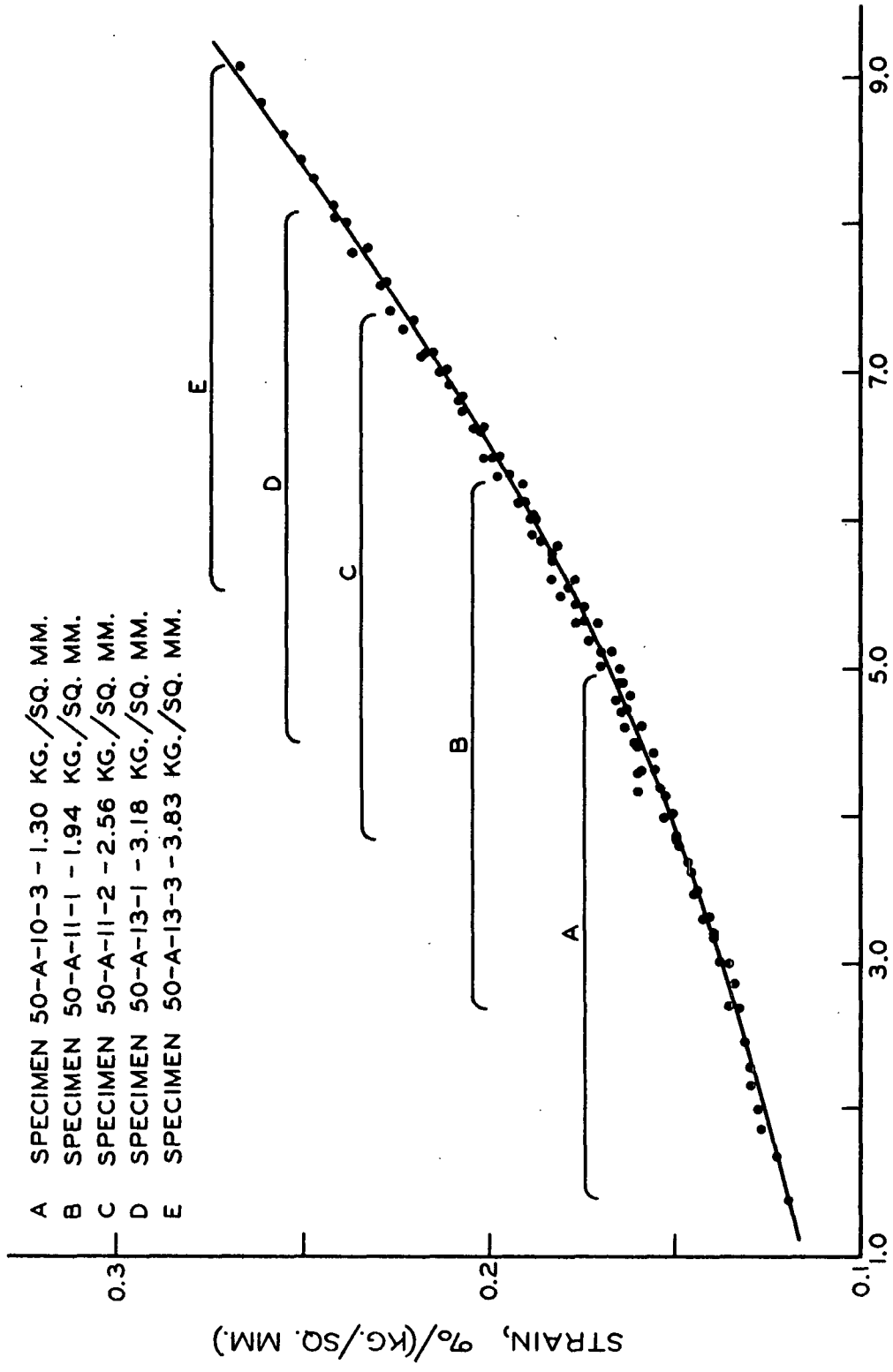

Figure 20. Master-Recovery Curve for Samples Used in Light-Scattering Studies

A comparison of Fig. 19 and 20 shows that all first-recovery curves had a sigmoidal shape whereas the master curve did not. This means that complete coincidence on the master curve was not achieved because each recovery curve tended to fall below it at high recovery times (10,000 to 86,400 seconds).

One possible explanation for this type of behavior is that compliance with a master curve concept was forced by the mathematical manipulations made in constructing the master curve. This is rather unlikely because no such phenomenon has ever been observed in any of the other instances in which the master curve concept was employed (16, 17, 33, 52).

Another and perhaps more plausible explanation is based on the assumption that an interfiber resistance to contraction develops during recovery. It is hypothesized that the cause of the increase in resistance is an increase in the magnitude of interfiber frictional effects during recovery. The result is that although recovery is induced by mechanisms compatible with a master curve concept (intrafiber contraction by molecular processes), the rate of response is decreased by an increase in interfiber frictional resistance which develops as a result of processes not in harmony with a master curve concept.

One of the most important objectives of this investigation was to determine the amount of energy irreversibly lost during creep-recovery cycles. In Appendix I it is demonstrated that this energy loss is proportional to the area enclosed by the load, creep, and deload curves

on a load-extension diagram of a creep-recovery cycle. Data obtained from both the load and deload portions of creep-recovery and stress-strain cycles are presented in Table III. These and other data not reported demonstrate that the load and deload curves (on a load-extension plot) of both types of cycle are essentially the same provided that the loading (not the time) schedules are identical. This was fortunate for it meant that the running of a few stress-strain curves allowed all of the data collected with the creep testers designed according to Brezinski (16, 17)[1] to be used in assessing the energy loss during creep-recovery cycles.

Figure 21 contains a plot of energy loss versus irreversible deformation[2] for a number of 48-hour creep-recovery cycles. The data were obtained through the use of 24-hour creep and 24-hour recovery tests carried out according to the parallel testing procedures. From Fig. 21 it can be seen that the energy loss per unit increase in irreversible deformation increased as the amount of deformation suffered by a specimen increased. This is a very important observation, as will be demonstrated later.

---

[1] The creep testers designed according to Brezinski were constructed in such a way that no estimate of the load and deload behavior of specimens could be obtained. Therefore, load and deload data had to be obtained from another source if energy loss estimates were to be made (see Appendix I).

[2] The irreversible deformation suffered by a specimen during a creep-recovery cycle was estimated by subtracting the total amount of recovery during the cycle from the total amount of creep.

TABLE III

COMPARISON OF STRESS-STRAIN AND CREEP-RECOVERY CYCLES

Stress-Strain Cycle[a]			Creep-Recovery Cycle[b]		
Load[c], kg.	Deformation, % Loading	Deloading	Load[c], kg.	Loading	Deloading
0.00	0.00	0.56	0.00	0.00	0.56
1.13	0.09	0.51	1.13	0.09	0.50
2.27	0.19	0.38	2.27	0.19	0.37
3.40	0.29	0.26	3.40	0.30	0.26
4.54	0.42	0.16	4.54	0.41	0.16
5.67	0.54	0.05	5.67	0.54	0.05
6.35	0.74	0.00	6.35	0.74	0.00

[a]The stress-strain cycle was run on an Instron tensile tester (51) at a strain rate of 2.54 cm./min. using IPC line contact clamps and a gage length of 12.70 cm.

[b]The creep-recovery cycle was run on the IPC load-elongation tester (39) with loading and deloading carried out at a strain rate of 2.54 cm./min. IPC line contact clamps and a gage length of 12.70 cm. were used in the test.

[c]Both specimens were 2.54 cm. wide and were prepared from a specimen typical of those used throughout the work. Specimen 50-A-4-3-2 was used in the stress-strain study while specimen 50-A-4-3-1 was used in the creep-recovery test.

OPTICAL PROPERTIES

One portion of this investigation involved a study of stress-induced changes in the scattering coefficient of paper. The objective of this work was to learn more about the effect of stress on the optically apparent exposed surface of a sheet. The first step taken in the study was to use the technique recommended by Ingmanson and Thode (53)

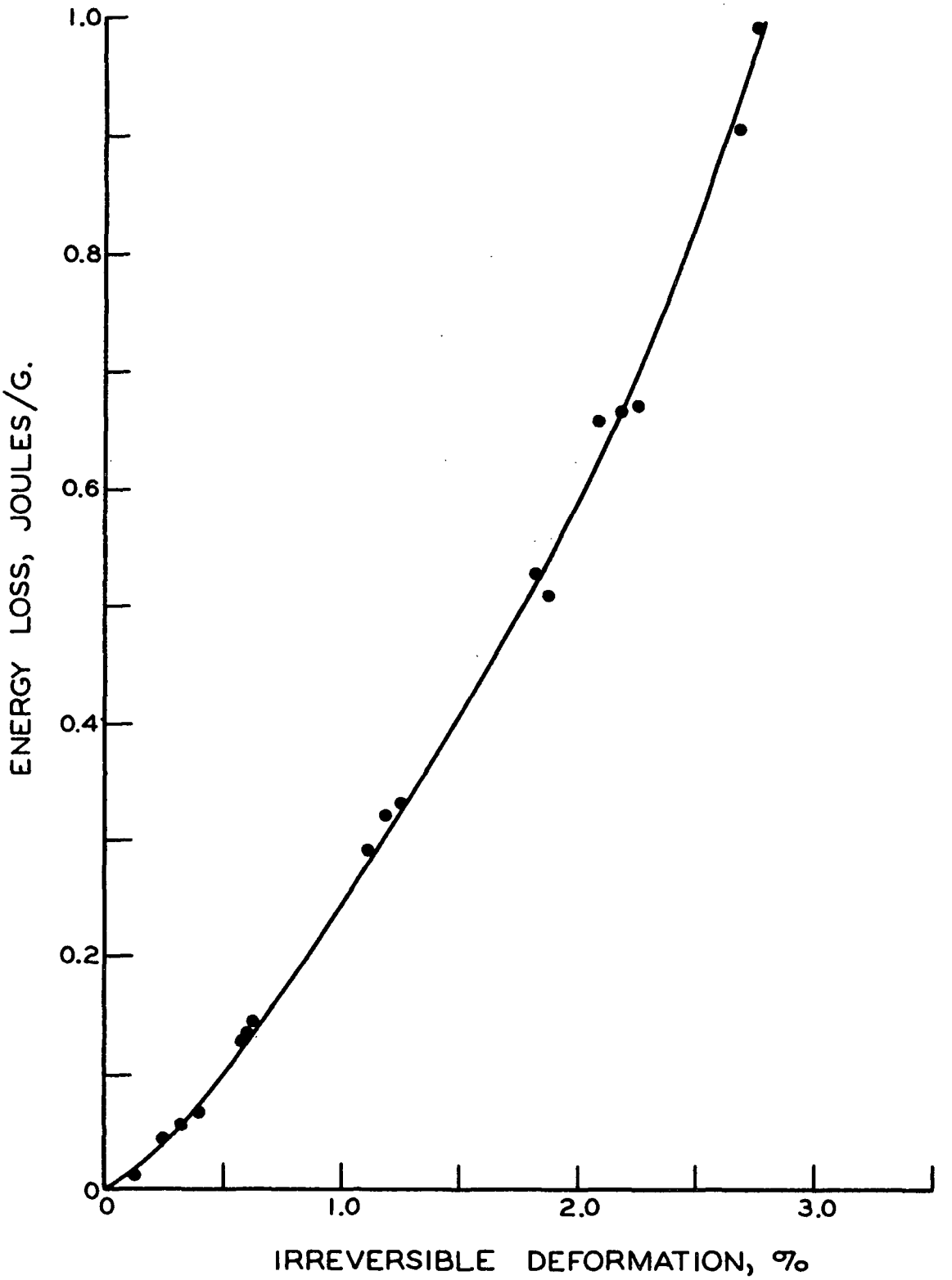

Figure 21. Energy Loss Versus Irreversible Deformation

to estimate the scattering coefficient of a water-dried, unbonded handsheet. A number of handsheets were formed, their dry-strengths were varied by wet pressing, and their tensile strengths and scattering coefficient were measured. The data obtained were used to construct a plot of scattering coefficient versus tensile strength which extrapolated to a scattering coefficient of 280 sq.cm./g. at zero tensile strength*. This figure was taken as being equivalent to the scattering coefficient of a water-dried, unbonded handsheet, and was used to calculate all of the changes in optically apparent exposed surface reported below through the use of the expression, $\Delta B_a = -\Delta s/s_{ub}$, where ΔB_a is the change in relative bonded area, Δs is the change in scattering coefficient, and s_{ub} is the scattering coefficient of a water-dried, unbonded sheet.

The second step taken in the study of stress-induced changes in optical properties was to use a parallel testing procedure to determine the magnitude of the changes in scattering coefficient that could be induced by stress. Forty-eight-hour creep-recovery cycles were used to induce the changes; the data obtained are presented in Table IV and Fig. 22 and 23.

Figure 22 shows that a linear relation between change in specimen relative bonded area and irreversible deformation (extrapolating to a slight positive intercept on the irreversible deformation axis) was found to exist. Such a relation is consistent with data previously reported

*This method of estimating the scattering coefficient of a water-dried, unbonded sheet is of dubious accuracy, but it was adequate for the present purposes because relative rather than absolute changes in optically apparent exposed surface were of interest.

TABLE IV

THE EFFECT OF DEFORMATION ON OPTICAL SCATTERING COEFFICIENT

Specimen	Applied Stress, kg./sq.mm.	Irreversible Deformation[a], %	Energy Loss[a], joules/g.	Change in Scattering Coefficient, sq.cm./g.	Change in Relative Bonded Area, %[b]
50-A-7-2	0.00	0.00	0.000	0.13	0.05
50-A-7-3	2.24	0.33	0.057	2.63	0.94
50-A-8-1	2.85	0.58	0.129	5.15	1.84
50-A-9-1	3.46	1.12	0.292	14.78	5.28
50-A-10-1	3.80	1.88	0.519	20.78	7.42
50-A-12-1	4.09	2.25	0.671	26.33	9.40
50-A-13-2	4.61	3.22	1.193	35.71	12.75
50-A-11-1	2.22	0.26	0.069	1.69	1.18
50-A-11-2	2.84	0.62	0.137	5.82	2.08
50-A-13-1	3.46	1.27	0.330	11.68	4.17
50-A-13-3	4.12	2.19	0.666	24.11	8.61
50-A-1-1	4.76	2.76	0.992	32.37	11.56
50-A-12-3	2.23	0.41	0.045	3.30	0.60
50-A-14-2	2.83	0.63	0.143	5.23	1.87
50-A-11-3	3.48	1.19	0.322	13.06	4.66
50-A-10-2	3.82	1.82	0.528	19.56	6.98
50-A-8-3	4.09	2.09	0.657	23.25	8.30
50-A-8-2	4.46	2.68	0.906	29.64	10.58

[a] The creep and recovery data for the cycles used during this study are summarized in Appendix B. Each cycle covered 48 hours with equal amounts of time (24 hours) being allowed for creep and for recovery.

[b] The change in relative bonded area was calculated through the use of the expression, $\Delta B_a = -\Delta s / s_{ub}$, where ΔB_a is the change in relative bonded area, Δs is the change in scattering coefficient, and s_{ub} the scattering coefficient of a water-dried but unbonded sheet.

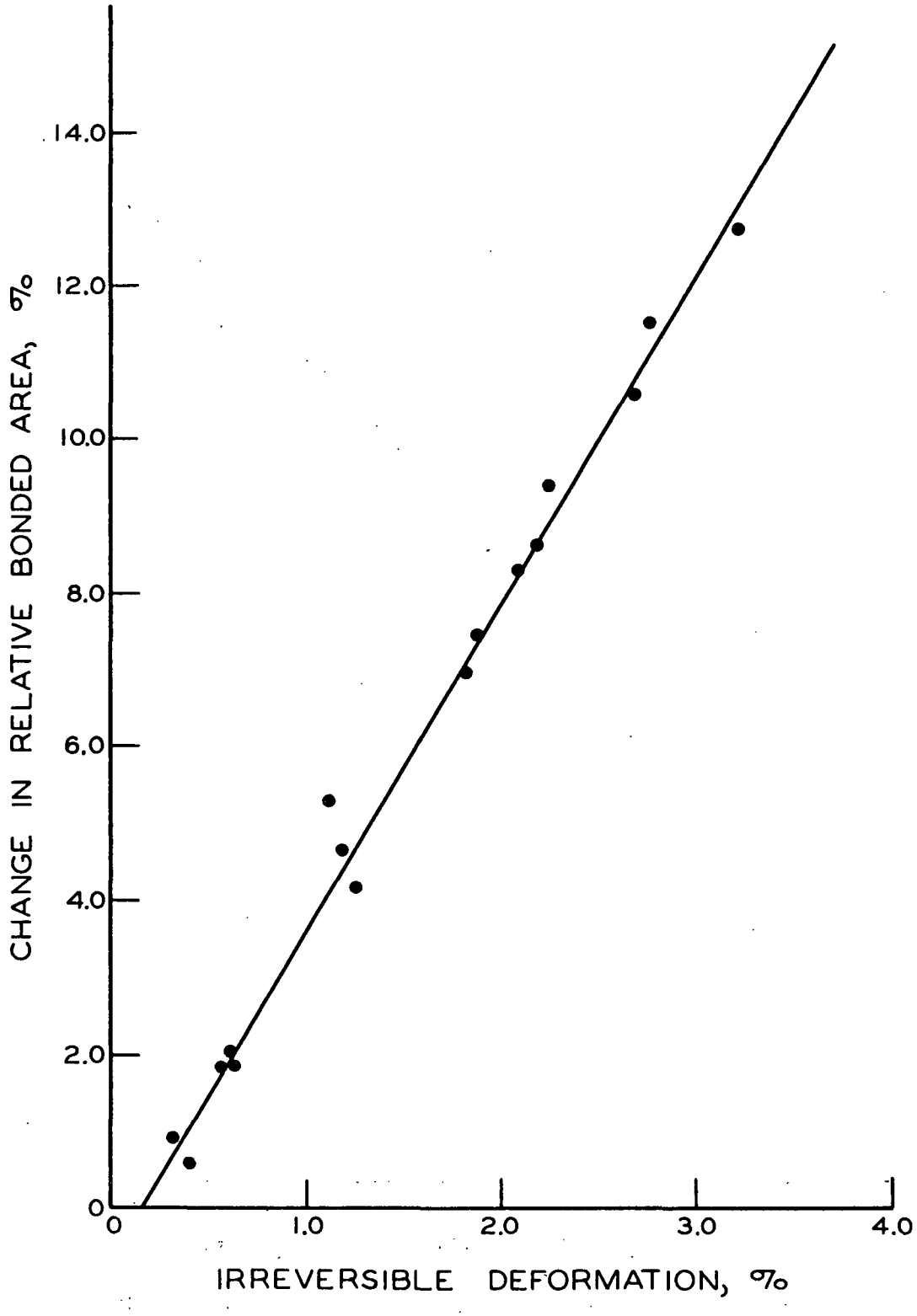

Figure 22. Change in Relative Bonded Area Versus Irreversible Deformation

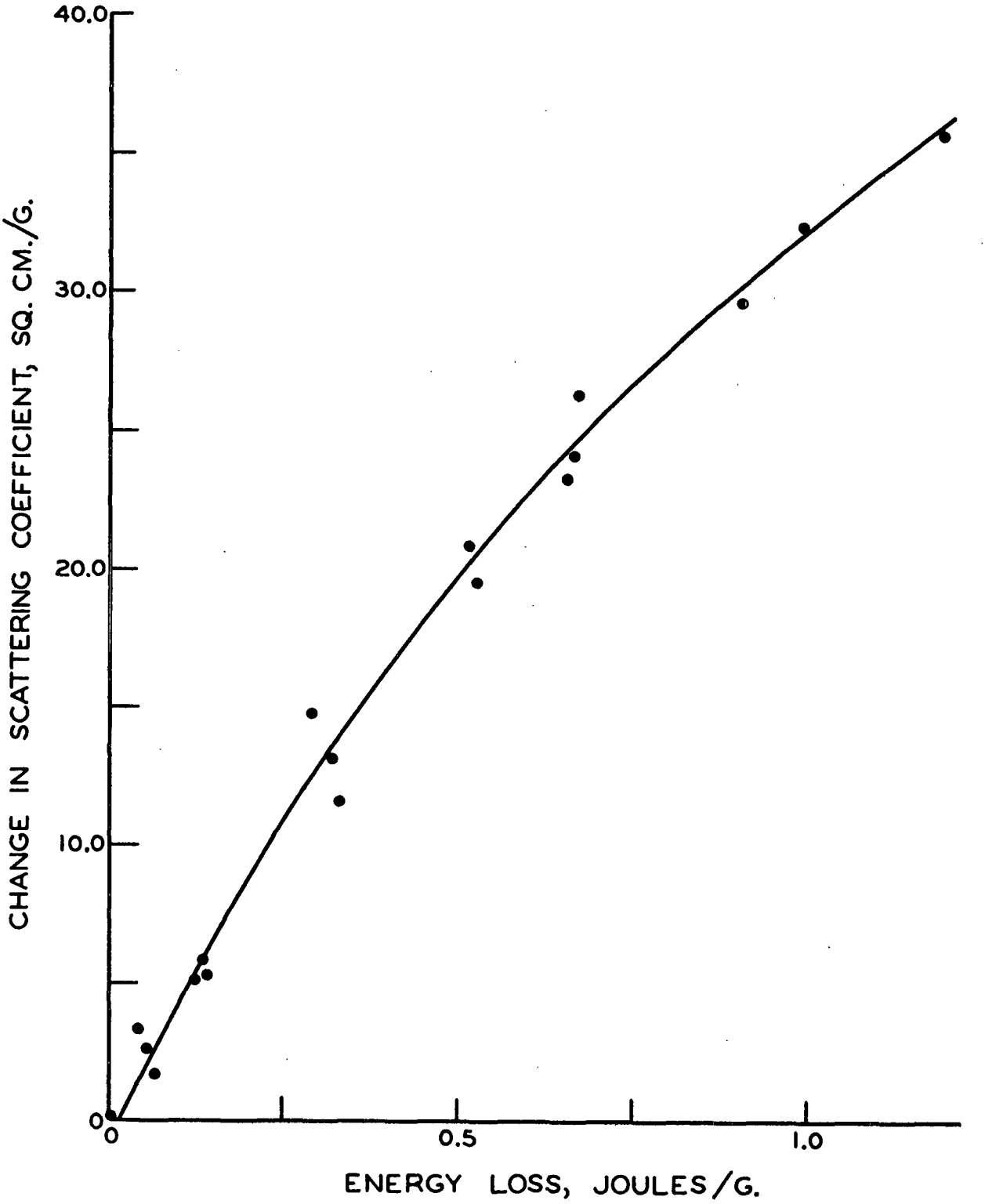

Figure 23. Change in Scattering Coefficient Versus Energy Loss

by Nordman, et al. (18-21)*. This means that the linearity of the interrelation between relative bonded area and irreversible deformation is probably not affected by the duration of a test. An interesting possibility (not checked during this work) is that the fracture of unit area of interfiber bonds may produce an irreversible deformation which is independent of the stress applied or the duration of testing.

A plot of change in scattering coefficient versus energy loss is presented in Fig. 23. The data in this plot do not agree with results previously reported by Nordman, et al. (18-21). Using short-term, mechanical tests, Nordman, et al. found a linear relation between change in scattering coefficient (or relative bonded area) and energy loss. In the present case it can be seen that the amount of energy associated with unit change in scattering coefficient (or relative bonded area) increased as the amount of irreversible deformation suffered by a specimen increased. The reason for the difference between these data and those reported by Nordman, et al. is rather difficult to determine.

If it is assumed (with Nordman, et al.) that all of the energy lost during deformation is consumed in breaking interfiber bonds, then it must be concluded that the increase in slope (of an energy loss versus change in scattering coefficient plot) is the result of an increase in either the number or strength of the interfiber bonds being broken to create unit area of fresh optically apparent exposed surface. The

*Andersson (23) has pointed out that linear plots of change in scattering coefficient (or relative bonded area) versus irreversible deformation can be derived from data collected by Nordman, et al. during short-term, stress-strain experiments.

weakness of this argument is that it is difficult to see why the specimens studied during this investigation should show an increase in either bond strength or number of bonds per unit area with irreversible deformation while the specimens studied by Nordman, et al. did not.

A more plausible explanation for the behavior observed is based on the observation that the interrelation between change in scattering coefficient (or relative bonded area) and energy loss is affected by variations in the duration of mechanical loading. This suggests that the interrelation is affected by long-term, viscoelastic effects. It seems unlikely that interfiber bonds can exhibit any great amount of viscoelasticity [e.g., Page and Tydeman (25) have observed that interfiber bonds never seem to reform after being severed]. It does seem logical, however, to hypothesize that appreciable amounts of energy are consumed in deforming the fiber elements within a sheet during deformation and that the change in slope noted in Fig. 23 (but not in the results reported by Nordman, et al.) is the result of an increase in the amount of energy absorbed by long-term, intrafiber creep.

The technique of estimating "bond strength" suggested by Nordman, et al. is based on the assumption that all the energy consumed by a sheet during deformation goes into the fracture of interfiber bonds and the creation of optically apparent exposed surface. If the hypothesis outlined in the preceding paragraph is correct, energy is also consumed in deforming fiber elements during straining. This would mean that the energy-absorbing capacity or "bond strength" of interfiber bonds could not be estimated from light scattering-energy loss data because an

indeterminate part of the energy loss would have been consumed in deforming fiber elements.

POROUS PROPERTIES

Another important objective of this investigation was to determine the effect of deformation on the porous properties of paper. Two techniques were used--the air permeability and the gas drive method. Before data collected with either of these methods could be evaluated, accurate estimates of specimen thickness had to be obtained. There are a number of techniques for measuring the thickness of paper--the electrical capacitance method, the mercury displacement method, etc.; but practical considerations (a lack of knowledge about the effect of structural changes on dielectric constant, etc.) led to the choice of a calipering technique using a Federal gage (48) to measure specimen thickness. Caliper measurements were made at an arbitrarily chosen platen pressure of 6.4 lb/sq.in. which was the lightest load at which measurements could be made with the Federal gage*.

The thickness data obtained on three typical specimens are presented in Table V and show that small amounts of deformation caused a rapid decrease in specimen thickness to a constant value. Careful analysis of these data led to the conclusion that the decrease in thickness was not due to specimen contraction in the z direction. It was hypothesized that

*It was decided that the thickness could be measured under these conditions despite the fact that the pressure was much greater than that encountered during permeation because experimental data showed that all specimens suffered similar changes in apparent thickness when platen pressure was varied.

TABLE V

THE EFFECT OF DEFORMATION ON SPECIMEN THICKNESS

Specimen 50-A-2-1

Applied stress, kg./sq.mm.	0.00	2.23	2.87	3.50	3.50	3.50	3.82
Irreversible deformation, %	0.00	0.25	0.73	1.56	2.00	2.42	3.00
Thickness, 10^{-3} cm.	14.7	14.4	14.2	13.8	13.8	13.8	13.8[a]

Specimen 50-A-3-3

Applied stress, kg./sq.mm.	0.00	2.15	2.76	3.37	3.37	3.37
Irreversible deformation, %	0.00	0.27	0.74	1.52	2.02	2.53
Thickness, 10^{-3} cm.	15.5	15.2	14.7	14.6	14.7	14.7[a]

Specimen 50-A-5-2

Applied stress, kg./sq.mm.	0.00	2.13	2.75	3.35	3.35	3.35
Irreversible deformation, %	0.00	0.33	0.72	1.60	2.00	2.50
Thickness, 10^{-3} cm.	15.6	15.3	14.8	14.7	14.7	14.7[a]

[a]These values were arbitrarily chosen as the sheet thicknesses to be used in all permeability and gas drive calculations.

the decrease was due to the removal of a cockle (caused by the peculiar method of drying) in the specimens, and photographs with grazing incidence light (2°) were taken of a specimen (50-A-6-3) both before and after it had been subjected to a number of extensions in an Instron tensile tester. Two of these photographs are presented in Fig. 24; they show that straining increased the surface smoothness of the specimen. This observation supports the contention that the decrease in specimen thickness caused by small amounts of deformation resulted from the removal of a cockle in the

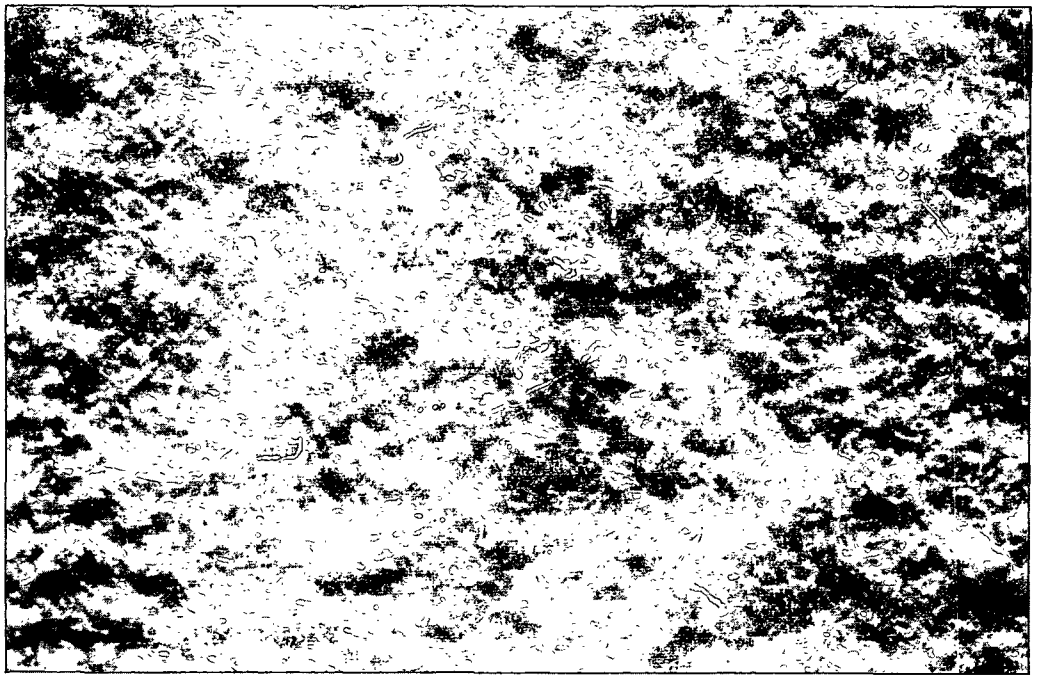

Figure 24a. Surface Photomicrograph - 15X
0.00% Irreversible Deformation

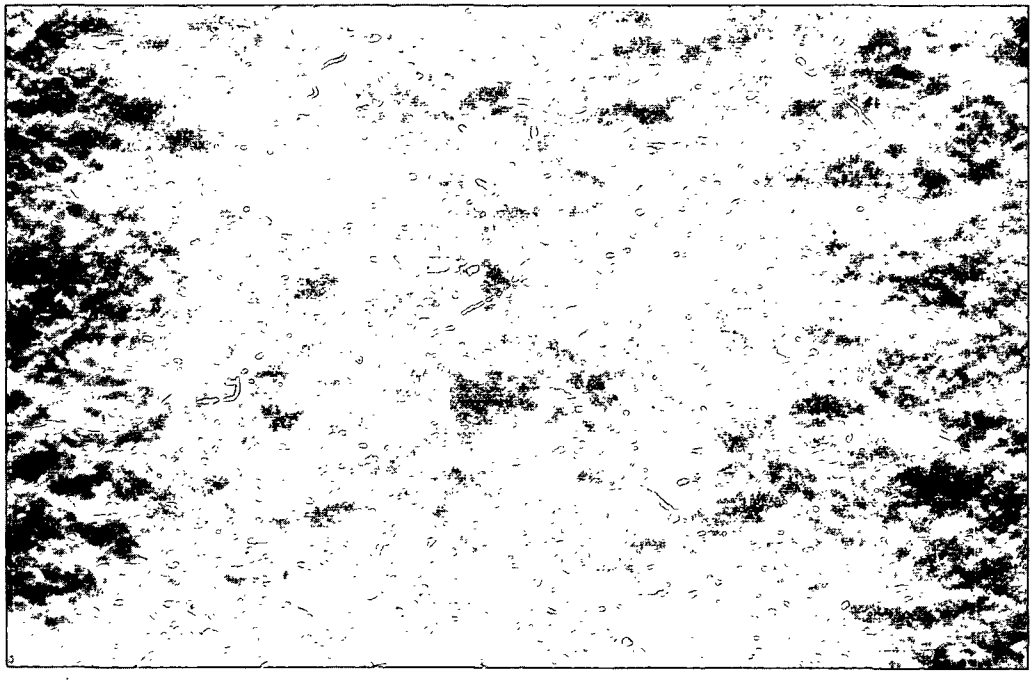

Figure 24b. Surface Photomicrograph - 15X
1.00% Irreversible Deformation

sheet. Therefore, the decrease in thickness during the early stages of deformation has been ignored, and it has been assumed that the effective thickness of a specimen to permeation processes is not altered appreciably by deformation.

AIR PERMEABILITY STUDIES

The objectives of the permeability studies that were carried out were to determine how deformation affected the permeability properties of paper and to see if the Kozeny-Carman approach (47) could be used to estimate the magnitude of stress-induced changes in the interfiber exposed surface of paper. Deformation was caused by 48-hour creep-recovery cycles, and the permeability data obtained were used to estimate the permeability, B_o, and slip constants, K_o, of specimens from the slope and intercept of plots similar to those shown in Fig. 25*. Appendix III contains all of the pertinent air permeability data collected during this investigation. These data were used to estimate the permeability, B_o, and slip constants, K_o, reported in Table VI. The permeability constants reported in Table VI have been used to construct the graphs shown in Fig. 26. These plots show that the permeability constants of the specimens increased linearly with irreversible deformation. Such an interrelation is not consistent with the Kozeny-Carman theory of permeation as will be demonstrated below.

*The flow rate - pressure drop data from which Curve A of Fig. 25 was derived are presented in Appendix III.

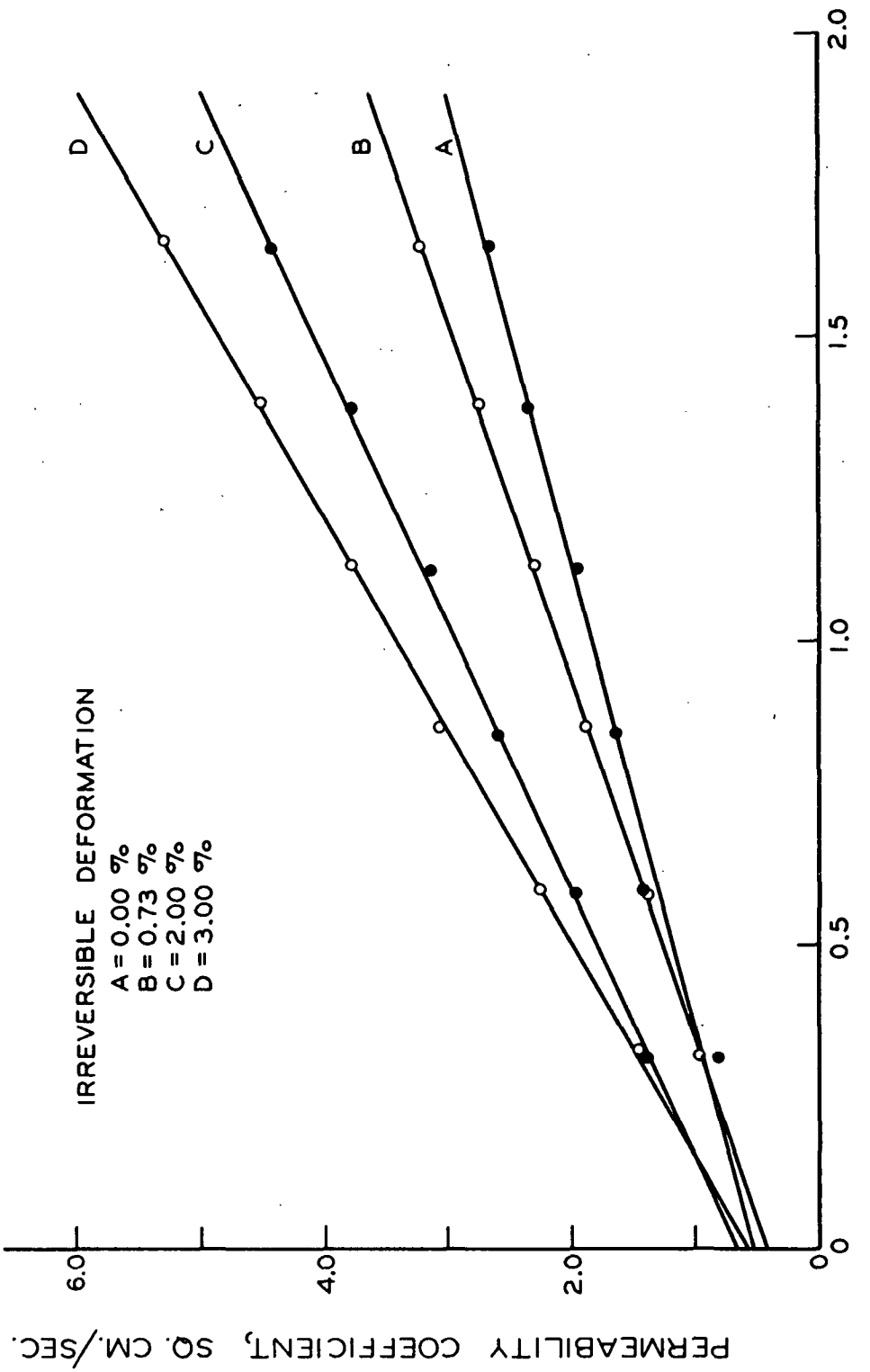

Figure 25. Permeability Coefficient Versus Mean Pressure

TABLE VI

THE EFFECT OF DEFORMATION ON AIR PERMEABILITY PROPERTIES

Specimen 50-A-2-1

Irreversible deformation, %[a]	0.00	0.25	0.73	1.56	2.00	2.42	3.00
Permeability constant, 10^{-10} sq. cm.	2.25	2.47	3.00	3.62	3.95	4.36	4.95
Slip constant, 10^{-5} cm.	0.79	0.71	0.68	0.83	1.03	0.88	0.89

Specimen 50-A-3-3

Irreversible deformation, %[a]	0.00	0.27	0.74	1.53	2.03	2.53
Permeability constant, 10^{-10} sq. cm.	3.82	4.30	4.60	5.29	5.83	5.94
Slip constant, 10^{-5} cm.	0.90	0.83	0.99	1.10	1.11	1.41

Specimen 50-A-5-2

Irreversible deformation, %[a]	0.00	0.33	0.72	1.50	2.00	2.42
Permeability constant, 10^{-10} sq. cm.	3.81	4.16	4.58	5.36	5.80	6.43
Slip constant, 10^{-5} cm.	0.88	0.86	0.98	1.07	1.31	1.20

[a]These data were obtained from 48-hour creep-recovery cycles carried out according to the series testing procedure (see Appendix II).

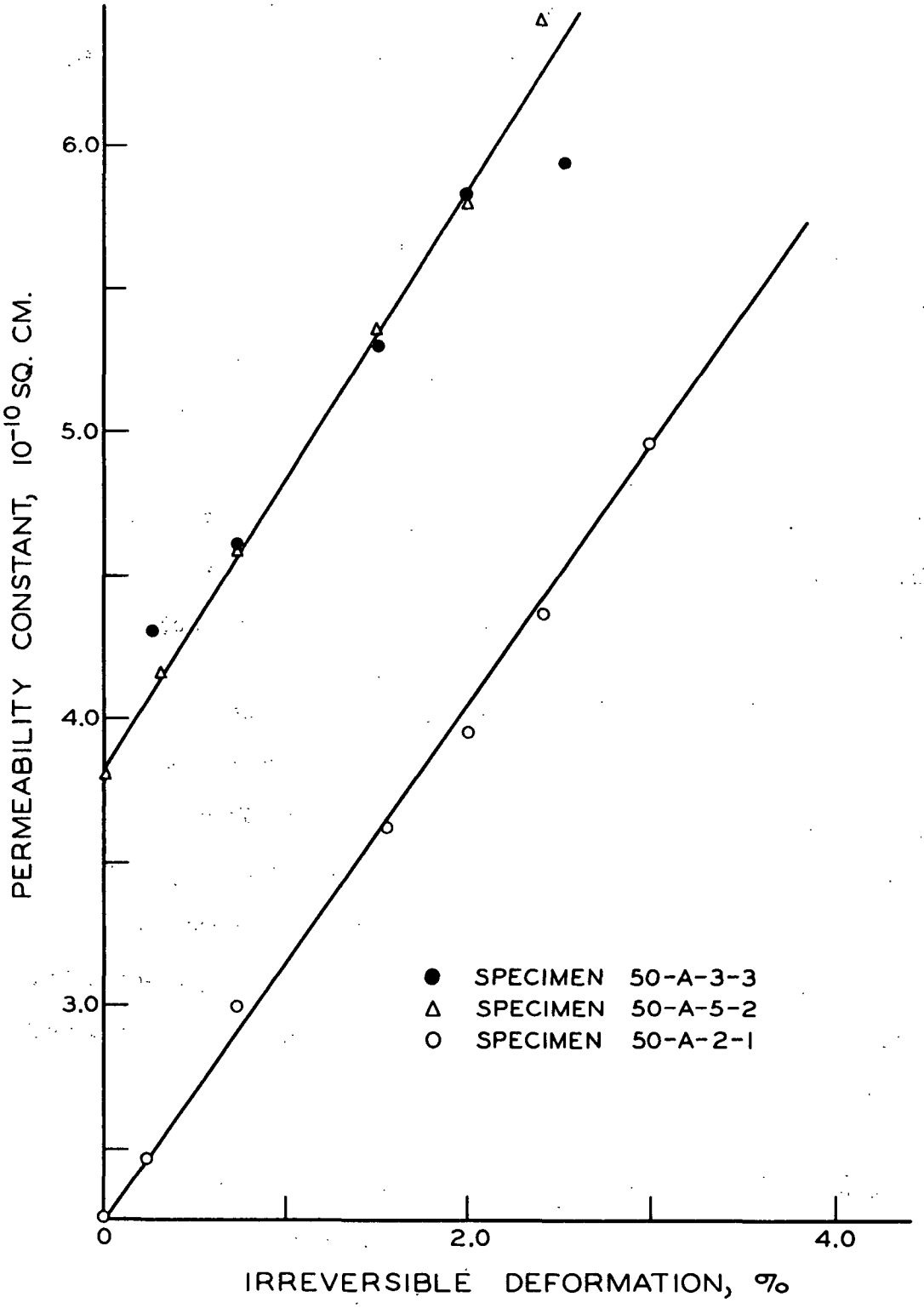

Figure 26. Permeability Constant Versus Irreversible Deformation

Another interesting observation derived from the data in Table VI was that the slip constants, K_o, of all specimens passed through a minimum as irreversible deformation increased. Analysis of the data available indicated that these minimums were not statistically significant and it was concluded that the effect was not real.

Because the slip constant data gathered during this study were not very precise, only permeability constant data were used to check the validity of the Kozeny-Carman approach (47). Interfiber exposed surfaces were calculated through the use of Equation (5), and in the case of Specimen 50-A-3-3 they ranged from a value of 11,000 sq.cm./g. for the undeformed specimen to 8750 sq.cm/g for the specimen which had been subjected to five 48-hour creep-recovery cycles*. (Similar figures were also obtained in the case of Specimens 50-A-2-1 and 50-A-5-2.)

Data collected by both Brown (55) and Estridge (54) indicate that the interfiber exposed surface of a sheet such as the one studied in this investigation should be about 4500 sq.cm./g. In addition, data obtained by Nordman, et al. (18-21) and Page, et al. (24, 25) indicate that the interfiber exposed surface of a sheet increases during deformation. This means that the Kozeny-Carman method of data reduction should not be used to analyze air-permeability data gathered on relatively thin sheets of paper. If the method is used to rectify such data two serious

*The porosity of all specimens was calculated by means of the expression, $p = 1 - (wV/aL)$, where p is porosity, w is specimen weight, a is the area of the specimen, L is specimen thickness, and V is the specific volume of the fibers within the specimens. Data reported by Estridge (54) was used to arrive at a figure of 1.0 cc./g. for fiber specific volume.

errors result. First, the calculated values of interfiber exposed surface are too high by a factor of about two; second, it appears that decreases in interfiber exposed surface are induced by stress. The specific reasons for the failure of the Kozeny-Carman treatment to characterize the interfiber structure of paper will become more evident during the discussion of the pore size distribution studies.

PORE SIZE DISTRIBUTION STUDIES

The objectives of the pore size distribution studies were to determine why the Kozeny-Carman equation cannot be used to analyze the flow of a gas through paper and to gain a more complete understanding of the effect of stress on the interfiber structure of paper. The gas drive technique was used to gather pore size distribution data, and all measurements were made on the same specimens from which the permeability data just discussed were obtained. These data were used to calculate the sheet parameters reported in Table VII and Appendix IV.

The pore size distribution plots shown in Fig. 27 demonstrate that deformation caused a shift in the distribution of pore sizes within a specimen by increasing the number of large pores (5 to 10 μ) at the expense of small pores (3.5 μ or less). This had a pronounced effect on the permeability characteristics of the specimens and was one of the important causes for the inability of the Kozeny-Carman method to characterize stress-induced changes in the interfiber structure of paper.

The effect of a stress-induced shift in specimen pore size distribution on specimen permeability properties is demonstrated by Fig. 28 and 29.

TABLE VII

GAS DRIVE DATA

Radius, μ	$\frac{dN}{dR}$, $cm.^{-1}$	$\log_{10} \frac{dN}{dR}$	Rel. Perm. Const.,[a] 10^{-11} sq. cm.	Perm. Const., 10^{-10} sq. cm.	Rel. Perm.,[b] %	$(\frac{p}{t'})^{c}$ x 10^{2}
Specimen 50-A-2-1-0: applied stress = 0.00 kg./sq.mm.; irr. deform. = 0.00%.[d]						
9.04	7.57×10^{6}	6.879	--	2.25	--	--
7.03	3.16×10^{8}	8.499	0.063	2.25	0.28	0.005
5.75	1.79×10^{9}	9.252	0.202	2.25	0.90	0.025
4.86	8.35×10^{9}	9.922	0.424	2.25	1.88	0.072
4.22	2.19×10^{10}	10.340	0.748	2.25	3.32	0.168
3.72	5.13×10^{10}	10.710	1.081	2.25	4.80	0.312
3.33	1.03×10^{11}	11.012	1.423	2.25	6.32	0.513
3.01	1.69×10^{11}	11.228	1.774	2.25	7.88	0.783
2.75	2.40×10^{11}	11.380	2.052	2.25	9.12	1.080
Specimen 5-A-2-1-25: applied stress = 2.87 kg./sq.mm.; irr. deform. = 0.73%.[d]						
9.04	2.61×10^{7}	7.416	--	3.00	--	--
7.03	6.58×10^{8}	8.818	0.125	3.00	0.42	0.010
5.75	2.98×10^{9}	9.474	0.376	3.00	1.25	0.045
4.86	1.07×10^{10}	10.029	0.668	3.00	2.23	0.113
4.22	3.05×10^{10}	10.484	1.122	3.00	3.75	0.252
3.72	6.80×10^{10}	10.832	1.574	3.00	5.26	0.454
3.33	1.08×10^{11}	11.033	1.968	3.00	6.56	0.709
3.01	1.60×10^{11}	11.204	2.292	3.00	7.64	1.010
2.75	2.27×10^{11}	11.356	2.545	3.00	8.50	1.350
Specimen A-2-1-30I: applied stress = 3.50 kg./sq.mm.; irr. deform. = 1.56%.[d]						
9.04	3.13×10^{7}	7.496	--	3.62	--	--
7.03	7.04×10^{8}	8.847	0.188	3.62	0.52	0.015
5.75	3.93×10^{9}	9.594	0.457	3.62	1.26	0.055
4.86	1.59×10^{10}	10.202	0.955	3.62	2.64	0.162
4.22	4.22×10^{10}	10.624	1.532	3.62	4.24	0.344
3.72	7.05×10^{10}	10.848	2.072	3.62	5.72	0.597
3.33	1.07×10^{11}	11.029	2.500	3.62	6.91	0.881
3.01	1.59×10^{11}	11.202	2.772	3.62	7.65	1.220
Specimen A-2-1-30III: applied stress = 3.50 kg./sq.mm.; irr. deform. = 2.42%.[d]						
9.04	4.28×10^{7}	7.631	--	4.36	--	--
7.03	9.29×10^{8}	8.968	0.224	4.36	0.51	0.0182
5.75	4.99×10^{9}	9.698	0.601	4.36	1.38	0.073
4.86	1.91×10^{10}	10.282	1.159	4.36	2.66	0.196
4.22	4.07×10^{10}	10.609	1.843	4.36	4.23	0.414
3.72	7.03×10^{10}	10.846	2.580	4.36	5.92	0.687
3.33	1.07×10^{11}	11.029	3.125	4.36	7.17	1.090

TABLE VII (Continued)

Radius, μ	dN/dR, $cm.^{-1}$	Log_{10} dN/dR	Rel. Perm. Const.,[a] 10^{-11} sq.cm.	Perm. Const., 10^{-10} sq.cm.	Rel. Perm.,[b] %	$(p/t')^c$ x 10^2
Specimen 50-A-2-1-33: applied stress = 3.82 kg./sq.mm.; irr. deform. = 3.00%.[d]						
9.04	8.45×10^7	7.926	--	4.95	--	--
7.03	9.31×10^8	8.969	0.313	4.95	0.63	0.025
5.75	5.92×10^9	9.772	0.748	4.95	1.51	0.091
4.86	2.13×10^{10}	10.328	1.422	4.95	2.88	0.241
4.22	4.44×10^{10}	10.647	2.138	4.95	4.32	0.480
3.72	7.23×10^{10}	10.859	3.045	4.95	6.15	0.820
3.33	1.39×10^{11}	11.143	3.840	4.95	7.76	1.280

[a]The relative permeability constant was calculated through the use of the expression, $K_e = QnL/A\Delta P$.

[b]The relative permeability was calculated through the use of the expression, $K_r = 100K_e/B_o$.

[c]Porosity-tortuosity ratio.

[d]The creep and recovery data from which these values were derived are summarized in Appendix II.

Figure 28 presents plots of relative permeability constant, K_e,[1] versus irreversible deformation with minimum effective pore radius[2] as a parameter. These plots show that the relative permeability constants, K_e, (at constant minimum effective pore radius) increased linearly with irreversible

[1]The relative permeability constant, K_e, of a porous medium has the same physical significance as its permeability constant, B_o, except that it is measured while a specimen is partially saturated with a nonswelling liquid.

[2]The minimum effective pore radius is calculated from the capillary pressure equation, $\Delta P = 2\gamma/R$. It is the radius of the smallest cylindrical capillary opened up in a specimen by a given pressure differential, ΔP. In Fig. 28, 29, and 30, the minimum effective pore radius is simply a measure of the smallest pores available to flow under a given set of experimental conditions. This means that the physical properties presented in these figures are controlled by the pores with effective radii greater than the minimum effective pore radius stated.

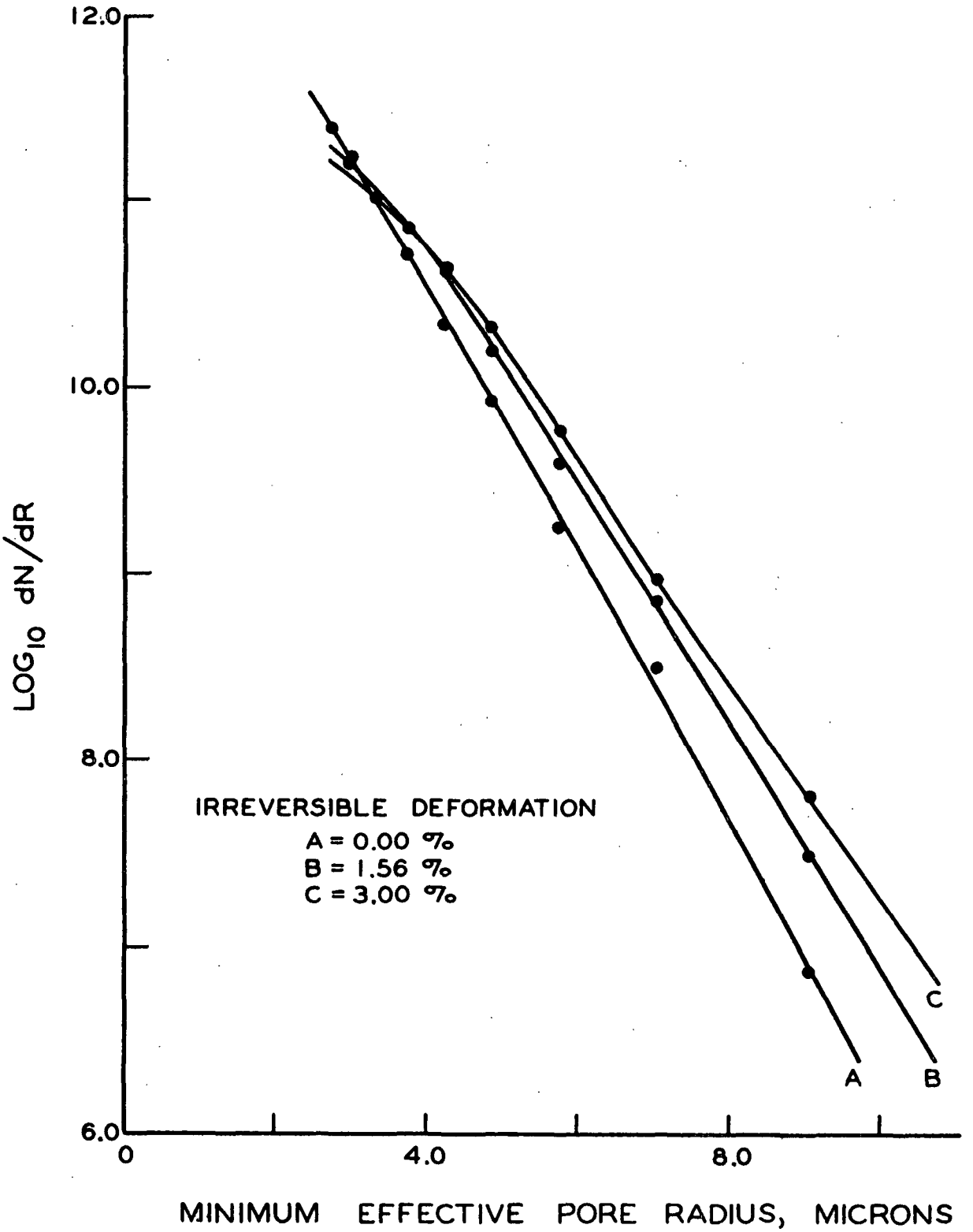

Figure 27. Pore Size Distribution Plots

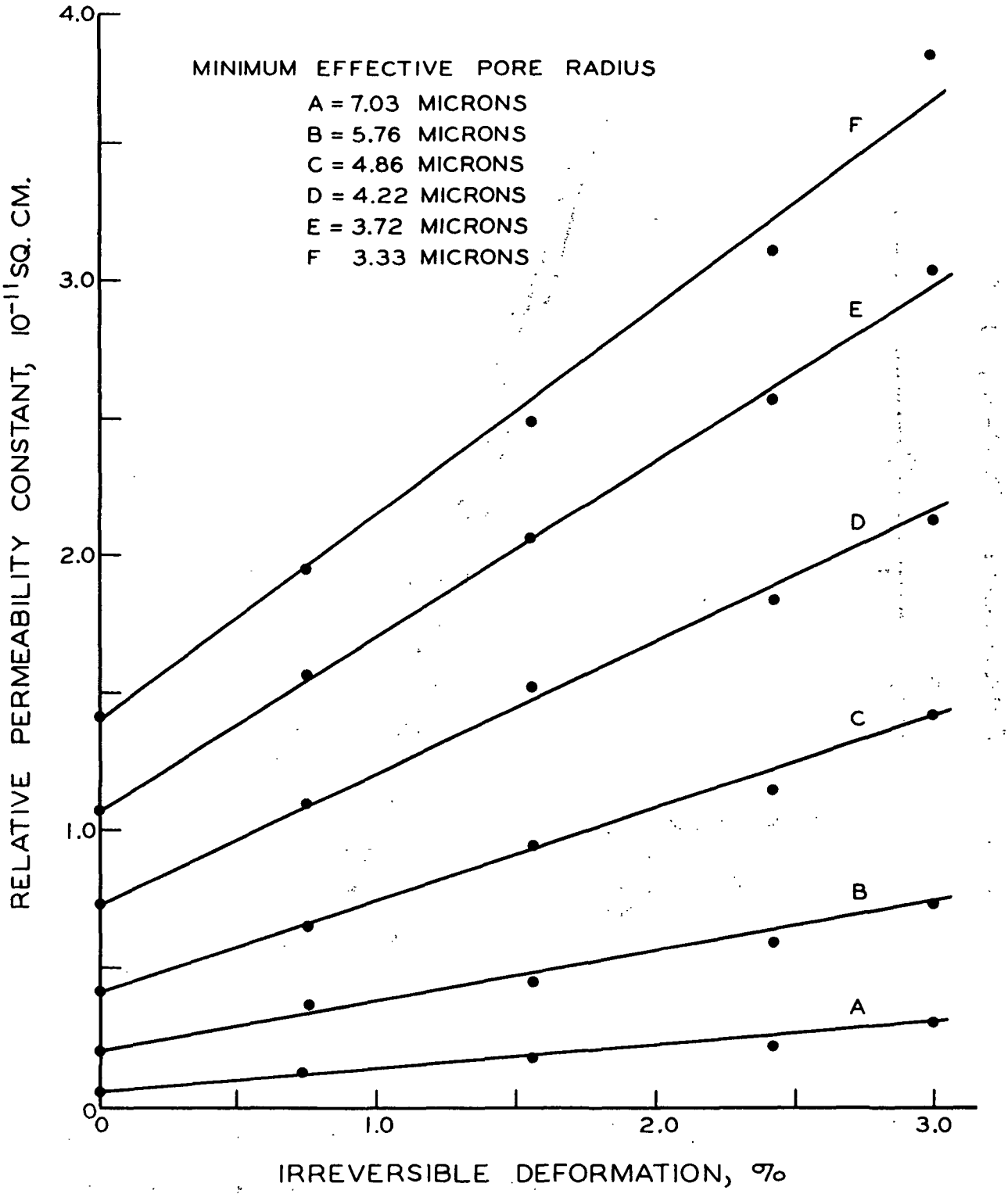

Figure 28. Relative Permeability Constant Versus Irreversible Deformation

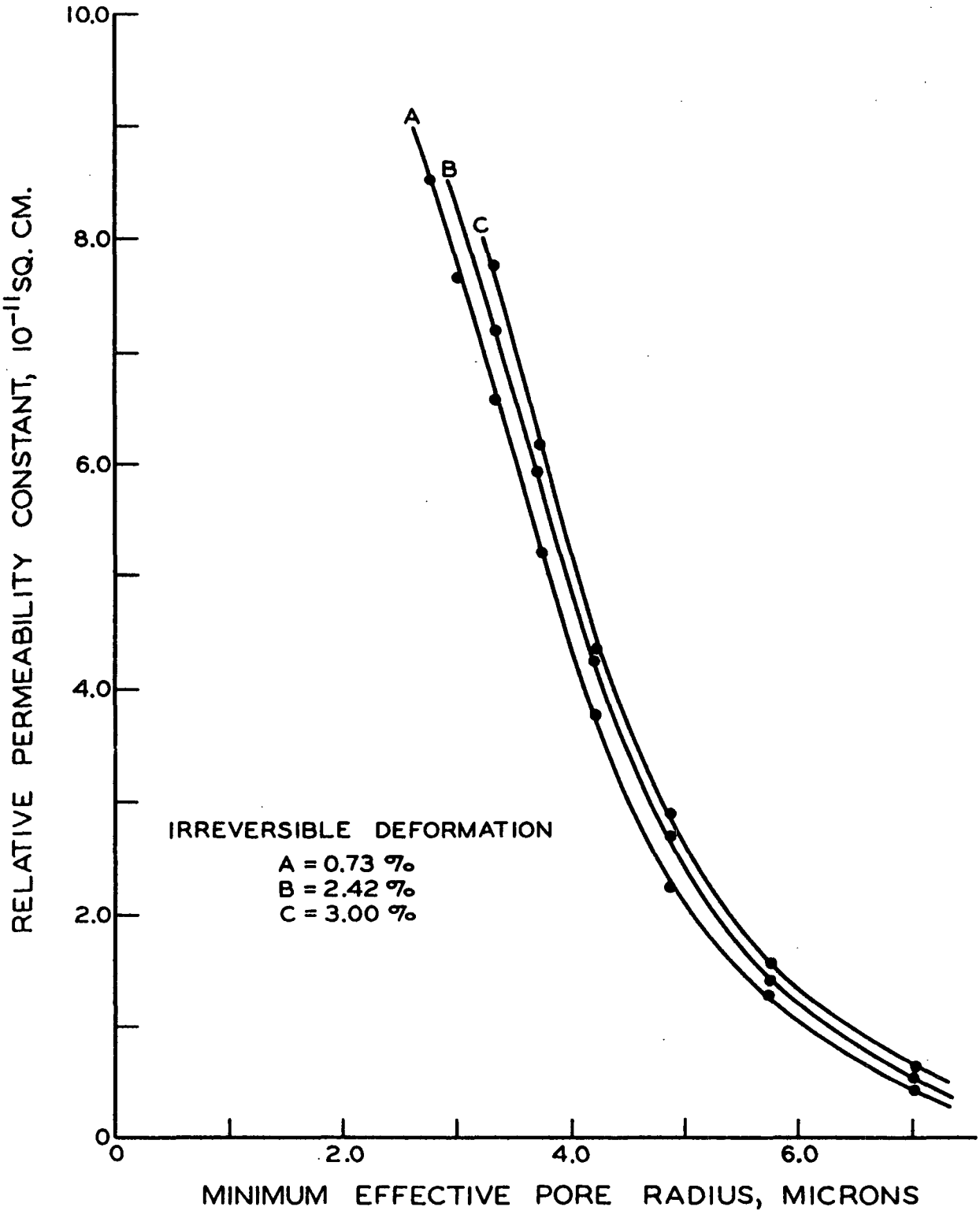

Figure 29. Relative Permeability Constant Versus Effective Pore Radius

deformation and suggest that changes in the number of large pores (5 μ or greater) within a sheet were primarily responsible for the linearity of the relation between the permeability constant, B_o, of a specimen and irreversible deformation. This would seem to indicate that the air permeability technique is not particularly sensitive to stress-induced changes in the fine interfiber structure of paper.

Still more information concerning the effect of shifts in pore size distribution on permeability properties can be obtained by constructing plots of relative permeability[1] versus minimum effective pore radius with irreversible deformation as a parameter. This has been done and the result is given in Fig. 29, which shows that deformation does not cause an undue amount of gas to flow through a selected group of pores; instead, it causes a rather uniform increase in the flow rate through all of the pores characterized. From this, it was concluded that deformation did not cause the preferential creation of a few large pinholes within a sheet.

The data reported in Fig. 27, 28, and 29 supply further evidence that deformation causes considerable interfiber structural damage. The increases in the permeability and relative permeability constants were both greater than could be accounted for by changes in porosity, which showed about a 3% increase[2]. This, along with the data indicating that

[1]The relative permeability of a specimen is the ratio of its relative permeability constant to its permeability constant expressed as a percentage.

[2]Porosity increases were calculated from stress-induced increases in specimen length assuming specimen width and thickness to remain constant during deformation. The effect of the porosity increases was estimated through the use of a Kozeny-Carman type of relationship.

deformation caused an appreciable change in pore size distribution, was taken to mean that stress not only caused an increase in the porosity of specimens but also altered their interfiber structure in such a way that more gas could flow through at equivalent porosities.

During the course of the pore size distribution study, it was noted that the relative permeabilities of specimens never rose above 10% (see Fig. 29). These low relative permeabilities could not be explained by the unavailability of small pores (3 μ or less). Therefore, it was hypothesized that many large pores contained constrictions which prevented the wetting fluid from draining away during gas drive measurements, but allowed appreciable amounts of gas to flow during air permeability measurements. This hypothesis was checked by recalling that Carman (56) had used beds of sand to demonstrate that the internal surface area exposed during any portion of a gas drive experiment was equal to the quotient, $\Delta P/\gamma$, where ΔP is the displacing pressure and γ is the surface tension of the wetting liquid. It was assumed that this relation also held, at least qualitatively, for paper, and the effect of deformation on the porosity-tortuosity ratio, p/t', of partially saturated specimens was evaluated through the use of the expression, $p/t' = K_e(\Delta P/\gamma)^2$ (50). Part of the data which resulted is given in Table VII (see Appendix IV for the rest of the data), and it was used to construct the plots of porosity-tortuosity ratio versus irreversible deformation (with minimum effective pore radius as a parameter) shown in Fig. 30.

These plots show that the porosity-tortuosity ratio increased linearly with irreversible deformation at all minimum effective pore radii, which

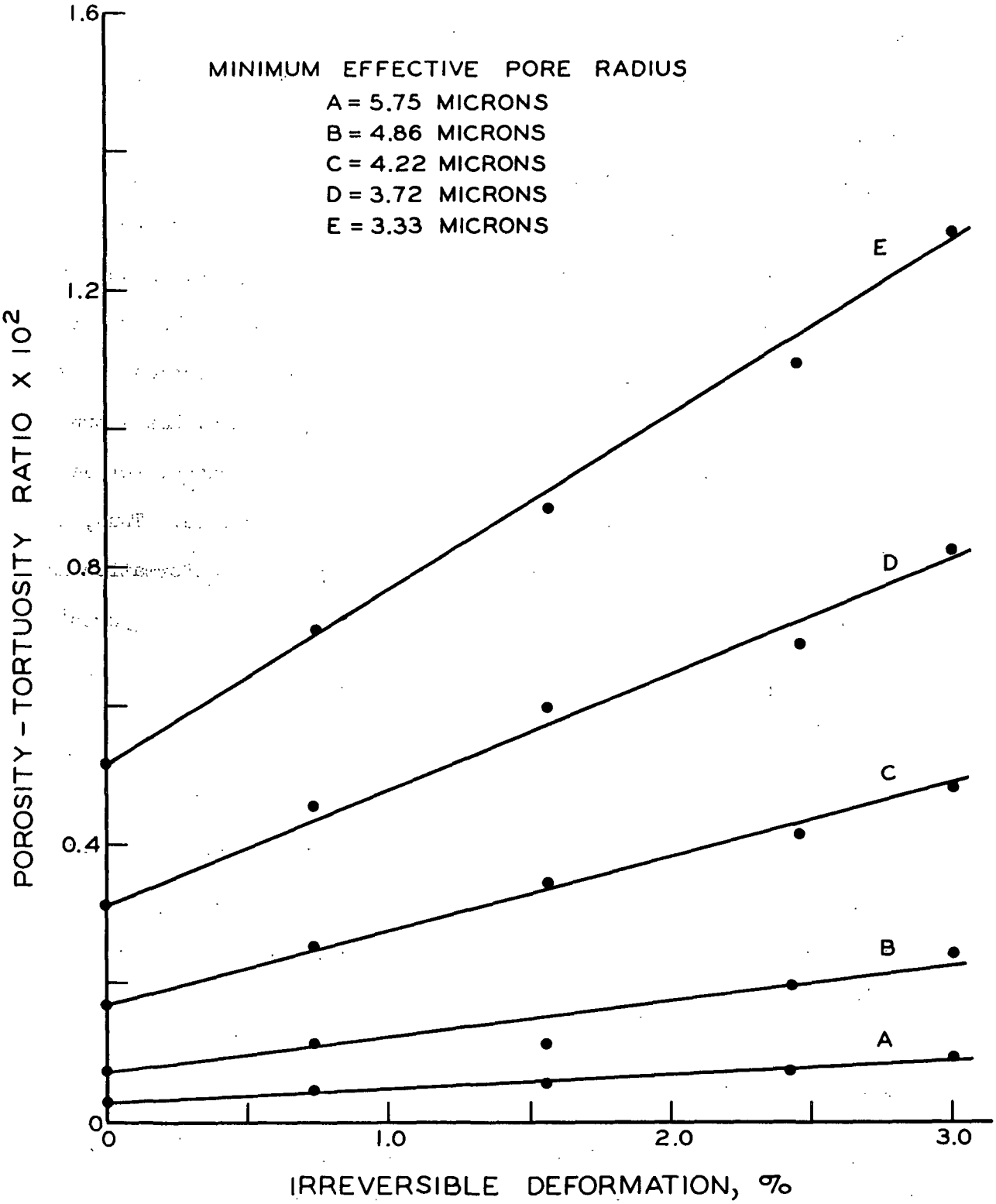

Figure 30. Porosity-Tortuosity Ratio Versus Irreversible Deformation

would seem to indicate that stress-induced variations in porosity-tortuosity ratio were primarily responsible for the stress-induced changes in specimen permeability and relative permeability constants. Further, it can also be shown that the porosity-tortuosity ratio increased at a much greater rate than could be explained by changes in porosity. Consequently, it is hypothesized that the apparent tortuosity of the specimens was decreased rather drastically during deformation. This drastic decrease in apparent tortuosity cannot be explained by a decrease in pore tortuousness alone (the tortuosity decreased by a factor of two or more). Petersen (57), on the other hand, has shown that the elimination of pore constrictions can easily account for decreases in apparent tortuosity by a factor of three or more. Thus, it seems that the increase in specimen permeability during deformation is the result of both an increase in porosity and a decrease in apparent tortuosity brought about (primarily) by the elimination of pore constrictions.

The above conclusions and hypothesis concerning the effect of deformation on porous properties have an important bearing on the question of how deformation affects interfiber structure. For example, the fact that the specimens suffered an increase in permeability during deformation indicates that their interfiber structure was changed. The fact that specimen porosity increased indicates that pores were opened up and fibers were separated. The partial justification of the hypothesis that apparent tortuosity was decreased by the elimination of pore constrictions suggests that fibers were separated at points of contact and indicates that interfiber bonds were broken during deformation.

SUMMARY AND CONCLUSIONS

The primary objective of this investigation was to learn more about how paper responds to stress. Interfiber processes of deformation were of particular interest. The paper studied was prepared from a bleached sulfite pulp which had been lightly refined in a ball mill and classified, with only that portion held on a 20-mesh screen being retained. Each specimen had a basis weight of about 100 g./sq.m. and was dried by a special technique which allowed it to be dried under pressure. The method of attack followed in characterizing interfiber processes of deformation was to use creep-recovery tests to characterize specimen mechanical properties and light scattering, air permeability, and pore size distribution tests to study changes in structure. The data obtained indicate that:

1. The paper studied conforms to a master creep curve concept.
2. The paper studied appears to conform well with a master recovery curve concept, but there is some indication that a resistance to recovery developed at long recovery times.
3. During this investigation it was found that the shapes of both the load and deload curves (on a load-extension plot) obtained for a specimen during a creep-recovery cycle was the same as the shapes of the load and deload curves obtained for a similar specimen during a stress-strain cycle (provided that both specimens were subjected to the same maximum load).

4. The amount of energy required to produce unit increase in irreversible deformation increases as the amount of irreversible deformation suffered by a specimen during a creep-recovery cycle increases.
5. The scattering coefficient of a specimen increases linearly with the amount of irreversible deformation suffered during a creep-recovery cycle (this means that the relative bonded area decreases linearly with increasing irreversible deformation).
6. The amount of energy associated with unit change in optically apparent exposed surface increases as the amount of irreversible deformation suffered by a specimen during a creep-recovery cycle increases.
7. The removal of a cockle in the specimens caused an apparent decrease in thickness (to a constant value) when they were subjected to stress.
8. Both the permeability constant and relative permeability constant (at a fixed minimum effective pore radius) of the specimens studied during this investigation increase linearly with irreversible deformation.
9. Stress-induced deformation causes a shift in the pore size distribution within a specimen due to an increase in the number of large pores (5 to 10 μ).
10. The porosity-tortuosity ratio (at a fixed minimum effective pore radius) as estimated from gas drive data increases linearly with the amount of irreversible deformation suffered by the specimens.

These experimental observations led to the following conclusions:

1. The stress-induced increases in air permeability constant, relative permeability constant, and porosity-tortuosity ratio as well as the shift in pore size distribution were taken as good evidence that stress-induced deformation alters the porous interfiber structure of paper by breaking interfiber bonds.
2. Because the interrelation between change in scattering coefficient and energy loss was affected by the duration of testing, it was hypothesized that appreciable amounts of energy might be absorbed by the fiber elements within a sheet during deformation. If this hypothesis is correct it would invalidate any attempt to calculate the energy-absorbing capacity or "bond strength" of interfiber bonds from light scattering - energy loss data.

ACKNOWLEDGMENTS

The author would like to express his sincere appreciation to Dr. J. A. Van den Akker, the chairman of his thesis advisory committee, and to Dr. W. L. Ingmanson and Mr. J. W. Swanson for their invaluable advice and encouragement during the course of his studies.

The aid of the following is also gratefully acknowledged.

Messrs. L. R. Dearth and W. M. Shillcox of The Institute of Paper Chemistry for their assistance in measuring the optical properties of the specimens studied.

The Physical Chemistry Group of The Institute of Paper Chemistry for help in determining the total exposed surface of specimens studied during the investigation.

Mr. T. D. McDonald, with whom the author constructed the flow rate-pressure drop apparatus used during the study.

The staff of the Engineering Department and Machine Shop of The Institute of Paper Chemistry for aid in the design and construction of equipment used during the investigation.

Dr. A. L. Lathrop for his assistance in preparing photomicrographs of various specimens and for his help in programming the IBM-610 computer.

Dr. G. R. Sears for his continued interest and helpful advice throughout the investigation.

Mr. R. L. Jones for his comments and advice during the preparation of the dissertation.

Mrs. E. A. Cary for the typing of the dissertation.

Mrs. Carlene Sanborn, without whose encouragement and steadfast support none of this would have been possible.

NOMENCLATURE

A = cross-sectional area available to flow, sq.cm.

a = specimen area, sq.cm.

B_a = relative bonded area, %

B_o = permeability constant, sq.cm.

f_l = fraction of molecules reflected diffusely from pore walls.

I_r = intensity of reflected light, lumens

I_t = intensity of transmitted light, lumens

K = permeability coefficient, sq.cm./sec.

K_e = relative permeability constant, sq.cm.

K_r = relative permeability, %

K_o = slip constant, cm.

k = specific absorption coefficient, sq.cm./g.

k' = Kozeny constant

k_o = shape factor

L = thickness, cm.

m = mean hydraulic radius, cm.

N = number of pores

n = viscosity, poise

$\overline{P}$ = mean pressure, bars

ΔP = pressure drop across bed, dynes/sq.cm.

p = porosity

Q = volume flow rate, sq.cm./sec.

Q_v = volume flow rate through pores in the interval, dN, sq.cm./sec.

R_o = reflectance when backed by a black body

$\underline{R}$ = effective pore radius, cm.

$\underline{S}$ = exposed surface per unit volume of bed solids, $cm.^{-1}$

$\underline{s}$ = specific scattering coefficient, sq.cm./g.

$\underline{s}_{\underline{ub}}$ = specific scattering coefficient of a water-dried, unbonded sheet, sq.cm./g.

$\Delta\underline{s}$ = change in specific scattering coefficient, sq.cm./g.

$\underline{T}$ = transmittance

$\underline{t}'$ = tortuosity

$\underline{u}$ = linear velocity of permeating fluid, cm./sec.

$\underline{V}$ = fiber specific volume, cc./g.

$\underline{\bar{v}}$ = mean thermal molecular velocity, cm./sec.

$\underline{W}$ = sheet basis weight, g./sq.m.

$\underline{w}$ = specimen weight, g.

δ_1 = slip coefficient

γ = surface tension, dynes/cm.

LITERATURE CITED

1. Houston, P. L., Paper Trade J. 71, no. 11:34-6(1920).

2. Bercsi, J. G., Paper Trade J. 84, no. 7:68-71(1927).

3. Gibbon, E. R., Paper Makers' Assoc. Gt. Brit. and Ireland, Proc. Tech. Sect. 25:199-210(1944).

4. Farebrother, T. H., Paper Makers' Assoc. Gt. Brit. and Ireland, Proc. Tech. Sect. 25:210-16(1944).

5. Steenberg, B., Svensk Papperstidn. 50, no. 6:127-40(1947).

6. Steenberg, B., Svensk Papperstidn. 50, no. 15:346-50(1947).

7. Ivarsson, B., and Steenberg, B., Svensk Papperstidn. 50, no. 18: 419-32(1947).

8. Ivarsson, B., Svensk Papperstidn. 51, no. 17:383-8(1948).

9. Andersson, O., Ivarsson, B., Nissan, A. H., and Steenberg, B., Paper Makers' Assoc. Gt. Brit. and Ireland, Proc. Tech. Sect. 30: 43-56(1949).

10. Rance, H. F. The mechanical properties of paper. In Meredith's Mechanical properties of wood and paper. p. 99-298. New York, Interscience, 1953.

11. Nissan, A. H., Textile Research J. 25, no. 9:780-8(1955).

12. Nissan, A. H., Tappi 39, no. 2:93-7(1956).

13. Nissan, A. H., Tappi 42, no. 12:928-33(1959).

14. Rance, H. F., Paper Makers' Assoc. Gt. Brit. and Ireland, Proc. Tech. Sect. 29:449-76(1948).

15. Rance, H. F. The rheological behavior of paper. In Harrison's Some recent developments in rheology. London, England, United Trade Press Ltd., 1950. 90 p.

16. Brezinski, J. P. A study of the viscoelastic properties of paper by means of tensile creep tests. Doctor's Dissertation. Appleton, Wis., The Institute of Paper Chemistry, 1955. 242 p.

17. Brezinski, J. P., Tappi 39, no. 2:116-28(1958).

18. Nordman, L., Gustafsson, C., and Olofsson, G., Paper and Timber (Finland) 34, no. 3:47-52(1952).

19. Nordman, L., Gustafsson, C., and Olofsson, G., Paper and Timber (Finland) 36, no. 8:315-20(1954).

20. Nordman, L., Gustafsson, C., and Olofsson, G., Tappi 38, no. 12: 724-7(1955).

21. Nordman, L. In Bolam's Fundamentals of papermaking fibres. p. 333-47. Kenley, England, Tech. Sect. British Paper and Board Makers' Assoc., 1958.

22. Van den Akker, J. A. In Bolam's Fundamentals of papermaking fibres. p. 365-6. Kenley, England, Tech. Sect. British Paper and Board Makers' Assoc., 1958.

23. Andersson, O. In Bolam's Fundamentals of papermaking fibres. p. 368-9. Kenley, England, Tech. Sect. British Paper and Board Makers' Assoc., 1958.

24. Page, D. H., Paper Technol. 1, no. 4:407-11(1960).

25. Page, D. H., and Tydeman, P. A., Paper Technol. 1, no. 5:519-30(1960).

26. Corte, H. In Bolam's Fundamentals of papermaking fibres. p. 301-31. Kenley, England, Tech. Sect. British Paper and Board Makers' Assoc., 1958.

27. Kallmes, O., and Corte, H., Tappi 43, no. 9:737-52(1960).

28. Onogi, S., and Sasaguri, K., Parupu Kami Kogyo Zasshi 11, no. 4:18-23(1957).

29. Van den Akker, J. A. Work to be presented at the symposium on The Formation and Structure of Paper, Oxford, England, Sept. 25-29, 1961.

30. Petterson, D. R. The mechanics of nonwoven fabrics. Doctor's Dissertation. Cambridge, Mass., The Massachusetts Institute of Technology, 1958. 291 p.

31. Van den Akker, J. A., Tappi 42, no. 12:940-7(1959).

32. Van den Akker, J. A., Lathrop, A. L., Voelker, M. H., and Dearth, L. R., Tappi 41, no. 8:416-25(1958).

33. Jayne, B. A., Tappi 42, no. 6:461-7(1959).

34. Hardacker, K. W., Lathrop, A. L., and Van den Akker, J. A. Personal communication, 1961.

35. Schulz, J. H. The effect of strain applied during drying on the viscoelastic behavior of paper. Doctor's Dissertation. Appleton, Wis., The Institute of Paper Chemistry, 1961. 161 p.

36. Institute Method 402, 1951.

37. Institute Method 415, 1951.

38. Wink, W. A., and Van Eperen, R. H. Unpublished work, 1960.

39. Hardacker, K. W. Unpublished work, 1951.

40. Kubelka, D., and Munk, F., Z. Tech. Physik 12:593-601(1931).

41. Steele, F. A., Paper Trade J. 100, no. 12:37-42(1935).

42. Van den Akker, J. A., Tappi 32, no. 11:498-501(1949).

43. Kubelka, D., J. Opt. Soc. Am. 38, no. 5:448-57(1948).

44. Hardy, A. C., J. Opt. Soc. Am. 28, no. 10:360-4(1938).

45. Michaelson, J. L., J. Opt. Soc. Am. 28, no. 10:365-71(1938).

46. Dearth, L. R., and Shillcox, W. M. Personal communication, 1960.

47. Carman, P. C. Slip flow, free molecular flow, and diffusional flow. In Carman's Flow of gases through porous media. p. 62-80. New York, Academic Press, 1956.

48. Staff of The Institute of Paper Chemistry, Paper Trade J. 109, no. 13:18-22(1939).

49. Carson, F. T., Paper Trade J. 99, no. 16:196-204(1934).

50. Scheidegger, A. E. Multiple phase flow. In Scheidegger's The physics of flow through porous media. p. 153-63, 181-90. New York, Macmillan, 1957.

51. Van den Akker, J. A., and Hardacker, K. W., Tappi 41, no. 8:224-31A(1958).

52. Catsiff, E., Alfrey, T., Jr., and O'Shaughnessy, M. T., Textile Research J. 23, no. 11:808-20(1953).

53. Ingmanson, W. L., and Thode, E. F., Tappi 42, no. 1:83-93(1959).

54. Estridge, R. The use of air permeability in studying hygroexpansivity. Special Studies. Appleton, Wis., The Institute of Paper Chemistry, 1958. 54 p.

55. Brown, J. C., Jr. Determination of the exposed surface area of pulp fibers from air permeability measurements using a modified Kozeny equation. Doctor's Dissertation. Appleton, Wis., The Institute of Paper Chemistry, 1949. 146 p.

56. Carman, P. C., Soil Sci. 52, no. 1:1-14(1941); C.A. 35:8181.

57. Petersen, E. E., A.I.Ch.E. Journal 4, no. 3:343-5(1958).

APPENDIX I

DESCRIPTION OF METHOD USED TO CALCULATE ENERGY LOSS

The purpose of this presentation is to demonstrate that the energy lost during a creep-recovery cycle is proportional to the area enclosed by the load, creep, and deload curves on a load-extension plot (see Fig. 31b).

Consider a system such as the one shown in Fig. 31a. It can be shown from first principles that the work done on or by such a system is equal to the integral $\int \underline{F}.\underline{dx}$, where $\underline{F}$ is force and $\underline{x}$ is displacement. The load-extension curve for a typical creep-recovery cycle is presented in Fig. 31b. This plot is essentially a record of the force exerted on the system shown in Fig. 31a, and the displacement which resulted. From Fig. 31b it can be seen that the system suffers an extension when a load, $\underline{L}$, is applied. The path followed (on a load-extension plot) is ABC; the work done is proportional to the area ABCDA. Later, when the load, $\underline{L}$,

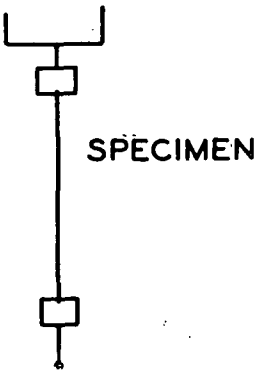

Figure 31a. Schematic Sketch of System

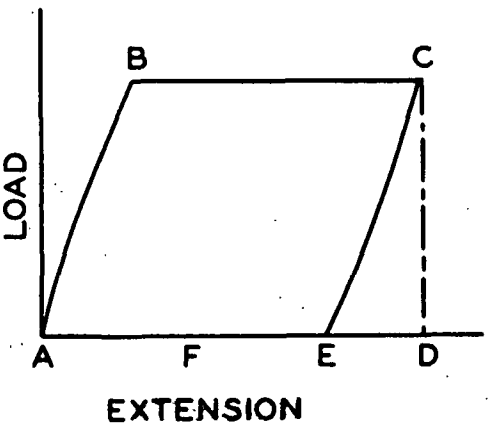

Figure 31b. Load-Extension Diagram

is removed the system contracts along the path CEF, and the work recovered is proportional to the area CDEC. The net result is that work is done on the system during a creep-recovery cycle and that this work was proportional to the area ABCEA. This work is expended in deforming the system irreversibly by an amount AF and is referred to as the amount of energy lost during a creep-recovery cycle.

In actual practice, stress-induced energy losses were estimated by using stress-strain data obtained on an Instron tensile tester to get an estimate of the shapes of AB and CE. The points C and F were located through the use of creep-recovery data collected with a Brezinski (16, 17) type of apparatus. With these data at hand it was possible to make a plot of the loop ABCEA and measure its area. The area of the loop was estimated by cutting it out, weighing it, and calculating its area from a knowledge of the weight per unit area of the paper on which the plot was constructed.

APPENDIX II

CREEP AND CREEP-RECOVERY DATA

The creep and recovery data used to construct the creep and recovery curves presented in Fig. 17 through 20 are contained in Table VIII. All creep and recovery data gathered during this study are summarized in Table IX.

TABLE VIII[a]

CREEP AND RECOVERY DATA

Time, sec.	Specimen					
	50-A-10-3	50-A-11-1	50-A-11-2	50-A-13-1	50-A-13-3	50-A-1-1
			Creep Deformation			
25	--	17.1	26.1	40.8	75.7	130.6
50	10.3	17.6	27.6	44.1	78.2	141.1
75	10.7	18.2	28.4	45.9	81.9	147.8
100	11.3	18.5	29.0	47.5	84.7	151.2
150	11.4	18.9	29.9	50.3	90.2	158.0
200	11.4	19.3	30.8	51.6	92.6	162.5
300	11.5	19.5	32.9	54.0	97.5	168.5
500	11.6	19.9	33.6	57.5	103.3	175.5
750	12.3	20.2	34.8	60.6	108.3	181.7
1,000	12.6	20.5	35.8	62.8	113.0	186.0
1,500	12.7	21.1	37.5	64.1	117.0	191.7
2,000	12.9	21.5	38.5	67.9	120.8	195.5
3,000	13.1	22.1	40.0	71.0	125.2	199.9
5,000	13.3	23.0	42.1	74.7	129.9	206.5
7,500	13.8	24.2	44.0	78.9	133.6	break
10,000	12.7	24.8	45.6	81.7	137.1	
15,000	13.9	25.8	47.2	85.3	141.9	
20,000	14.5	26.7	49.0	88.1	145.9	
30,000	15.3	27.9	51.8	91.0	150.3	
50,000	16.3	29.8	55.7	94.1	155.9	
86,400	17.5	31.6	59.1	101.6	160.7	
Applied stress	(1.58)	(2.22)	(2.84)	(3.46)	(4.12)	(4.76)

TABLE VIII (Continued)[a]

Time, sec.	Specimen 50-A-10-3	50-A-11-1	50-A-11-2	50-A-13-1	50-A-13-3	50-A-1-1
			Recovery Deformation			
25	7.8	13.2	19.0	--	34.4	
50	8.0	13.4	19.5	25.7	35.6	
75	8.2	13.6	19.8	26.2	36.1	
100	8.3	13.7	20.3	26.6	36.7	
150	8.4	14.0	20.5	27.1	37.2	
200	8.4	14.2	20.8	27.6	37.8	
300	8.5	14.4	21.1	28.1	38.6	
500	8.6	14.6	21.8	28.8	39.7	
750	8.7	14.9	22.2	29.7	40.4	
1,000	8.8	15.4	22.5	30.2	41.0	
1,500	9.1	15.6	23.0	30.8	--	
2,000	9.3	15.9	23.4	31.6	--	
3,000	9.4	16.1	24.0	32.1	43.6	
5,000	9.5	16.5	24.6	33.1	44.5	
7,500	9.7	16.8	25.2	33.9	45.6	
10,000	9.9	17.2	25.7	34.6	46.2	
15,000	10.4	17.5	26.1	35.4	47.3	
20,000	10.4	17.7	26.5	35.9	47.9	
30,000	10.4	17.7	26.9	36.4	48.9	
50,000	10.6	18.3	27.7	37.6	50.0	
86,400	10.6	18.5	28.1	38.3	51.1	
Removed stress	(1.30)	(1.94)	(2.56)	(3.18)	(3.83)	

[a]All gage lengths used were 5.002 in. All deformations expressed in mils.

TABLE IX

SUMMARIZED CREEP, RECOVERY AND ENERGY LOSS DATA

Specimen	Applied Stress, kg./sq.mm.	Removed Stress, kg./sq.mm.	Immed. Deform., mils	Total Deform., mils	Immed. Recovery, mils	Total Recovery, mils	Irrevers. Deform., mils	Energy Loss, joules/g.
50-A-10-3	1.58	1.30	10.0	17.5	8.0	10.6	6.9	0.014
50-A-11-1	2.22	1.94	14.5	31.6	13.0	18.5	13.1	0.045
50-A-11-2	2.84	2.56	19.6	59.1	18.6	28.1	31.0	0.137
50-A-13-1	3.46	3.18	25.9	101.6	24.0	38.3	63.3	0.330
50-A-13-3	4.12	3.83	36.8	160.7	32.6	51.1	109.6	0.666
50-A-1-1	4.76	4.47	62.6	206.5	43.6	68.3	138.2	0.992
50-A-12-3	2.23	1.95	14.7	39.6	13.0	19.3	20.3	0.069
50-A-14-2	2.83	2.55	19.4	59.9	18.6	28.3	31.6	0.143
50-A-11-3	3.48	3.20	24.7	97.5	24.0	37.8	59.7	0.322
50-A-10-2	3.82	3.54	31.1	137.3	28.4	46.2	91.1	0.528
50-A-8-3	4.10	3.81	36.5	156.9	32.6	52.2	104.7	0.657
50-A-8-2	4.46	4.18	47.7	195.3	39.2	61.3	134.0	0.906
50-A-7-3	2.24	1.95	14.7	35.7	13.0	19.0	16.7	0.057
50-A-8-1	2.85	2.56	19.6	56.9	18.6	28.0	28.9	0.129
50-A-9-1	3.46	3.18	25.9	93.4	24.0	37.3	56.1	0.292
50-A-10-1	3.80	3.52	30.8	139.8	28.4	45.8	94.0	0.519
50-A-12-1	4.09	3.81	36.0	165.1	32.6	52.4	112.7	0.671
50-A-13-2	4.61	4.31	54.1	225.6	39.2	64.4	161.2	1.193
50-A-2-1[a]	2.23	2.23	15.8	39.0	15.4	26.5	12.5	0.069
50-A-2-1	2.87	2.87	21.4	63.4	21.0	39.4	24.0	0.166
50-A-2-1	3.50	3.50	29.2	88.3	26.6	46.7	41.6	0.289
50-A-2-1	3.50	3.50	27.0	69.4	26.8	47.3	22.1	0.201
50-A-2-1	3.50	3.50	27.2	65.8	26.8	44.8	21.0	0.184
50-A-2-1	3.82	3.82	37.0	83.8	33.4	54.9	28.9	0.252

TABLE IX (Continued)

Specimen	Applied Stress, kg./sq.mm.	Removed Stress, kg./sq.mm.	Immed. Deform., mils	Total Deform., mils	Immed. Recovery, mils	Total Recovery, mils	Irrevers. Deform., mils	Energy Loss, joules/g.
50-A-3-3[a]	2.15	2.15	15.8	36.5	15.4	22.9	13.6	0.062
50-A-3-3	2.76	2.76	21.4	57.7	21.0	34.2	23.5	0.135
50-A-3-3	3.37	3.37	29.2	83.3	26.6	43.9	39.4	0.247
50-A-3-3	3.37	3.37	27.0	68.8	26.8	44.0	24.8	0.186
50-A-3-3	3.37	3.37	27.2	69.2	26.8	43.9	25.3	0.184
50-A-5-2[a]	2.13	2.13	15.8	43.8	15.4	27.2	16.6	0.076
50-A-5-2	2.75	2.75	21.4	63.3	21.0	44.0	19.3	0.156
50-A-5-2	3.35	3.35	29.2	88.4	26.6	49.4	39.0	0.271
50-A-5-2	3.35	3.35	27.0	70.2	26.8	44.9	25.3	0.194
50-A-5-2	3.35	3.35	27.2	69.0	26.8	48.3	20.7	0.187

[a]These creep tests were carried out in series according to the series testing procedure.

APPENDIX III

AIR PERMEABILITY DATA

A considerable amount of air permeability data was gathered during this investigation. The technique used was to collect a few (usually four) flow rate-pressure drop measurements at a number (usually six) of different mean pressures. These data were used to calculate specimen permeability coefficients, and this parameter was plotted against mean permeation pressure to give curves similar to those shown in Fig. 25. Figure 32 contains a plot of the flow rate-pressure drop data obtained for Specimen 50-A-2-1 before deformation. Plots of similar accuracy were obtained for all the rest of the specimens. The permeability coefficients calculated from these data are recorded in Table X.

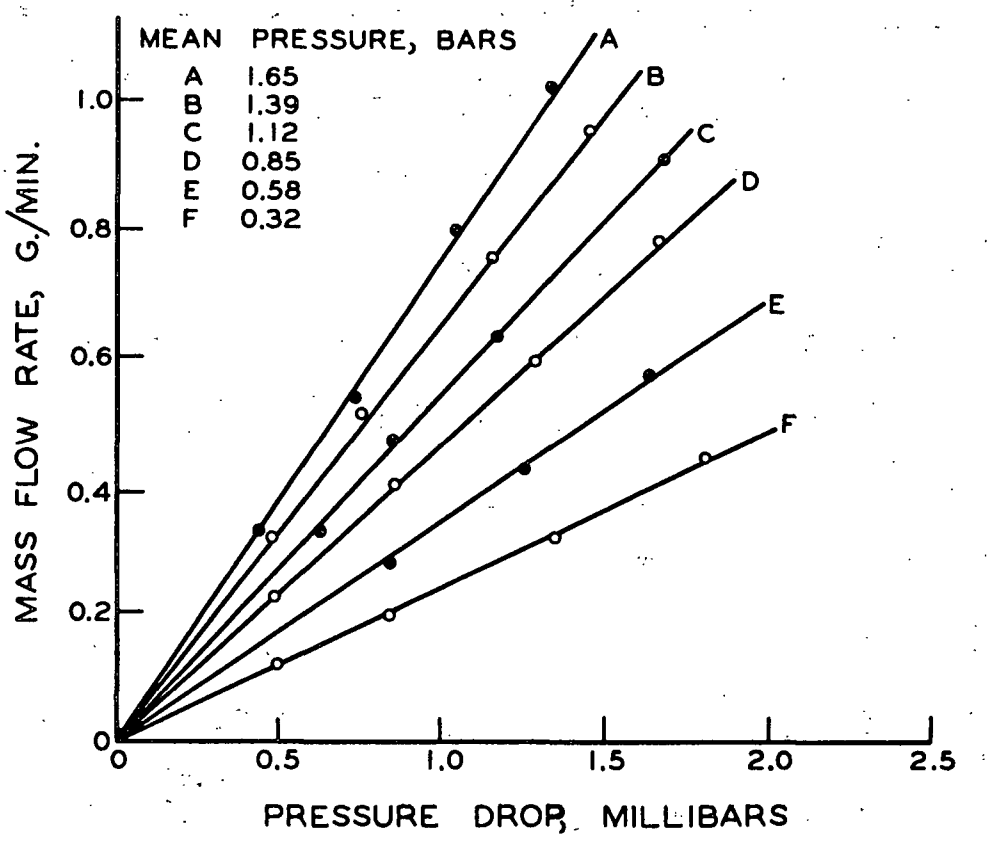

Figure 32. Flow Rate - Pressure Drop Curves for Specimen 50-A-2-1-0

TABLE X

PERMEABILITY COEFFICIENT - MEAN PRESSURE DATA

Specimen 50-A-2-1-0 Applied Stress - 0.00 kg./sq.mm. Irr. Def. - 0.00%

Mean Pressure, bars	1.65	1.39	1.12	0.85	0.58	0.32
Permeability Coeff., sq.cm./sec.	2.82	2.50	2.06	1.76	1.48	0.88

Specimen 50-A-2-1-20 Applied Stress - 2.23 kg./sq.mm. Irr. Def. - 0.25%

Mean Pressure, bars	1.66	1.40	1.13	0.86	0.60	0.33
Permeability Coeff., sq.cm./sec.	2.96	2.49	2.12	1.79	1.35	0.95

Specimen 50-A-2-1-25 Applied Stress - 2.87 kg./sq.mm. Irr. Def. - 0.73%

Mean Pressure, bars	1.66	1.39	1.12	0.86	0.59	0.32
Permeability Coeff., sq.cm./sec.	3.37	2.87	2.39	1.96	1.47	1.01

Specimen 50-A-2-1-30I Applied Stress - 3.50 kg./sq.mm. Irr. Def. - 1.56%

Mean Pressure, bars	1.66	1.39	1.13	0.86	0.59	0.33
Permeability Coeff., sq.cm./sec.	3.99	3.40	2.78	2.32	1.76	1.20

Specimen 50-A-2-1-30II Applied Stress - 3.50 kg./sq.mm. Irr. Def. - 2.00%

Mean Pressure, bars	1.65	1.38	1.12	0.85	0.58	0.32
Permeability Coeff., sq.cm./sec.	4.41	3.77	3.12	2.60	1.96	1.38

Specimen 50-A-2-1-30III Applied Stress - 3.50 kg./sq.mm. Irr. Def. - 2.42%

Mean Pressure, bars	1.66	1.40	1.13	0.86	0.60	0.33
Permeability Coeff., sq.cm./sec.	4.68	4.04	3.30	2.73	2.09	1.32

Specimen 50-A-2-1-33 Applied Stress - 3.82 kg./sq.mm. Irr. Def. - 3.00%

Mean Pressure, bars	1.66	1.39	1.13	0.86	0.60	0.33
Permeability Coeff., sq.cm./sec.	5.26	4.49	3.75	3.05	2.24	1.47

Specimen 50-A-3-3-0 Applied Stress - 0.00 kg./sq.mm. Irr. Def. - 0.00%

Mean Pressure, bars	1.65	1.39	1.12	0.85	0.59	0.32
Permeability Coeff., sq.cm./sec.	4.45	3.75	3.14	2.65	1.98	1.30

Specimen 50-A-3-3-20 Applied Stress - 2.16 kg./sq.mm. Irr. Def. - 0.27%

Mean Pressure, bars	1.66	1.39	1.13	0.86	0.59	0.33
Permeability Coeff., sq.cm./sec.	4.81	4.05	3.35	2.79	2.02	1.39

TABLE X (Continued)

Specimen 50-A-3-3-25 Applied Stress - 2.76 kg./sq.mm. Irr. Def. - 0.74%

Mean Pressure, bars	1.66	1.40	1.12	0.86	0.59	0.32
Permeability Coeff., sq.cm./sec.	5.00	4.27	3.56	2.89	2.20	1.47

Specimen 50-A-3-3-30I Applied Stress - 3.37 kg./sq.mm. Irr. Def. - 1.52%

Mean Pressure, bars	1.66	1.39	1.13	0.86	0.59	0.33
Permeability Coeff., sq.cm./sec.	5.65	4.91	4.08	3.30	2.47	1.65

Specimen 50-A-3-3-30II Applied Stress - 3.37 kg./sq.mm. Irr. Def. - 2.02%

Mean Pressure, bars	1.66	1.40	1.13	0.86	0.60	0.33
Permeability Coeff., sq.cm./sec.	6.27	5.29	4.43	3.65	2.68	1.77

Specimen 50-A-3-3-30III Applied Stress - 3.37 kg./sq.mm. Irr. Def. - 2.53%

Mean Pressure, bars	1.65	1.39	1.12	0.85	0.59	0.32
Permeability Coeff., sq.cm./sec.	6.48	5.64	4.64	3.82	2.90	1.95

Specimen 50-A-5-2-0 Applied Stress - 0.00 kg./sq.mm. Irr. Def. - 0.00%

Mean Pressure, bars	1.65	1.39	1.12	0.85	0.59	0.32
Permeability Coeff., sq.cm./sec.	4.49	3.75	3.14	2.62	1.93	1.32

Specimen 50-A-5-2-20 Applied Stress - 2.13 kg./sq.mm. Irr. Def. - 0.27%

Mean Pressure, bars	1.66	1.39	1.13	0.86	0.60	0.33
Permeability Coeff., sq.cm./sec.	4.68	3.98	3.30	2.78	2.05	1.34

Specimen 50-A-5-2-25 Applied Stress - 2.75 kg./sq.mm. Irr. Def. - 0.74%

Mean Pressure, bars	1.66	1.39	1.13	0.86	0.59	0.33
Permeability Coeff., sq.cm./sec.	4.88	4.15	3.47	2.84	2.07	1.35

Specimen 50-A-5-2-30I Applied Stress - 3.35 kg./sq.mm. Irr. Def. - 1.53%

Mean Pressure, bars	1.66	1.39	1.12	0.86	0.59	0.33
Permeability Coeff., sq.cm./sec.	5.77	4.93	4.11	3.40	2.50	1.64

Specimen 50-A-5-2-30II Applied Stress - 3.35 kg./sq.mm. Irr. Def. - 2.03%

Mean Pressure, bars	1.65	1.39	1.13	0.86	0.59	0.33
Permeability Coeff., sq.cm./sec.	6.29	5.49	4.48	3.74	2.81	1.89

Specimen 50-A-5-2-30III Applied Stress - 3.35 kg./sq.mm. Irr. Def. - 2.53%

Mean Pressure, bars	1.65	1.39	1.12	0.85	0.59	0.32
Permeability Coeff., sq.cm./sec.	6.78	5.94	4.79	4.02	2.92	1.88

APPENDIX IV

PORE SIZE DISTRIBUTION DATA

The gas drive technique was used to characterize the pore size distribution of specimens during this study. Gas drive data were gathered by saturating a specimen with technical-grade hexyl alcohol (density - 0.817 g./cc.; surface tension - 21.1 dynes/cm.), and then making flow rate - pressure drop measurements on it. Some typical flow rate - pressure drop data obtained from Specimen 50-A-3-3 before deformation are presented in Fig. 33. All the specimen parameters reported in Table XI were calculated from such plots.

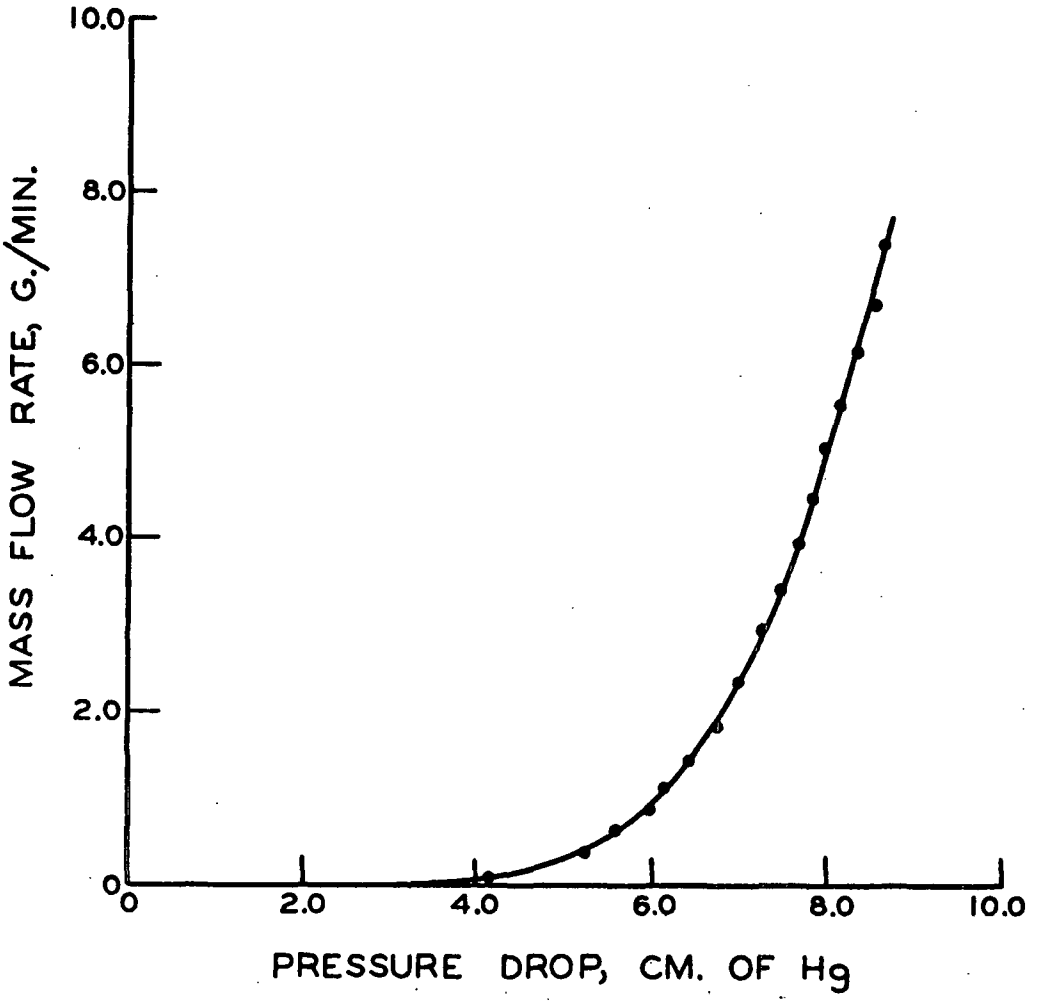

Figure 33. Gas Drive Data for Specimen 50-A-3-3-0

TABLE XI

GAS DRIVE DATA

Radius, μ	$\frac{dN}{dR}$, $cm.^{-1}$	$\log_{10} \frac{dN}{dR}$	Rel. Perm. Const., 10^{-11} sq. cm.	Perm. Const., 10^{-10} sq. cm.	Rel. Perm., %	Porosity/ Tortuosity x 10^4
Specimen 50-A-3-3-0: Applied stress = 0.00 kg./sq.mm.; irr. ext. = 0.00%.						
7.91	1.65×10^8	8.217	0.054	3.82	0.14	0.04
6.32	1.45×10^9	9.161	0.223	3.82	0.58	0.22
5.27	7.64×10^9	9.882	0.550	3.82	1.44	0.79
4.52	2.74×10^{10}	10.438	1.150	3.82	3.01	2.17
3.95	3.45×10^{10}	10.538	1.745	3.82	4.57	4.48
3.51	1.05×10^{11}	11.021	2.300	3.82	6.02	7.47
3.16	1.58×10^{11}	11.198	2.740	3.82	7.17	10.98
Specimen 50-A-3-3-20: Applied stress = 2.15 kg./sq.mm.; irr. ext. = 0.27%.						
7.91	2.27×10^8	8.356	0.065	4.30	0.15	0.04
6.32	1.76×10^9	9.246	0.300	4.30	0.70	0.30
5.27	9.97×10^9	9.998	0.726	4.30	1.69	1.05
4.52	3.35×10^{10}	10.525	1.448	4.30	3.37	2.84
3.95	5.96×10^{10}	10.775	2.130	4.30	4.95	5.46
3.51	9.41×10^{10}	10.974	2.630	4.30	6.12	8.53
3.16	1.42×10^{11}	11.152	3.020	4.30	7.02	12.09
Specimen 50-A-3-3-25: Applied stress = 2.76 kg./sq.mm.; irr. ext. = 0.74%.						
7.91	3.19×10^8	8.504	0.086	4.60	0.19	0.06
6.32	2.13×10^9	9.328	0.343	4.60	0.75	0.34
5.27	1.20×10^{10}	10.079	0.896	4.60	1.95	1.30
4.52	3.55×10^{10}	10.562	1.612	4.60	3.50	3.16
3.95	6.25×10^{10}	10.796	2.320	4.60	5.04	5.95
3.51	9.89×10^{10}	10.994	2.840	4.60	6.17	9.22
3.16	1.49×10^{11}	11.173	3.240	4.60	7.04	12.98
Specimen 50-A-3-30I: Applied stress = 3.37 kg./sq.mm.; irr. ext. 1.53%.						
7.91	4.50×10^8	8.653	0.097	5.29	0.18	0.06
6.32	2.90×10^9	9.462	0.480	5.29	0.91	0.48
5.27	1.49×10^{10}	10.173	1.162	5.29	2.20	1.68
4.52	3.71×10^{10}	10.569	1.988	5.29	3.76	3.90
3.95	6.50×10^{10}	10.812	2.710	5.29	5.12	6.95
3.51	1.03×10^{11}	11.012	3.260	5.29	6.16	10.58

TABLE XI (Continued)

Radius, μ	$\frac{dN}{dR}$, $cm.^{-1}$	$\log_{10} \frac{dN}{dR}$	Rel. Perm. Const., 10^{-11} sq.cm.	Perm. Const., 10^{-10} sq.cm.	Rel. Perm., %	Porosity/ Tortuosity x 10^4
Specimen 50-A-3-30II: Applied stress = 3.37 kg./sq.mm.; irr. ext. = 2.03%.						
7.91	4.71×10^{8}	8.673	0.174	5.83	0.30	0.10
6.32	3.28×10^{9}	9.516	0.607	5.83	1.04	0.61
5.27	1.48×10^{10}	10.170	1.334	5.83	2.29	1.93
4.52	3.64×10^{10}	10.561	2.190	5.83	3.76	4.30
3.95	6.14×10^{10}	10.788	2.870	5.83	4.92	7.36
3.51	9.70×10^{10}	10.986	3.380	5.83	5.80	10.97
Specimen 50-A-3-30III: Applied stress = 3.37 kg./sq.mm.; irr. ext. = 2.53%.						
7.91	5.10×10^{8}	8.707	0.228	5.94	0.38	0.15
6.32	3.33×10^{9}	9.522	0.634	5.94	1.07	0.63
5.27	1.64×10^{10}	10.215	1.449	5.94	2.44	2.09
4.52	3.65×10^{10}	10.562	2.340	5.94	3.94	4.59
3.95	6.17×10^{10}	10.790	3.030	5.94	5.10	7.77
3.51	9.24×10^{10}	10.965	3.500	5.94	5.89	11.36
Specimen 50-A-5-2-0: Applied stress = 0.00 kg./sq.mm.; irr. ext. = 0.00%.						
7.91	8.72×10^{7}	7.940	0.044	3.81	0.12	0.03
6.32	1.46×10^{9}	9.164	0.190	3.81	0.50	0.19
5.27	6.54×10^{9}	9.815	0.579	3.81	1.52	0.83
4.52	2.36×10^{10}	10.373	1.021	3.81	2.68	2.01
3.95	6.00×10^{10}	10.778	1.610	3.81	4.22	4.14
3.51	1.07×10^{11}	11.029	2.175	3.81	5.71	7.06
3.16	1.61×10^{11}	11.207	2.630	3.81	6.90	10.53
Specimen 50-A-5-2-20: Applied stress = 2.13 kg./sq.mm.; irr. ext. = 0.33%.						
7.91	1.89×10^{8}	8.276	0.065	4.16	0.16	0.04
6.32	2.02×10^{9}	9.306	0.316	4.16	0.76	0.32
5.27	8.94×10^{9}	9.951	0.727	4.16	1.75	1.05
4.52	2.86×10^{10}	10.456	1.331	4.16	3.20	2.62
3.95	6.31×10^{10}	10.800	1.988	4.16	4.78	5.10
3.51	1.00×10^{11}	11.000	2.520	4.16	6.06	8.18
3.16	1.50×10^{11}	11.176	2.930	4.16	7.04	11.73

TABLE XI (Continued)

Radius, μ	$\frac{dN}{dR}$, $cm.^{-1}$	$\log_{10} \frac{dN}{dR}$	Rel. Perm. Const., 10^{-11} sq.cm.	Perm. Const., 10^{-10} sq.cm.	Rel. Perm., %	Porosity/ Tortuosity x 10^4
Specimen 50-A-5-2-25: Applied stress = 2.75 kg./sq.mm.; irr. ext. = 0.72%.						
7.91	1.78×10^8	8.250	0.097	4.58	0.21	0.06
6.32	2.08×10^9	9.318	0.334	4.58	0.73	0.33
5.27	1.06×10^{10}	10.025	0.805	4.58	1.76	1.16
4.52	3.05×10^{10}	10.484	1.462	4.58	3.19	2.87
3.95	6.67×10^{10}	10.824	2.145	4.58	4.68	5.51
3.51	1.06×10^{11}	11.025	2.715	4.58	5.93	8.80
3.16	1.59×10^{11}	11.202	3.145	4.58	6.87	12.60
Specimen 50-A-5-2-30I: Applied stress = 3.35 kg./sq.mm.; irr. ext. = 1.50%.						
7.91	3.98×10^8	8.600	0.113	5.36	0.21	0.07
6.32	2.78×10^9	9.444	0.488	5.36	0.91	0.49
5.27	1.36×10^{10}	10.134	1.088	5.36	2.03	1.57
4.52	3.05×10^{10}	10.584	1.921	5.36	3.58	3.78
3.95	5.63×10^{10}	10.751	2.675	5.36	4.99	6.87
3.51	9.32×10^{10}	10.969	3.235	5.36	6.04	10.50
Specimen 50-A-5-2-30II: Applied stress = 3.35 kg./sq.mm.; irr. ext. = 2.00%.						
7.91	3.60×10^8	8.556	0.173	5.80	0.30	0.11
6.32	3.00×10^9	9.477	0.548	5.80	0.94	0.55
5.27	1.90×10^{10}	10.279	1.599	5.80	2.76	2.30
4.52	3.67×10^{10}	10.564	2.135	5.80	3.68	4.19
3.95	6.21×10^{10}	10.793	2.830	5.80	4.88	7.27
3.51	9.85×10^{10}	10.994	3.350	5.80	5.78	10.88
Specimen 50-A-5-2-30III: Applied stress = 3.35 kg./sq.mm.; irr. ext. = 2.42%.						
7.91	5.38×10^8	8.730	0.216	6.43	0.34	0.14
6.32	3.19×10^9	9.504	0.590	6.43	0.92	0.59
5.27	2.12×10^{10}	10.326	1.747	6.43	2.72	2.52
4.52	3.69×10^{10}	10.567	2.295	6.43	3.57	4.50
3.95	6.21×10^{10}	10.793	2.985	6.43	4.64	7.66
3.51	9.86×10^{10}	10.994	3.505	6.43	5.45	11.37